Report

presented to obtain

THE HABILITATION TO SUPERVISE RESEARCH

University Paul Sabatier, Toulouse 3

Field:

Applied Mathematics

by

Marie - Hélène VIGNAL

TITLE :

Mathematical modeling and asymptotic preserving scheme in the quasi-neutral limit for plasmas and the transport of particles

Defended the 12th december 2007

Jury

François Bouchut, CNRS, École Normale Supérieure

Yann Brenier, CNRS, University of Nice-Sophia-Antipolis

François Castella, University of Rennes 1

Thierry Colin, University of Bordeaux 1

Pierre Degond, CNRS, University of Toulouse 3

Thierry Gallouët, University of Provence

Mohamed Masmoudi, University of Toulouse 3

Eric Sonnendrücker, University L. Pasteur of Strasbourg

Referees

François Bouchut, CNRS, École Normale Supérieure

Yann Brenier, CNRS, University of Nice-Sophia-Antipolis

Haïliang Liu, Iowa State University

AKNOWLEDGEMENTS

Mes premiers remerciements vont à Pierre Degond. C'est grace à lui que j'ai découvert, entre autres, le monde passionnant de la modélisation de particules chargées. De part son dynamisme et le large spectre de ses connaissances, collaborer avec lui a été une expérience exceptionnellement enrichissante et agréable. Je tiens à lui exprimer toute ma profonde gratitude ainsi que toute mon amitié.

Je remercie François Bouchut, Yann Brenier et Haïliang Liu qui se sont penchés sur ce document. Je tiens à leur dire à quel point je suis honorée qu'ils aient accepté d'être mes rapporteurs.

C'est une grande joie pour moi, que Thierry Gallouët ait accepté de faire parti de mon jury. C'est lui, en tant que directeur de thèse, qui a guidé mes premiers pas en recherche. Ses qualités humaines, scientifiques et pédagogiques ont contribué à façonner la chercheuse que je suis aujourd'hui, merci Thierry.

Je tiens également, à remercier particulièrement Thierry Colin, François Castella, Mohamed Masmoudi et Eric Sonnendrücker de me faire l'honneur de participer à mon jury.

Je salue tous mes collaborateurs, Pierre Crispel, Fabrice Deluzet, Pierre Degond, Kim-Claire Le Than, Jian-Guo Liu, Céline Parzani, Rachid Talaalout et Dominique Savelief. Travailler avec eux a été et est toujours un réel plaisir.

Je remercie chaleureusement Raphaël Loubère et Francis Filbet pour leur chasse aux erreurs dans ce document.

La très bonne ambiance qui règne à MIP est telle que c'est un plaisir de venir travailler. Je souhaite pour cela exprimer ma reconnaissance à tous les membres du laboratoire, et tout particulièrement à Christine Marty, Jean-Michel Roquejoffre, Komla Domelevo, Luc Mieussens, Naoufel Ben Abdallah, Marjolaine Puel, Mohammed Lemou, Pierre Raphaël et Philippe Laurençot, sans oublier ceux qui sont déjà partis Christophe Besse, Florian Mehats et Xavier Antoine. Les pauses cigarettes ont souvent été l'occasion de riches discussions (mathématiques ou autres) et les bonnes bouffes bien arrosées le week-end ont largement contribué à mon équilibre moral.

Enfin et surtout, merci à vous, Thierry et Léo (mon petit soleil) pour vos présences à mes côtés et pardon pour tous ces moments que je vous ai volés pour travailler.

Table of Contents

Chapter 1

Introduction

1.1 Research activities

The research activities presented in this report are related to three different fields: First the coupling of models describing plasmas and containing both quasi-neutral and non quasi-neutral zones, then the development and the analysis of an asymptotic preserving scheme in the quasi-neutral limit and finally the modeling of transport of charged or non charged particles.

Before describing these three different studies, I summarize in Chapter 2 the work performed in my PhD studies. It deals with the numerical analysis of finite volume schemes for elliptic and hyperbolic equations, with a particular interest in boundary condition problems. Even if the research done after my PhD studies is not closely related to my PhD work, the knowledge that I have gained during this period has guided me all along my work: First, on criteria to construct an efficient finite volume scheme and above all for boundary condition problems. Furthermore, I have paid a particular attention on recent developments published since this period.

The first field of my research is devoted to the coupling of models describing the expansion of a quasi-neutral plasma bubble between two electrodes. The plasma, containing electrons and one ion species, is injected from the cathode and expands in the gap between the electrodes. During expansion, some electrons are attracted by the positive anode potential and form a beam in the vacuum. Then, two regions with different properties are present in the domain. The first region being the plasma bubble: It is quasi-neutral, meaning that electric unbalances take place at a very small scale length called the Debye length. The second region is the electron beam. This zone contains only electrons and so can not be at equilibrium. Thus, the Debye length is of order one in the beam.

We start with a fluid model constituted by the isentropic Euler equations for each species coupled with the Poisson equation for the description of electric effects. This model is called the two-fluid Euler-Poisson model. Unfortunately, classical discretizations of this model are subject to severe numerical constraints in quasi-neutral zones. Moreover, numerical simulations are two much expensive to be performed in practical multi-dimensional cases.

There are two possible ways to overcome this limitation. The first way, described in Chapter 3, consists in finding an asymptotic model for which discretizations are not constrained. Starting from the two-fluid Euler-Poisson model, we derive a quasi-

neutral model describing the plasma bubble. However, this model is not valid anymore in non quasi-neutral zones. Next, we derive a Child-Langmuir model describing the beam. Then, it is necessary to determine the dynamics of the interface between the different regions, and couple the models. We propose two descriptions based on different assumptions. The first description consists in a quasi-neutral model with a vanishing current for the plasma bubble coupled to the Child-Langmuir model for the beam. The coupling is done using the Rankine-Hugoniot relations of the two-fluid Euler-Poisson model. The numerical simulations of this model show that it correctly describes the interface dynamics. On the other hand, the electron mass conservation is not satisfied at the plasma-beam interface. The consequence is a spurious peak of plasma density near the interface. To correct this problem, we consider a new description giving a quasi-neutral model with a non vanishing current for the plasma bubble. This new description is coupled with the Child-Langmuir model for the beam studying a transmission problem at the plasma-beam interface. We, mathematically and numerically, study this new model. This gives us the validity domain of the quasi-neutral model with a non vanishing current. In one space dimension, the numerical simulations of this model show a very good agreement with the results given by two-fluid Euler-Poisson model. We propose different extensions of this work related to the full Euler equations and two dimensional problems.

Unfortunately, the numerical simulations of the plasma expansion test case near the plasma-beam interface, reaches a regime outside the validity domain of the quasi-neutral model with a non vanishing current. For this reason, we consider a new approach in Chapter 4. In this chapter, we develop an asymptotic preserving scheme in the quasi-neutral limit for the two-fluid Euler-Poisson model. Using this scheme, we do not have to follow any interface since only one model is used for the description of quasi-neutral and non quasi-neutral regions. Moreover, this scheme has the same cost as classical schemes without being subject to quasi-neutral constraints. We prove the good behavior of this scheme while performing numerical simulations and studying its stability for a linearized one-fluid Euler-Poisson model. Furthermore, we study a boundary layer problem at the injection point. Indeed, we numerically show that boundary conditions not well adapted to the quasi-neutral regime, lead to numerical constraints as severe as the previously encountered ones. We derive and study a boundary layer problem. This allows to determine well-adapted boundary conditions. These well-adapted boundary conditions are numerically tested on the previous plasma expansion test case. Results show that all numerical constraints related to quasi-neutrality, are removed.

The last chapter of this report presents some work related to kinetic descriptions of particles. First, we study a problem of particles confined close to a wall by an applied potential. To reduce the cost of numerical simulations, we derive a two dimensional model starting from a three dimensional kinetic description. This asymptotic analysis is done rigorously in the case of non charged particles and formally when the coupling with the Poisson equation is considered. We illustrate this work with numerical simulations of a primary discharge problem occurring in the study of electric arc phenomena on satellite solar panels. Finally, I conclude this report with the mathematical study of a simplified diphasic model. This model describes the transport of

droplets in a gas. It is constituted of the Vlasov equation for the droplets description coupled to the Burgers equation for the gas. We study the existence, the uniqueness and the limit of the different viscous solutions.

1.2 Publication list

1.2.1 Articles or proceedings during the PhD work

[**Th1**] M.-H. Vignal, Convergence of a finite volume scheme for an elliptic-hyperbolic system, RAIRO Modélisation Mathématique et Analyse Numérique **30** (1996) no. 7, 841–872.

[**Th2**] S. Verdière, M.-H. Vignal, Numerical and theoretical study of a dual mesh method using finite volume schemes for two phase flow problems in porous media, Numerische Mathematik **80** (1998) no. 4, 601–639.

[**Th3**] T. Gallouët, R. Herbin, M.-H. Vignal, Error estimates on the approximate finite volume solution of convection diffusion equations with general boundary conditions, SIAM Journal on Numerical Analysis **37** (2000) no. 6, 1935–1972.

[**Th4**] M.-H. Vignal, Convergence of Finite Volumes Schemes for an elliptic hyperbolic system with boundary conditions, Proceeding of the First International Symposium on Finite Volumes for Complex Applications, ed. F. Benkhaldoun et R. Vilsmeier, Hermes (1996) 145–152. This proceeding is not published in an article.

1.2.2 Notes published after the PhD work

[**N1**] K. Domelevo, M.-H. Vignal, Limites visqueuses pour des systèmes de type Fokker-Planck-Burgers unidimensionnels, Comptes Rendus de l'Académie des Sciences. Série I. Mathématique **332** (2001) no. 9, 863–868. This not is not published in an article.

[**N2**] P. Degond, C. Parzani, M.-H. Vignal, Un modèle d'expansion de plasma dans le vide, Comptes Rendus de l'Académie des Sciences. Série I. Mathématique **335** (2002), no. 4, 399–404. This note is not published in an article.

[**N3**] P. Degond, C. Parzani, M.-H. Vignal, A one-dimensional model of plasma expansion, Mathematical and Computer Modeling **38** (2003) no. 10, 1093–1099. This note summarizes the results published in [**A1**].

[**N4**] P. Crispel, P. Degond, C. Parzani, M.-H. Vignal, Trois formulations d'un modèle de plasma quasi-neutre avec courant non nul, Comptes Rendus de l'Académie des Sciences. Série I. Mathématique **338** (2004) no. 4, 327–332. This note summarizes the results published in [**A2**].

[**N5**] P. Crispel, P. Degond, M.-H. Vignal, An asymptotically stable discretization for the Euler-Poisson system, Comptes Rendus de l'Académie des Sciences. Série I. Mathématique **341** (2005) no. 5, 323–328. This note summarizes the results published in [**A4**].

1.2.3 Articles published after the PhD work

[**A1**] P. Degond, C. Parzani, M.-H. Vignal, Plasma expansion in vacuum: modeling the breakdown of quasineutrality, Multiscale Modeling and Simulation, SIAM **2** (2003) no. 1, 158–178.

[**A2**] P. Crispel, P. Degond, M.-H. Vignal, Quasi-neutral fluid models for current-carrying plasmas, Journal of computational Physics, **205** (2005) no. 2, 408–438.

[**A3**] P. Degond, C. Parzani, M.-H. Vignal, A Boltzmann model for trapped particles in a surface potential, Multiscale Modeling & Simulation, SIAM **5** (2006) no. 2, 364–392.

[**A4**] P. Crispel, P. Degond, M.-H. Vignal, An asymptotic preserving scheme for the two-fluid Euler-Poisson model in the quasi-neutral limit, Journal of computational Physics **223** (2007) no. 1, 208–234.

[**A5**] P. Crispel, P. Degond, M.-H. Vignal, A plasma expansion model based on the full Euler-Poisson system, Mathematical Models & Methods in Applied Sciences **17** (2007) no. 7, 1129–1158.

[**A6**] K.-C. Le Thanh, C. Parzani, M.-H. Vignal, A Volume Of Fluid method for a two-dimensional plasma expansion problem, Journal of computational Physics **225** (2007) 1937–1960.

[**A7**] J.-G. Liu, P. Degond, M.-H. Vignal, Analysis of an asymptotic preserving scheme for the Euler-Poisson system in the quasineutral limit, submitted.

[**A8**] Vignal M.-H., A boundary layer problem for an asymptotic preserving scheme in the quasi-neutral limit for the Euler-Poisson system, submitted.

1.2.4 Proceedings published after the PhD work

[**CR1**] P. Degond, R. Talaalout, M.-H. Vignal, Electron transport and secondary emission in a surface of solar cell, proceeding of the Workshop ESA-CNES, 4th and 6th september 2000, ESTEC, Noordwijk, the Netherlands. This proceeding is not published in an article.

[**CR2**] P. Degond, C. Parzani, M.-H. Vignal, On plasma expansion in vacuum, proceedings of the conference on Free Boundary Problems, Theory and applications, Trento, juin 2002, International Series of Numerical Mathematics, Birkaüser, Editors P. Colli, C. Verdi, A. Visinti, **147** 103–112. This proceeding is not published in an article.

[**CR3**] N. Ben Abdallah, P. Degond, F. Deluzet, V. Latocha, R. Talaalout, M.-H. Vignal, Diffusion limits of kinetic models, proceedings of the conference on Hyperbolic problems: theory, numerics, applications, Springer, Berlin, (2003) 3–17. The work regarding me, in this proceeding is published in [**CR1**].

Chapter 2

Summary of the PhD work: Numerical analysis of finite volume schemes

During my PhD, I worked on numerical analysis of finite volume schemes for elliptic or hyperbolic equations on bounded domains. The originality of my work consists in the study of boundary conditions and in the elliptic-hyperbolic coupling.

Finite volume schemes are intensively used in industry, among others in petroleum industry. They are particularly well adapted for the discretization of conservation equations. The principle of finite volumes is the following. A family of cells (or control volumes) are considered. An unknown is associated to each cell and, we obtain one equation for one unknown, by integrating the considered equation on each control volume. This integration yields flux terms modeling the exchange between cells. These flux terms are discretized using finite differences.

First, I have considered a linear hyperbolic equation coupled to a linear elliptic equation on a multi-dimensional domain. This system is discretized using a "four points" finite volume scheme for the elliptic equation, studied in [26], and the upwind scheme for the hyperbolic equation. I show the convergence of the approximate solution towards the exact solution of the system. For the elliptic equation, I establish an error estimate in a discrete H^1 norm of order Δx, where Δx is the size of the mesh. Furthermore, using discrete Sobolev embedding inequalities, I establish error estimates in L^r for all r such that $1 \leq r \leq +\infty$. For the hyperbolic equation, I prove the convergence of the approximate solution towards the exact solution in L^∞ for the weak-$\star$ topology. This work is published in [**Th1**].

Then, in collaboration with Sophie Verdière, I consider a diphasic flow problem in porous media. This work is published in [**Th2**]. The model couples a linear elliptic equation with a non linear hyperbolic equation. The parameters of this problem are given by geophysicists as constant functions over each cell of a very fine mesh. This mesh can be made of several millions of cells. The discretization of the elliptic equation leads to a linear system too large to be resolved on the fine mesh. For this reason, this equation is discretized on a coarse grid. However, in order to keep the information given on the fine mesh, the hyperbolic equation is resolved on this fine mesh. Then, a dual mesh method is obtained. Since the equations are coupled, we have to reconstruct some the information from the coarse grid on the fine grid. We study two reconstruction methods. On a simplified linear model, we prove the

convergence of the scheme. Furthermore, for the non linear system, we perform numerical simulations for more complex physical applications.

In **[Th3]**, we consider a convection-diffusion equations with general boundary conditions: Dirichlet, Neumann or Fourier. We discretize this equation with a finite volume scheme on a Voronoï mesh (including triangles and rectangles). Assuming the solutions at least in H^2, we prove error estimates in a discrete H_0^1 norm of the domain and in a discrete L^2 norm of the boundary. A Sobolev embedding inequality gives an error estimate in L^2 norm of the domain. This work has been done in collaboration with Thierry Gallouët and Raphaèle Herbin.

Then, I consider the non linear case for the hyperbolic equation set on a bounded domain. The equation is discretized with a general finite volume scheme. Using L^∞ and "weak BV" estimates, I show the convergence of the approximate solution towards an entropy process solution of the problem in L^∞ for the weak-$\star$ topology. This solution, introduced in [21] in the unbounded case, is built using the repartition function of a Young measure. If the exact solution has bounded variations, I can prove that this entropy process solution is the weak entropy solution of the problem. For this, we use a technique introduced by S.N. Kruzkov in [30]. Furthermore, for a particular family of fluxes, we prove error estimates in L^1 norm of order $\Delta x^{1/4}$ where Δx is the size of the mesh. This work is partially published in **[Th4]**.

Chapter 3

Coupling of models for a plasma expansion problem

3.1 Introduction

In this chapter, I describe the mathematical and numerical modeling of the expansion of a plasma bubble between two electrodes. This work has been published in [**N2**], [**N3**], [**N4**], [**A1**], [**A2**], [**A5**], [**A6**] and [**CR2**]. It is a collaboration with Pierre Crispel, Pierre Degond, Kim-Claire Le Thanh and Céline Parzani. It has been done in the context of two industrial projects and was supported by several contracts.

The first project deals with the study of high current diodes. It has been proposed by Franck Assous, Jacques Segré and Kim-Claire le Thanh from the CEA (French Atomic Energy Center) of Bruyères le châtel. It covers the period from 2001 until 2004. The second project has been proposed by Jean-Pierre Catani and Denis Payan from the CNES (French space center) and Jean-François Roussel from Onera in Toulouse. It covers the period from 2003 until 2005, and deals with the electric arc phenomena on satellite solar panels.

The physical scenari of these two phenomena are identical, only the scales of physical parameters change. In both cases, we consider two plane electrodes. A plasma is injected from the cathode. Due to some thermal effects, the plasma bubble expands in the gap between the electrodes. During its expansion, electrons are attracted by the positive potential of the anode. They are emitted in the gap between the plasma-beam interface and the anode, and form an electron beam in the "vacuum". The plasma is supposed to be fully ionized and constituted of electrons and of one ion species. We use a fluid description given by the following two-fluid Euler-Poisson model

$$\partial_t n_i + \partial_x(n_i u_i) \;=\; 0, \tag{3.1}$$

$$m_i\,\left(\partial_t(n_i u_i) + \partial_x(n_i u_i^2)\right) + \partial_x p_i(n_i) \;=\; -e\,n_i\,\partial_x\phi, \tag{3.2}$$

$$\partial_t n_e + \partial_x(n_e u_e) \;=\; 0, \tag{3.3}$$

$$m_e\,\left(\partial_t(n_e u_e) + \partial_x(n_e u_e^2)\right) + \partial_x p_e(n_e) \;=\; e\,n_e\,\partial_x\phi, \tag{3.4}$$

$$-\partial_{xx}^2\phi \;=\; \frac{e}{\epsilon_0}(n_i - n_e), \tag{3.5}$$

where t is the time, x is the space variable and where the quantities for ions are

indexed by i and those for electrons by e. For $j = i$ or e, we denote by m_j the mass of the particles j, by n_j their density, by u_j their velocity and by p_j their pressure law assumed adiabatic and given by $p_j(n) = C_j\, n^{\gamma_j}$ where $C_j > 0$ and $\gamma_j > 1$. Furthermore, $e > 0$ is the positive elementary charge, ϕ is the electric potential and ϵ_o the vacuum permittivity.

This model describes all the device (plasma, interface, beam), but it is subject to such severe numerical constraints that the model is unusable in practice. The computational cost in one space dimension is already huge although the aim is to simulate cases in two or three dimensions of space. These numerical constraints are related to two physical parameters well known in plasma physics (see [7], [28]): the Debye length and the plasma period, respectively denoted by λ_D and τ_p. They are given by

$$\lambda_D = \left(\frac{\epsilon_0\, k_B\, T_0}{e^2\, n_0}\right)^{1/2} \qquad \text{and} \qquad \tau_p = \left(\frac{\epsilon_0\, m_e}{e^2\, n_0}\right)^{1/2}, \tag{3.6}$$

where k_B is the Boltzmann constant, n_0 and T_0 are the typical density and temperature of the plasma.

The Debye length measures the scale of the distance at which electric effects take place in the plasma. If we consider a particular charge q in the plasma, then a cloud of opposite charges is formed around this charge. This cloud screens the electric effect of the charge q beyond the distance λ_D. The charges outside the effective area do not interact with the charge q. The plasma period is related to these charge unbalances. When an unbalance occurs (of the order λ_D), electric forces tend to restore the particles towards their equilibrium position. Then, the particles oscillate around this position. The period of the electron oscillations is given by τ_p. It is possible to define the ion period by switching m_e by m_i. But, this period is larger than τ_p since ions are heavier than electrons. In the problem that we consider here, the densities in the plasma bubble are very large. Thus, the Debye length and the plasma period are very small comparing to the macroscopic scales, i.e. the size of the device (distance cathode-anode) and the final time of the simulatation.

In practice, when we use a classical scheme, the time discretization must resolve the plasma period otherwise an instability appears. This result is proved in [23] for a one-fluid Euler-Poisson system linearized around a stationary solution. Furthermore, we will see in section 4.4, that a boundary layer of size λ_D at the cathode, leads in general to another numerical constraint. The space discretization must resolve the Debye length to ensure the stability of the scheme. These constraints are too much penalizing to perform two dimensional numerical simulations.

Two ways are possible to overcome these limitations. They consist in freeing from the small scales λ_D and τ_p either at the level of the modeling or at the discretization level. Here, we describe the first approach, the second approach is developed in Chapter 4.

In the first approach, we choose to use a quasi-neutral model in the plasma bubble. This model is obtained from the two-fluid Euler-Poisson model when the Debye length tends to zero. It is not constrained to resolve the scale τ_p. But, it is only valid in quasi-neutral zones, i.e. the plasma bubble. So, it is necessary to derive another model to describe the electron beam. Then, we have to determine the regions where

each model is valid and, as a result, follow the plasma-beam interface. Finally, we have to reconnect the models at the interface.

3.2 The physical context and the Euler-Poisson model

I begin with the description of the physical context of the projects already mentioned in the introduction. In a conventional plane diode, a high potential is applied at the anode leading to an electron emission in the gap between the electrodes. For all electron emission process, this extracted current is limited by a threshold value, called the Child-Langmuir current or limited current by space charge effects. This threshold current is inversely proportional to the square of the distance between the electrodes, see [31], [14], [18], [19].

To overcome this limitation, physicists have developed new devices: the high current diodes. In high current diodes, the cathode is made of a material with a regular micro spike lattice. Several materials are used like cathodes in dielectric metal, in carbon fiber or velvet cathodes, see [44]. According to physicists, the current increase has two origins. The enhanced electric field near the spikes (called in physics literature "enhanced field particle emission") and the explosive erosion of the cathode produce a very dense plasma, see [29], [33]. Here, we are interested in the modeling of the expansion of the dense plasma.

While the plasma expands, electrons are emitted from the plasma-beam interface. The plasma being quasi-neutral, all the difference of potential is concentrated between the plasma-beam interface and the anode. The plasma-beam interface plays the role of a virtual cathode. As the distance between the virtual cathode and the anode decreases, the extracted current increases.

Now, I describe the physical context of the electric arc phenomena on satellites. To be supplied in energy, satellites have solar panels constituted of strings of solar cells. In order to respond to high power demands, constructors increase the number of cells contained in each string. But, when this number exceeds the threshold value of fifty Volts, electric arcs may appear and could damage the concerned string.

The physical scenario can be split into three steps. In the first step, an electrostatic discharge, called primary discharge, ignites near a metallic part of a cell. This primary discharge creates a very high density plasma which expends in the gap between two cells. The cells are at different potentials. When the plasma has filled up all the gap, the electric arc may occur. Here, we are interested in the transition from the primary discharge towards the electric arc, i.e. the plasma expansion.

We start from the two-fluid Euler-Poisson model (3.1)-(3.5) for $x \in [0, L]$ and $t > 0$ where L is the distance between the electrodes. We close the system with initial and boundary conditions. At the beginning of the process, the domain is supposed devoid of plasma. Then, we set $n_i|_{t=0} = n_e|_{t=0} = 0$. The cathode and the anode are respectively located at $x = 0$ and $x = 1$, thus

$$\phi|_{x=0} = 0, \quad \text{and} \quad \phi|_{x=0} = \phi_L > 0. \tag{3.7}$$

Finally, for the fluid quantities, at the point $x = L$, we assume a super-sonic regime

and no boundary condition is necessary. At the point $x = 0$, we consider that a quasi-neutral plasma with the same velocity for ions and electrons, is present outside the domain for $x < 0$. The boundary conditions are given by

$$(n_i, u_i)(0,t) = (n_{i0}, u_{i0})(t), \qquad (n_e, u_e)(0,t) = (n_{e0}, u_{e0})(t), \tag{3.8}$$

for all $t > 0$ and where (n_{i0}, u_{i0}) and (n_{e0}, u_{e0}) are given by the resolution of electron and ion Riemann problems where the left states are identical and given by (n_0, u_0), the state outside the domain. The right states are given by $(n_{i,e}, u_{i,e})(0^+, t) = \lim_{x\to 0^+}(n_{i,e}, u_{i,e})(x,t)$.

3.3 One dimensional asymptotic model

Here, I describe the results published in [**N2**], [**N3**] and [**A1**]. I recall that the two-fluid Euler-Poisson model (3.1)-(3.5), (3.7)-(3.8), is valid in all the domain: the plasma bubble, the interface and the beam. But it must resolve the small scale of the plasma period.

The aim of this study is to derive a model not constrained to resolve this small scale. For this, we begin with the rescaling of physical quantities in (3.1)-(3.5). The rescaling is different in each zone since they have different physical properties.

We begin with the rescaling of the plasma region. We choose the following characteristic quantities: the size of the domain L for the space variable, the density and velocity n_0 and u_0, the time $t_0 = L/u_0$, the ion pressure $p_0 = n_0\, m_i\, u_0^2$ and the anode potential ϕ_L. The rescaled variables are defined by $\tilde{x} = x/L$, $\tilde{t} = t/t_0$, $\tilde{n}_{i,e} = n_{i,e}/n_0$, $\tilde{u}_{i,e} = u_{i,e}/u_0$, $\tilde{p}_{i,e}(\tilde{n}_{i,e}) = p_{i,e}(n_{i,e})/p_0$ and $\tilde{\phi} = \phi/\phi_L$. We denote by $\tilde{X}(\tilde{t})$ the plasma-beam interface in rescaled variables for all $\tilde{t} > 0$. Omitting the "tildes", we obtain, for all $x \in [0, X(t)]$ and all $t > 0$

$$\partial_t n_i + \partial_x(n_i u_i) \;=\; 0, \qquad \partial_t(n_i u_i) + \partial_x(n_i u_i^2) + \partial_x p_i(n_i) \;=\; -\frac{n_i\, \partial_x \phi}{\eta}, \tag{3.9}$$

$$\partial_t n_e + \partial_x(n_e u_e) \;=\; 0, \qquad \varepsilon\, \big(\partial_t(n_e u_e) + \partial_x(n_e u_e^2)\big) + \partial_x p_e(n_e) \;=\; \frac{n_e\, \partial_x \phi}{\eta}, \tag{3.10}$$

$$-\lambda\, \partial_{xx}^2 \phi \;=\; (n_i - n_e), \tag{3.11}$$

where ε, η and λ are three dimensionless parameters defined by

$$\varepsilon = \frac{m_e}{m_i}, \qquad \eta = \frac{m_i\, u_0^2}{e\, \phi_L}, \qquad \lambda = \frac{\epsilon_0\, \phi_L}{e\, n_0\, L^2} = \frac{e\, \phi_L}{e^2/(\epsilon_0\, (n_0\, L^2)^{-1})}.$$

They respectively measure the ratio between electron and ion masses, the ratio between thermal energy and potential energy and the ratio between potential energies due to the applied potential and the Coulombian interactions (see [7]).

We are interested in situations such that λ is of order 1 and η is very small. These values agree with those observed in high current diodes (see [50]). In practice, ε is small but can not be neglected. Indeed, although the electrons' inertia is small, they

undergo large accelerations. Therefore, ε will be considered as an order 1 quantity. It is important to note that the rescaled Debye length, i.e. the ratio between the Debye length and the macroscopic scale L, is given by $\sqrt{\lambda\,\eta}$. Furthermore, the rescaled plasma period, i.e. the ratio between the plasma period and the macroscopic time t_0, is given by $\sqrt{\varepsilon\,\lambda\,\eta}$. Thus, η small gives a small Debye length and a small plasma period.

In the beam region there are only electrons. The characteristic quantities chosen for the rescaling are the same as previously, for the space variable, the time, the density, the potential and the pressure. But electrons are accelerated to large velocities by the electric field. We expect energies of order of the potential energy $e\phi_L$. Thus, we choose for characteristic electron velocity $\sqrt{e\phi_L/m_e}$. We set $\bar{u}_e = \sqrt{\varepsilon\,\eta}\,u_e$ where u_e is the rescaled velocity in the plasma region. We obtain the Euler-Poisson model in the beam region $[X(t), 1]$:

$$\sqrt{\varepsilon\eta}\,\partial_t n_e + \partial_x(n_e\bar{u}_e) = 0\,, \qquad -\lambda\partial^2_{xx}\phi = -n_e\,, \tag{3.12}$$

$$\varepsilon\left(\sqrt{\varepsilon\eta}\,\partial_t(n_e\bar{u}_e) + \partial_x(n_e\bar{u}_e^2)\right) + \varepsilon\eta\,\partial_x p_e(n_e) = \varepsilon\,n_e\partial_x\phi\,, \tag{3.13}$$

where the boundary conditions at the point $x = X(t)$ are such that n_e, $\bar{u}_e$, ϕ match the values of the corresponding quantities for the two-fluid Euler-Poisson model in the plasma region. Note that since $u_e = O(1)$ in the plasma region, we have $\bar{u}_e|_{x=X(t)} = (\varepsilon\eta)^{1/2}u_e|_{x=X(t)} = O((\varepsilon\eta)^{1/2}) \to 0$ as $\eta \to 0$. Similarly, since $\phi \to 0$ in the plasma region, we have $\phi|_{x=X(t)} \to 0$ as $\eta \to 0$. Finally, we recall that $\phi|_{x=1} = 1$.

Now, we can establish an asymptotic model in each region. We begin with the beam region.

3.3.1 Asymptotic model in the beam region

The asymptotic models in the beam are identical in references **[N2]**, **[N3]** and **[A1]**. Let us denote by n_e^η, $\bar{u}_e^\eta$, ϕ^η a solution of system (3.12)-(3.13) with the above specified boundary conditions. The limit $\eta \to 0$ is analyzed in the following proposition based on the results established in [14] and [18].

Proposition 3.1 *As $\eta \to 0$, n_e^η, $\bar{u}_e^\eta$, ϕ^η converge to n_e, $\bar{u}_e$, ϕ, a solution of the Child-Langmuir problem on $[X(t), 1]$:*

$$\partial_x(n_e\bar{u}_e) = 0\,, \quad \partial_x(n_e\bar{u}_e^2) = n_e\,\partial_x\phi\,, \quad -\lambda\partial^2_{xx}\phi = -n_e\,,$$

with the boundary conditions $\bar{u}_e|_{x=X(t)} = 0$, $\phi|_{x=X(t)} = 0$, $\phi|_{x=1} = 1$. We set $\bar{j}_e = n_e\bar{u}_e$. Then, $\bar{j}_e$ does not depend of x on $[X(t), 1]$. We introduce the Child-Langmuir current:

$$\bar{j}_{CL}(t) = \frac{4\sqrt{2}\lambda}{9\,(1 - X(t))^2}\,. \tag{3.14}$$

Then, for all values $\bar{j}_e \in [0, \bar{j}_{CL}(t)]$, there exists a unique solution n_e, $\bar{u}_e$, ϕ, with ϕ positive on $]X(t), 1]$, given by $n_e = \bar{j}_e/\sqrt{2\phi}$, $\bar{u}_e = \sqrt{2\phi}$. The potential ϕ is implicitly

determined by

$$\int_0^{\phi(x,t)} \frac{d\psi}{\sqrt{(\partial_x\phi|_{x=X(t)})^2 + 2\sqrt{2}\,\lambda^{-1}\bar{j}_e\sqrt{\psi}}} = x - X(t)\,. \tag{3.15}$$

Remark that the knowledge of $\partial_x\phi|_{x=X(t)}$ *and the boundary conditions at* $x = 1$ *on the potential, implicitly give* $\bar{j}_e$*. Indeed, writing (3.15) at* $x = 1$*, yields an equation linking* $\partial_x\phi|_{x=X(t)}$ *and* $\bar{j}_e$*. There is no solution if* $\bar{j}_e \notin [0, \bar{j}_{CL}(t)]$ *and* $\bar{j}_e \in [0, \bar{j}_{CL}(t)]$ *corresponds to an electric field at the interface* $\partial_x\phi|_{x=X(t)} \in [0, 1/(1-X)]$*. In particular, for* $\partial_x\phi|_{x=X(t)} = 0$*, we are in a maximal current regime and* $\bar{j}_e = \bar{j}_{CL}(t)$ *and* $\phi = ((x-X)/(1-X))^{4/3}$*.*

Going back to the scaling used in the plasma region, the electron flux j_e and the Child-Langmuir current j_{CL} are given by $j_e, j_{CL} = (\varepsilon\eta)^{-1/2}\bar{j}_e, \bar{j}_{CL}$.

3.3.2 Asymptotic model in the plasma and reconnection at the interface

The asymptotic models for the plasma region as well as the reconnection models at the plasma-beam interface are different in references [**N2**] and [**N3**], [**A1**].

In [**N2**], we assume that the limit of the current, when $\eta \to 0$, is zero in the plasma, i.e. electron and ion velocities are identical. If $n^\eta_{e,i}$, $u^\eta_{e,i}$ and ϕ^η are solutions of (3.9)-(3.11), the formal limit $\eta \to 0$ gives $n^\eta_{e,i} \to n$, $u^\eta_{e,i} \to u$ and $\phi^\eta \to 0$. The quasi-neutral density n and the total momentum $(1+\varepsilon)\,n\,u$ satisfy the classical isentropic Euler model on $[0, X(t)]$

$$\begin{cases} \partial_t n + \partial_x(n\,u) = 0\,, \qquad \phi(x) = 0, \\ (1+\varepsilon)\ (\partial_t(n\,u) + \partial_x(n\,u^2)) + \partial_x\left(p_i(n) + p_e(n)\right) = 0. \end{cases} \tag{3.16}$$

We close and couple the Child-Langmuir model for the beam (given in Proposition 3.1) and the classical isentropic Euler model for the plasma with the following result.

Proposition 3.2 *We assume that the quasi-neutral limit is valid until the interface* $X(t)$*, that the electron density is continuous across the interface while the electron velocity is discontinuous. Furthermore, we suppose that the electron emission in the beam is done in a maximal current regime and that a reaction pressure force exerted by the beam onto the plasma is localized at the interface. The left state at the interface is given by* $n_{e-} = n_{i-} = n_-$*,* $u_{i-} = u_{e-} = u_-$*,* $\phi_- = 0$ *and* $(\phi_x)_- = 0$*, and the right state by* $n_{e+} = n_-$*,* $n_{i+} = 0$*,* $n_{e+}u_{e+} = j_{CL}$ *and* $(\phi_x)_+ = 0$ *where for all function* f*, we denote by* $f_\pm = \lim_{x\to X(t)^\pm} f$*, and where* n_- *and* u_- *are the density and the velocity on the left-hand side of* $X(t)$ *given by the quasi-neutral model (3.16). Moreover,* j_{CL} *is given by* $j_{CL} = (\varepsilon\eta)^{-1/2}\bar{j}_{CL}$ *where* $\bar{j}_{CL}$ *is given by (3.14). Thus, the interface position velocity and the reaction pressure force exerted by the beam onto the plasma are given by*

$$\frac{dX}{dt} = u_-, \qquad \left(p_i + p_e\right)(n_-) = \varepsilon j_{CL}\left(\frac{j_{CL}}{n_-} - u_-\right) + p_e\,(n_-)\,.$$

The proof of this result relies on the passage to the limit $\eta \to 0$ in the Rankine-Hugoniot relations written for the conservation equations of ion mass and total momentum.

We perform numerical simulations with values close to those given in high current diodes. We compare the two-fluid Euler Poisson model (3.9)-(3.11) valid in all

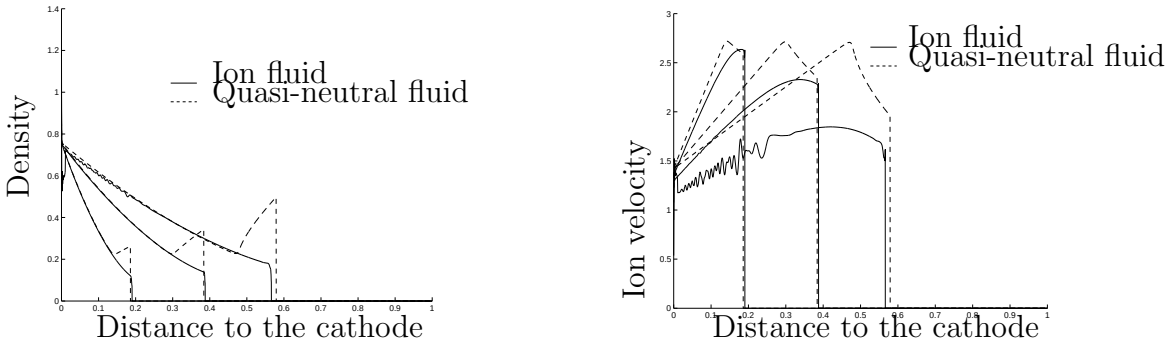

Figure 3.1: Rescaled density and velocity of the ion fluid given by the two-fluid and quasi-neutral models: observed quantities between the cathode $x = 0$ and the interface at the rescaled times $t = 0.07$, $t = 0.15$ and $t = 0.24$.

the domain, to the asymptotic model constituted of the classical isentropic Euler model (3.16) for the plasma region and the Child-Langmuir model in the beam, connected by the relations given in Proposition 3.2. The discretization is a finite volume scheme with an HLLE solver (see [51]) or a degree 2 polynomial solver (see [17]) which are order 1 Roe type solvers. We use a uniform mesh in space (Δx =constant) except in the neighborood of the plasma-beam interface where the mesh matches the interface. This allows to take into account the reaction pressure force since along the interface the flux is given by the total pressure. The interface velocity is given by the ion velocity in the last cell which contains plasma. The numerical scheme is detailed for a similar model in [**A1**]. We set $\eta = 10^{-4}$, $\lambda = 10^{-3}$, $\varepsilon = 0.5$, $C_i = C_e = 1$, $\gamma_i = \gamma_e = 2$ and $\Delta x = 2 \times 10^{-4}$. Let us remark that these values give a rescaled Debye length and plasma period respectively given by $\sqrt{\lambda\,\eta} \approx 3.2 \times 10^{-4}$ and $\sqrt{\varepsilon\,\lambda\,\eta} \approx 2.2 \times 10^{-4}$.

Figure 3.2 shows that the Child-Langmuir model is valid in the beam. Indeed, after the plasma-beam interface the results of the two-fluid Euler-Poisson model are identical to those of the Child-Langmuir model. But, Figure 3.1 shows that the isentropic Euler model in the plasma yields several problems. First, we can see a peak on the density curve near the interface. This peak is not present in the two-fluid Euler-Poisson model curve. It is the consequence of the vanishing current assumption in the plasma and implies an important physical inconsistency. Indeed, the electron mass conservation is not satisfied across the interface and the electron mass before the interface is overestimated. Furthermore, we have to penalize the reaction pressure term at the interface. If we do not, the plasma-beam interface given by the asymptotic model is moving slower than the interface given by the two-fluid model.

All the drawbacks of the previous model lead us naturally to consider in [**N3**]

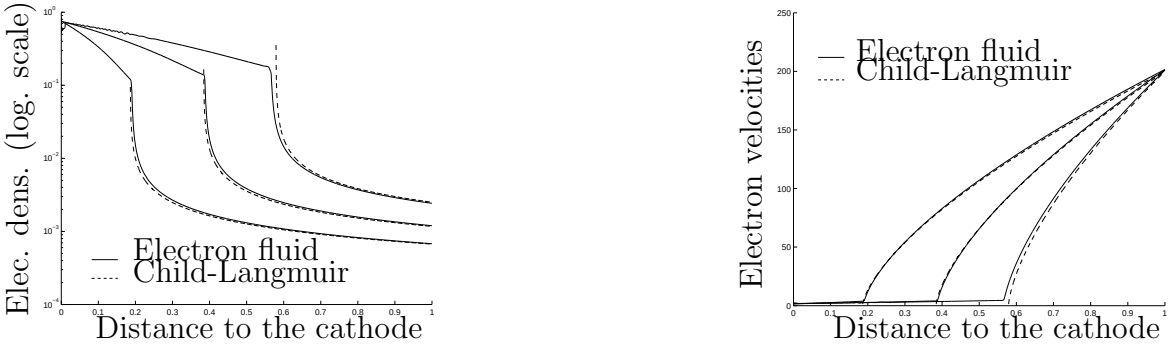

Figure 3.2: Rescaled density and velocity of the electron fluid given by the two-fluid and Child-Langmuir models: observed quantities between the interface $x = X(t)$ and the anode $x = 1$ at the rescaled times $t = 0.07$, $t = 0.15$ and $t = 0.24$.

and [**A1**], another modeling of the plasma and interface regions. First, we suppose a non vanishing current in the plasma and so different velocities for ions and electrons. However, we note that the limit being still quasi-neutral $n_i = n_e$, the density conservation laws give a constant current, $j = n_i\, u_i - n_e\, u_e$. In [**N3**] and [**A1**], we establish the following formal result.

Proposition 3.3 *If n_e^η, n_i^η, u_e^η, u_i^η, ϕ^η are solutions of (3.9)-(3.11), the formal limit $\eta \to 0$ in $[0, X(t)]$, gives*

$$n_e^\eta, n_i^\eta \to n, \quad u_i^\eta \to u, \quad u_e^\eta \to u - j/n, \quad \phi^\eta \to 0,$$

where n, u, j and ϕ are solutions of the quasi-neutral model with a non vanishing current:

$$\partial_t n + \partial_x(nu) = 0\,, \quad \partial_x j = 0\,, \quad \phi = 0\,, \tag{3.17}$$

$$(1+\varepsilon)\left(\partial_t(nu)+\partial_x(nu^2)\right) + \partial_x\left(p_i(n)+p_e(n)\right) + \varepsilon\,\partial_x\left(-2uj+\frac{j^2}{n}\right) = \varepsilon\,\partial_t j\,. \tag{3.18}$$

The current j is unknown at this stage and will be specified further during the connexion of the models. Its value depends on the electron emission in the beam region and so on the Child-Langmuir model. Furthermore, note that the formal analysis does not ensure that the boundary conditions are kept. Here, we assume that this holds true for the quasi-neutral density and the ion velocity. But, we will see in Chapter 4 that the presence of a boundary layer transforms the boundary conditions. If $j \neq 0$, the conditions for u_e^η are lost since $u_e|_{x=0} = 1 - j \neq 1$.

In (3.18), the additional flux terms, compared to the classical isentropic Euler model, $\varepsilon\,\partial_x(-2uj + j^2/n)$, express the lost momentum due to the electron emission, like the recoil of a shotgun when a bullet is fired.

If $j \neq 0$, system (3.17), (3.18) is not unconditionally hyperbolic. When $\gamma_i = \gamma_e = \gamma$, this system is strictly hyperbolic if and only if the plasma density n, satisfies the condition $n > n_H(j)$ where

$$n_H(j) = \left(\frac{\varepsilon j^2}{(c_i + c_e)\gamma(1+\varepsilon)}\right)^{1/(\gamma+1)}\,. \tag{3.19}$$

In the hyperbolicity domain, $n \in [n_H(j), \infty)$, the characteristic velocities are given by

$$\mu_\pm = u - \frac{\varepsilon\, j}{(1+\varepsilon)\, n} \pm \left(\frac{\gamma\,(c_i + c_e)\, n^{\gamma-1}}{1+\varepsilon} - \frac{\varepsilon\, j^2}{(1+\varepsilon)^2\, n^2} \right)^{1/2} .$$

Finally, note that the plasma region is characterized by the presence of ions, thus, the plasma-beam interface $X(t)$, moves with the ion velocity u.

It remains to connect the models and specify the current at the interface since it is unknown both in the plasma and beam regions. First, let us look at how many boundary conditions we have to impose on the quasi-neutral model (3.17), (3.18) at $x = X(t)$. In a frame moving with the plasma-beam interface, the boundary becomes fixed and the hyperbolic problem has eigenvalues $\mu_- - u$ and $\mu_+ - u$. We shall be considering cases where $j < 0$. Indeed, electron emission at the plasma-beam interface requires that electrons are accelerated to velocities larger than the ion ones, thereby leading to a negative current. Then, obviously, $\mu_+ + u > 0$ and the corresponding characteristic field is outgoing relative to the domain $[0, X(t)]$. Now, an easy computation shows that $\mu_- - u > 0$ if and only if $n < n_P(j)$ where

$$n_P(j) = \left(\frac{\varepsilon j^2}{(c_i + c_e)\gamma} \right)^{1/(\gamma+1)} > n_H(j)\,. \tag{3.20}$$

Therefore, if $n > n_P(j)$, we must impose one additional boundary condition at the interface, whereas if $n_H(j) < n < n_P(j)$, no additional boundary condition is necessary.

To summarize, it remains to determine the current in both regions and give boundary conditions at the interface for the plasma model if the density is larger than $n_P(j)$. We do it analyzing a transmission problem. We go back to the two-fluid Euler-Poisson model (3.9)-(3.11) which is the only model valid on both sides of the interface. We change the position variable into the stretched variable $\xi = (x - X(t))/\eta^{1/2}$. This yields a traveling-wave problem and we look for solutions which reconnect to the solutions of the quasi-neutral model on the left-hand side, i.e. for $\xi \to -\infty$, and the solutions of the Child-Langmuir problem on the right-hand side, i.e. for $\xi \to \infty$. Additionally, since the interface is located at $\xi = 0$, we let $n_i = 0$ for $\xi > 0$. Furthermore, we demand that n_i be continuous at $\xi = 0$. Indeed, the ion fluid in the two-fluids Euler-Poisson model is an ordinary fluid. For an ordinary fluid, we know that no shock can border the vacuum [51], otherwise the Rankine-Hugoniot condition for the momentum equation can not be satisfied across the interface. We prove the following result

Proposition 3.4 *If $\gamma \geq 2$, there exists a (smooth or unsmooth) solution to the traveling-wave problem connecting the plasma to the beam and such that n_e is bounded, $n_i = 0$ for $\xi \geq 0$, and n_i is continuous across $\xi = 0$, if and only if the following relations hold:*

$$j = -j_e\,, \quad u_- = \frac{dX}{dt}\,, \quad n_- \in [n_H(j), n_P(j)]\,, \tag{3.21}$$

where $u_- = \lim_{x \to X(t)^-} u(x,t)$, $n_- = \lim_{x \to X(t)^-} n(x,t)$, u and n being respectively the ion velocity and quasi-neutral density in the plasma. Furthermore, $n_H(j)$ and $n_P(j)$ are given by (3.19) and (3.20).

The condition $\gamma \geq 2$ is a technical one. It can probably be removed at the expense of more analytical work.

Eqs. (3.21) provide some of the closure relations which connect the plasma and the beam models, but not all of them. First, they confirm that the interface dynamics is governed by ions. Then, they give the current continuity since they express that the plasma current of the quasi-neutral model must be equal to the electron flux in the beam region (up to a sign, due to the definitions of these quantities). However, it does not provide the exact value of this current. From the Child-Langmuir problem (see proposition 3.1), we know that $0 \leq j_e \leq j_{CL}$.

The last relation (3.21) gives an inequality constraint for the boundary condition at $x = X(t)$ of the quasi-neutral model. In view of the previous discussion, if $n_- \leq n_P(j)$, no additional condition at $X(t)$ is necessary since then, the fluid is supersonic. It is remarkable that the critical values n_H and n_P, previously defined, appear naturally in the transmission problem. This confirms their dominant role in the interface zone. Therefore, condition (3.21) expresses that the plasma must be supersonic at the interface. This condition is nothing but the Bohm sheath criterion when the beam region is viewed as a sheath (see [7], [24], [40], [46], [47], [49], [2] and [25]). It gives a boundary condition for the quasi-neutral model. Indeed, if the density at the interface in the plasma is such that a boundary condition is necessary, we impose the largest value such that the supersonic regime is reached, i.e. $n_P(j)$.

To close the model, we have to assign a value to $j_e = -j \in [0, j_{CL}]$, since this value can not be found from the formal asymptotic analysis. Based on our numerical experiments, we shall assume a maximal current regime and $j_e = -j = j_{CL} = (\varepsilon\eta)^{-1/2}\bar{j}_{CL}$ where $\bar{j}_{CL}$ is given by (3.14).

We performe numerical simulations with the values of the parameters previously used, i.e. $\eta = 10^{-4}$, $\lambda = 10^{-3}$, $\varepsilon = 0.5$, $C_i = C_e = 1$, $\gamma_i = \gamma_e = 2$. I recall that these parameters give a rescaled Debye length and plasma period respectively given by $\sqrt{\lambda\,\eta} \approx 3.2 \times 10^{-4}$ and $\sqrt{\varepsilon\,\lambda\,\eta} \approx 2.2 \times 10^{-4}$. We compare the two-fluid Euler-Poisson model (3.9)-(3.11) valid in all the domain, to the asymptotic model constituted of the quasi-neutral model with a non zero current (3.17), (3.18) for the plasma zone and of the Child-Langmuir model for the beam region, connected by the previous relations. We use a finite volume discretization with a HLLE solver (see [51]) or a degree 2 polynomial solver (see [17]) which are order 1 Roe type solvers. The mesh is uniform (Δx =constant) except at the interface where it matches the interface position. For the two-fluid model, we use a space step $\Delta x \leq 2.10^{-4}$ and for the asymptotic model the space step is given by $\Delta x = 10^{-3}$. Figure 3.3 shows the ion density and velocity in the plasma region $[0, X(t)]$ at different times. We can see that the quasi-neutral model with a non zero current leads to the right interface velocity and the right density and velocity profiles.

Figure 3.4 on the left-hand side, shows the electric potential given by the two-fluid model and the Child-Langmuir law. We can see again that the beam part is well described by the Child-Langmuir model.

Finally, on the right picture of Figure 3.4 we compare the current computed from the two-fluid model to the Child-Langmuir current computed with the asymptotic model. We can see that the Child-Langmuir current gives a very good approximation

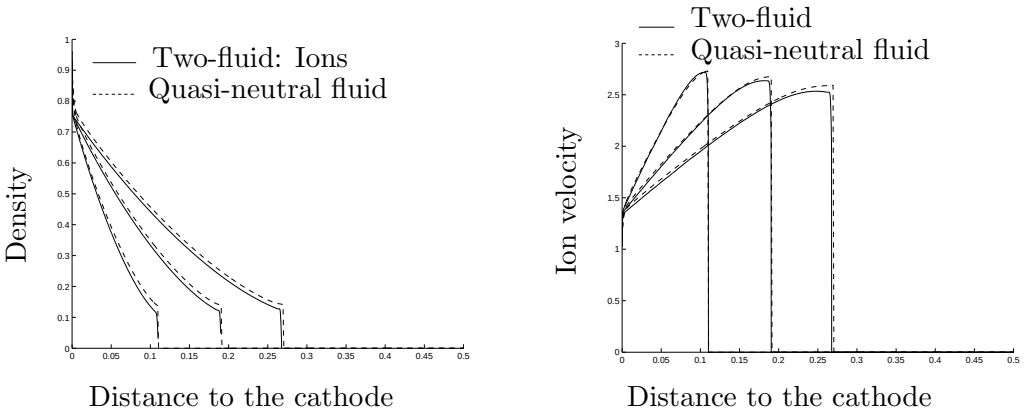

Figure 3.3: Ion density and velocity given by the two-fluid Euler-Poisson model (solid line) and the quasi-neutral model with a non zero current (dotted line). The values are observed between the cathode $x = 0$ and the plasma-beam interface $x = X(t)$ at the rescaled times $t = 0.04$, $t = 0.07$ and $t = 0.1$.

of the two-fluid current. The two-fluid model exhibits a current peak close to the interface. The existence of this peak can be explained thanks to the solution of the transmission problem. Indeed, the solution of the transmission problem satisfies $n_e(u_e - \sigma) = j_e$, $n_i(u_i - \sigma) = 0$, where j_e and $\sigma = dX/dt$ are constant by respect to x. Thus $j = n_i u_i - n_e u_e = -j_e + (n_i - n_e)\sigma$. Therefore, j is, up to constant, proportional to $n_i - n_e$. An analysis of the monotony of $n_i - n_e$ as a function of x easily shows that it has the same behavior as the one exhibited by the curves shown on Figure 3.4 (right).

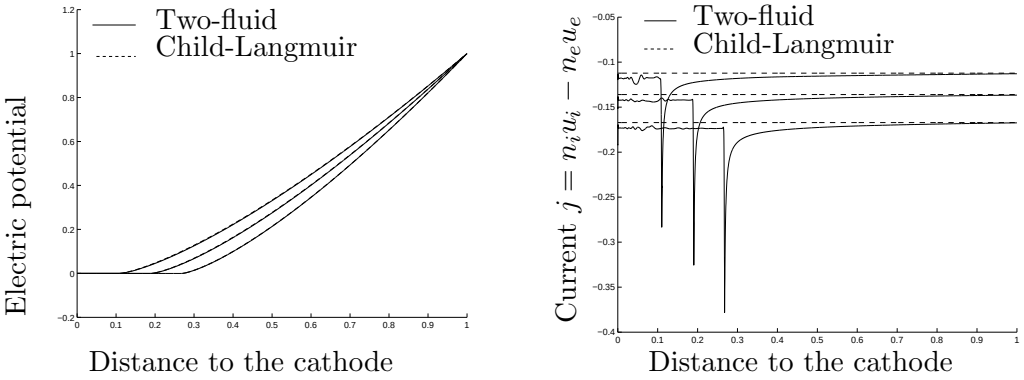

Figure 3.4: Electric potential (left-hand side) and current (right-hand side) given by the two-fluid Euler-Poisson model (solid line) and the Child-Langmuir model (dotted line). The values are observed at the rescaled times $t = 0.04$, $t = 0.07$ and $t = 0.1$.

Then, the asymptotic model gives a good approximation of the original two-fluid model with a lower numerical cost. However, our numerical method breaks down outside the hyperbolicity domain of the system (3.17)-(3.18) i.e. when the density becomes smaller than n_H defined by (3.19). And, this value is numerically reached at the rescaled time $t = 0.116$. In the last cell before the interface, at the plasma front, the hyperbolicity condition is not satisfied by the quasi-neutral model and the

numerical program stops. This problem does not depend on the mesh size and on the stability condition.

To find an answer to this problem, we introduce in [**N4**] and [**A2**] different formulations of the quasi-neutral model with a non vanishing current. I describe this work in the following section.

3.4 Different formulations of the quasi-neutral model with a non zero current

Here, I describe the results published in [**N4**] and [**A2**] in which we study different formulations of the quasi-neutral model with a non zero current. We hope that it can help us to overcome the loss of hyperbolicity in the numerical simulations presented in the previous section.

We start from the two-fluid Euler-Poisson model (3.9)-(3.11). First, remark that rescaling the potential, i.e. by switching ϕ by $\eta\phi$, yields the Debye length, and so the quasi-neutral limit, explicitly written in the system. Indeed, we obtain

$$\partial_t n_i + \nabla.(n_i u_i) = 0, \qquad \partial_t(n_i u_i) + \nabla.(n_i u_i \otimes u_i) + \nabla p_i(n_i) = -n_i \nabla\phi, \tag{3.22}$$

$$\partial_t n_e + \nabla.(n_e u_e) = 0, \qquad \partial_t(n_e u_e) + \nabla.(n_e u_e \otimes u_e) + \nabla p_e(n_e)/\varepsilon = n_e \nabla\phi/\varepsilon, \tag{3.23}$$

$$\lambda\eta\Delta\phi = n_i - n_e, \tag{3.24}$$

where $p_{i,e}(n) = C_{i,e}\, n^{\gamma_{i,e}}$. We recall that $\lambda_D^2/L^2 = \lambda\eta$ where λ_D is the Debye length given by (3.6) and L is the macroscopic length scale.

We write the system in general dimension, because we want to study if the different formulations are well-posed in dimensions larger than 1. The formal quasi-neutral limit $\lambda\eta \to 0$ of this system gives equations (3.22)-(3.23) and the quasi-neutrality constraint $n_i = n_e$. From this system, we deduce three formulations of the quasi-neutral model with a non zero current.

The first formulation, called the constrained two-fluid formulation, is obtained by noting that the quasi-neutrality constraint $n_i = n_e$ is equivalent (if the quasi-neutrality constraint is initially satisfied) to the divergence free current constraint. Thus, this formulation is given by (3.22), (3.23) and

$$\nabla.(n_i u_i - n_e u_e) = 0. \tag{3.25}$$

Equation (3.25) is an equation characterizing the potential ϕ. We will see in Chapter 4 that we can establish an elliptic equation for the potential.

The second formulation, called the 1.5-fluid formulation, is obtained from the constrained two-fluid formulation. It consists in taking into account the quasi-neutrality by keeping only one equation for the plasma density, denoted by $n = n_i = n_e$. Then, we write the conservation of the total momentum. The unknowns of this equation are the ion velocity and the current j given by $j = n_i u_i - n_e u_e$. An equation for the current is obtained by taking the difference between the momentum conservation laws. The non classical flux terms (as compared to the classical insentropic Euler system)

are moved to the right-hand side of the system and written as a potential force. The non physical potential ψ is defined by $\psi = -\left(p_i'(n)/(\gamma_i - 1) - p_e'(n)/(\varepsilon(\gamma_e - 1))\right) - (1 + 1/\varepsilon)\,\phi$. The 1.5-fluid formulation is given by

$$\partial_t n + \nabla.(nu_i) = 0, \tag{3.26}$$

$$(1+\varepsilon)\left[\partial_t(nu_i) + \nabla.(nu_i \otimes u_i)\right] + \nabla(p_i + p_e) = \varepsilon n \nabla\psi, \tag{3.27}$$

$$\partial_t j + \nabla.\left(u_i \otimes j + j \otimes u_i - j \otimes j/n\right) = n\nabla\psi, \tag{3.28}$$

$$\nabla.j = 0. \tag{3.29}$$

The "potential" ψ is a scalar quantity and is determined by the divergence free current constraint (3.29). As previously, an elliptic equation can be derived determining ψ. Note that the left-hand side operator of system (3.26)-(3.28) is hyperbolic but not strictly hyperbolic. If the space dimension $d = 1$, we easily show that two eigenvalues can be identical. Finally, remark that equation (3.28) on j does not express a physical conservation. When shocks occur, the Rankine-Hugoniot relation for this equation is not necessarily physically true. This contrasts with the constrained two-fluid formulation where the ion and electron momentum conservation equations express physical conservations.

The 1-fluid formulation, used in the previous section with $d = 1$ where d is the space variable, is obtained from the 1.5-fluid formulation eliminating the potential ψ. We obtain

$$\partial_t n + \nabla.(nu_i) = 0, \tag{3.30}$$

$$(1+\varepsilon)\left[\partial_t(nu_i) + \nabla.(nu_i \otimes u_i)\right] + \nabla(p_i + p_e) - \varepsilon\nabla.\left(u_i \otimes j + j \otimes u_i - j \otimes j/n\right) = \varepsilon\partial_t j, \tag{3.31}$$

$$\nabla.j = 0. \tag{3.32}$$

Remark that the 1-fluid formulation is ill-posed if the dimension d is larger than 1. Indeed, there are $2 + d$ equations for $1 + 2d$ unknowns. Furthermore, I recall that it is only conditionally hyperbolic. The hyperbolicity domain is characterized by $n > n_H(j)$ where n_H is defined by (3.19).

The aim of this study is to compare these different formulations to find the better one for our problem. We recall that the plasma expansion test case needs the coupling with a non quasi-neutral model modeling the beam region. To eliminate the problems coming from coupling, we introduce a new test case. It consists in a small periodic perturbation of a constant quasi-neutral plasma carrying a non zero current. This situation is described in [7] as a configuration generating an instability in high current plasmas, called two-stream instability. This instability is due to the electron drift velocity compared to ion velocity. For this test case, we can compute the exact solution of the linearized problem about the steady state. For small perturbations, the solution of the non-linear problem is believed to be close to the solution of the linearized problem. This gives two possible studies. The first one consists in calculating the stability conditions of the different linearized models using a modal analysis. The second one is the numerical comparison of the different non linear formulations to the corresponding analytical solution of the linearized problem.

Then, we linearize the two-fluid Euler Poisson model and the quasi-neutral model around the constant state $U^0 = (n_i^0 = 1, n_e^0 = 1, u_i^0 = 0, u_e^0 = u_D, E^0 = (-\partial_x \phi)^0 = 0)$. Note that the different formulations of the quasi-neutral model yield the same results. I briefly recall the principle of the modal analysis. The initial perturbation is periodic and we suppose that it can be expanded in Fourier series. Thus, we look for solutions written as $U = \overline{U}(t)\, e^{ik\,x}$ where $k \in \mathbb{R}$ is determined by the initial condition and where we denote $\overline{U} = (\overline{n}_i, \overline{n}_e, \overline{u}_i, \overline{u}_e, \overline{E})$. We obtain a differential system with constant coefficients and a matrix depending on k. The solutions are given by $U(x,t) = \overline{U}(0)\, e^{A\,t}\, e^{ik\,x}$. The system is unstable if the norm of the solution exponentially increases with the time, i.e. when an eigenvalue of $A(k)$ has a positive real part. Classically, in order that stable modes correspond to real quantities, instead of working with the eigenvalue μ, we work with the pulsation $\omega = i\mu$, for which the unstable modes correspond to negative imaginary parts.

We prove the following results

Proposition 3.5 *The dispersion relation (i.e. the characteristic polynomial function of the matrix A) of the two-fluid Euler-Poisson system linearized around U^0, is given by*

$$\lambda\eta = \frac{1}{\omega^2 - \gamma_i T_i^0\, k^2} + \frac{1}{\varepsilon\,(\omega - k u_D)^2 - \gamma_e T_e^0\, k^2}, \tag{3.33}$$

where $T_{i,e}^0 = p_{i,e}(n_{i,e}^0)/n_{i,e}^0$. Furthermore, if $T_i^0 = 0$, we have

- If $u_D^2 > (1+\varepsilon^{-1})\gamma_e T_e^0$, then, $\exists k^*$ such that the solution is unstable for $k < k^*$ and stable for $k \geq k^*$.

- If $\varepsilon^{-1}\gamma_e T_e^0 < u_D^2 < (1+\varepsilon^{-1})\gamma_e T_e^0$, then, $\exists k_1,\ k_2$ such that the solution is unstable for $k \in]k_1,\, k_2[$ and stable otherwise.

- If $u_D^2 < \varepsilon^{-1}\gamma_e T_e^0$ then the solution is unconditionally stable.

Proposition 3.6 *The dispersion relation of the quasi-neutral model linearized around U^0, is given by*

$$0 = \frac{1}{\omega^2 - \gamma_i T_i^0\, k^2} + \frac{1}{\varepsilon\,(\omega - k u_D)^2 - \gamma_e T_e^0\, k^2}. \tag{3.34}$$

Furthermore, we have

- If $u_D^2 > (1+\varepsilon^{-1})(\gamma_i T_i^0 + \gamma_e T_e^0)$, the solution is unstable for all k.

- If $u_D^2 \leq (1+\varepsilon^{-1})(\gamma_i T_i^0 + \gamma_e T_e^0)$, the solution is unconditionally stable.

First, let us remark that the formal limit $\lambda\eta \to 0$ of the two-fluid model dispersion relation gives the quasi-neutral dispersion relation. Furthermore, the resolution of (3.33) (in term of ω) reduces to the computation of roots of a 4-degree polynomial function, whereas the polynomial function of the quasi-neutral dispersion relation (3.34) is of degree 2. Then, the quasi-neutral model filters two non quasi-neutral modes and keeps only two quasi-neutral modes. Furthermore, if $\gamma_i = \gamma_e = \gamma$, the condition $u_D^2 \leq (1+\varepsilon^{-1})(\gamma_i T_i^0 + \gamma_e T_e^0)$ can be rewritten

$$n_{i0} = n_{e0} = n_0 \geq \left(\frac{\varepsilon\,(n_0\, u_D)^2}{(1+\varepsilon)\,(C_i + C_e)\,\gamma} \right)^{1/(\gamma+1)}.$$

We find again the hyperbolicity condition of the 1-fluid formulation (see (3.19)). This analysis being valid for all formulations, we already see that it will be not possible to solve the loss of hyperbolicity using a different formulation of the quasi-neutral model. Indeed, the hyperbolicity condition of the 1-fluid formulation exactly corresponds to the linear stability condition, and so to the validity domain of the quasi-neutral model with a non vanishing current. In the plasma expansion test case, this instability occurs close to the interface when the interface is sufficiently far in the domain. Note that the closer the interface to the anode, the larger the current. Indeed, the difference of potential is almost totally applied in the gap between the interface and the anode. Thus, the smaller this distance is, the larger the electric field and the larger the electron emission and the current. In this case, the non quasi-neutral modes may be excited, that the quasi-neutral model fails to describe.

We performed numerical simulations on the linear models which confirm these results. First, in order to select the best formulation of the quasi-neutral model when it is valid, we compare them in a stable case. We select parameters issued from plasma arc physics (see [9], [37]). We set $\gamma_i = \gamma_e = 5/3$, $C_i = C_e = 1$, $\varepsilon = 10^{-4}$, $\sqrt{\lambda\eta} = 10^{-3}$ and $u_D = 1$. The initial perturbation is chosen such that $k = 2\,\pi$ and $\overline{U}(t=0) = (\overline{n}_i, \overline{n}_e, \overline{u}_i, \overline{u}_e, \overline{E})(t=0) = (0, 0, 10^{-2}, 10^{-2}, 0)$. These parameters give the following values for the rescaled plasma frequency ω_p and sound speed v_s

$$\omega_p = \frac{1}{\sqrt{\varepsilon\lambda\eta}} = 10^5, \quad v_s = \left(\frac{\gamma_i T_i^0 + \gamma_e T_e^0}{1+\varepsilon}\right)^{1/2} = 11.47.$$

The values $\pm\omega_p$ and $\pm k v_s$ correspond to the roots ω of the Euler-Poisson dispersion relation calculated by a QR method. These roots are real numbers which corresponds to a stable regime. We notice that the high frequency modes correspond to the plasma frequency and the low frequency modes to the sound waves in the plasma.

The roots of the linearized quasi-neutral system are directly obtained by solving the dispersion equation (3.34) which leads to $\omega \simeq \pm k v_s = 11.47$ and corresponds to a stable case. Furthermore, high frequency modes of the Euler-Poisson model which are associated with plasma waves, disappeared in the quasi-neutral limit while low frequency acoustic waves remained. We can see that the quasi-neutral limit leads to a drastic reduction of the stiffness of the problem.

The space discretization is made via a finite volume scheme. The constrained 2-fluid model is delicate to discretize. Indeed, the quasi-neutrality constraint is not explicitly written in the system and numerically it can not be exactly satisfied. In general it is approximately verified up to the order of the scheme. We use two different Roe type solvers: the HLLE solver (see [51]) and the degree 2 polynomial solver (see [17]). In **[A2]**, we prove that the HLLE solver guarantees the exact quasi-neutrality if it is initially imposed. This is not the case for the polynomial solver. Then, in order to enforce the numerical quasi-neutrality, we have investigated two discretizations. The first one consists in projecting the ion and electron densities on an averaged density. We call this operation the projection step. The second one consists in using the polynomial scheme with an approximate numerical quasi-neutrality. We compare the discretizations of the constrained 2-fluid model to the 2-fluid Euler-Poisson model.

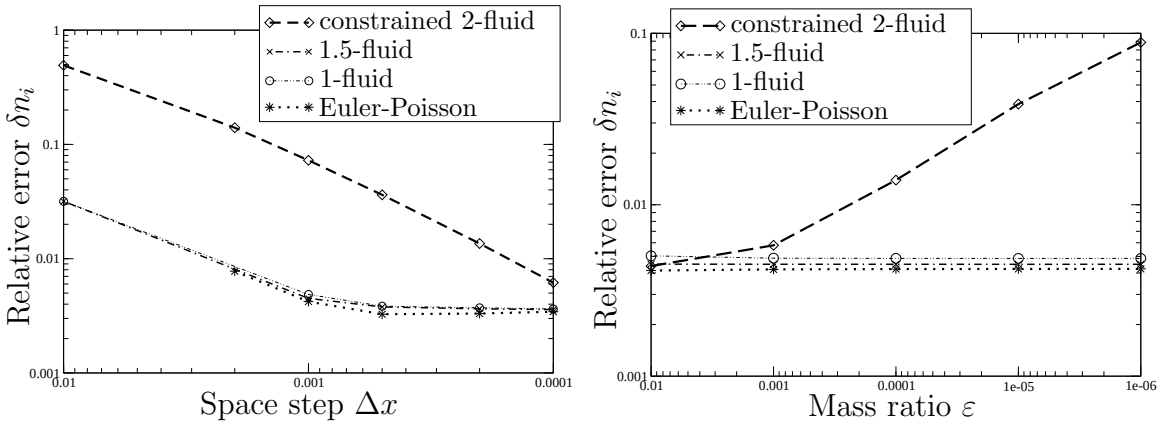

Figure 3.5: Relative error on the ion density at the rescaled time $t = 0.12$, on the left-hand side as a function of the space step Δx and on the right step as a function of the mass ratio ε for a given space step $\Delta x = 10^{-3}$.

Contrary to all expectations, the best results are obtained with the polynomial solver without the projection step, i.e. the only solver which does not ensure the exact quasi-neutrality. The results are presented in [**A2**].

Then, we use this solver to compare the different formulation of the quasi-neutral model to the two-fluid Euler-Poisson model. The results are given on Figure 3.5. We calculate the relative error between the approximate solution, of a given formulation, and the exact analytical solution of the linearized system. On Figure 3.5 on the left-hand side, we observe that the error decreases when the mesh size Δx decreases but eventually saturates to a finite value. Indeed, the error is computed by comparison with the analytical solution of the linearized model, while the schemes actually converge towards the one of the nonlinear model. This saturation reflects the difference between the solution of linearized and nonlinear models. Nonetheless, we can use these results before saturation to study the numerical efficiency of the different schemes. We observe that the order of convergence is $O(\Delta x)$ for all schemes. They are order 1 schemes.

Furthermore, we can see that the 1.5-fluid, 1-fluid and Euler-Poisson schemes are more accurate than the constrained two-fluid scheme. This loss of accuracy of the constrained two-fluid formulation appears to be related to the fact that ε multiplies the time derivative in the momentum equation, i.e. to an ill-conditioning of this equation. In the other formulations, ε never multiplies the time derivatives alone (only the factor $(1 + \varepsilon)$ does) and this conditioning problem does not occur. This conclusion is supported by the numerical determination of the orders of accuracy, see the right hand side of Figure 3.5, which is ε-dependent for the constrained 2-fluid model but ε-independent for the 1.5- and one-fluid models.

The second test case models the expansion of a plasma bubble between two electrodes. The numerical results are given in [**A2**]. They confirm the conclusion of the modal analysis: when the 1-fluid formulation loses its hyperbolicity, the constrained 2-fluid and the 1.5-fluid models develop numerical instabilities. Moreover,

these results also confirm that the 1.5-fluid formulation gives the best results.

After this study, it appears necessary to develop a model allowing the description of non quasi-neutral modes in situations such that they can not be eliminated every where (sheaths near the boundary or the interface). To do this, we began to derive a fictitious mixture model. These models are used in fluid mechanics (see [1, 43, 42], [45]). Doing this, we have found an other possible answer. It consists in a scheme preserving the quasi-neutral asymptotic and asymptotically stable for the two-fluid Euler-Poisson model. The study of this scheme is described in Chapter 4.

But before this, I finish this chapter presenting extensions of this work to the full Euler system and the two-dimensional case.

3.5 Extension to the full Euler system

We realized two extensions to the full Euler system. The first extension deals with the quasi-neutral model with a zero current (3.16) presented in section 3.3.2. This extension is done without additional difficulties compared to the isentropic case. This work is published in the proceeding **[CR2]**.

The second extension deals with the quasi-neutral model with a non vanishing current. This case needs more work. Here, I detail this study which is published in **[A5]**.

In the works detailed in the previous sections, we have considered a plasma injected from the cathode and, the emission occurring from the interface towards the anode, generating an electron beam. Here, we also consider the case of a plasma injected from the anode leading to an ion beam. We analyse the case of an ion beam and perform numerical simulations in both cases (electron and ion beams)

We start from the two-fluid full Euler-Poisson. I only consider the rescaled variables, the reader can refer to **[A5]** for the rescaling step. Furthermore, we rescale the potential as done in the previous section. In this way, the Debye length is explicitly written in the rescaled model. Here, we denote the Debye length by λ which was not the case in the previous section where it was given by $\sqrt{\lambda\,\eta}$. This is also the notation used in the following chapter. Thus, here we have

$$\lambda = \frac{\lambda_D}{L}, \tag{3.35}$$

where λ_D is the Debye length given by (3.6) and L is the macroscopic length scale. The quantities for ions are indexed by i and those for electrons by e. The densities, velocities, pressures and total energies for ions and electrons are respectively denoted by $n_{i,e}$, $u_{i,e}$, $p_{i,e}$ and $w_{i,e}$. The rescaled state laws are given by

$$w_i = \frac{p_i}{\gamma_i - 1} + \frac{n_i\,|u_i|^2}{2}, \quad w_e = \frac{p_e}{\gamma_e - 1} + \frac{\varepsilon\, n_e\,|u_e|^2}{2}\,.$$

The rescaled two-fluid full Euler-Poisson system writes

$$\partial_t n_i + \nabla \cdot (n_i\, n_i) = 0, \qquad \partial_t (n_i\, u_i) + \nabla (n_i\, u_i \otimes u_i) + \nabla p_i = -n_i\, \nabla \phi, \tag{3.36}$$

$$\partial_t w_i + \nabla \cdot ((w_i + p_i)\, u_i) = -n_i\, u_i \cdot \nabla \phi, \tag{3.37}$$

$$\partial_t n_e + \nabla \cdot (n_e\, n_e) = 0, \qquad \varepsilon \Big(\partial_t (n_e\, u_e) + \nabla n_e\, u_e \otimes u_e \Big) + \nabla p_e = n_e\, \nabla \phi, \tag{3.38}$$

$$\partial_t w_e + \nabla \cdot ((w_e + p_e)\, u_e) = n_e\, u_e \cdot \nabla \phi, \tag{3.39}$$

$$-\lambda^2\, \Delta \phi = n_i - n_e. \tag{3.40}$$

The parameter λ is the rescaled Debye length given by (3.35) and as previously, ε is the mass ratio given by $\varepsilon = m_e/m_i$, where m_i and m_e are the ion and electron masses. Like in the isentropic case the formal quasi-neutral limit, $\lambda \to 0$, leads to three formulations. The constrained 2-fluid formulation which is strictly hyperbolic, the 1.5-fluid formulation which is only hyperbolic and the 1-fluid formulation which is conditionally hyperbolic. This last formulation contains all the information of the quasi-neutral model in its hyperbolic operator. Indeed, in the isentropic case we have seen that the hyperbolicity domain exactly coincides with the validity domain of the quasi-neutral model. Thus, in **[A5]**, we study this formulation. The first essential difference with the isentropic case is that the 1-fluid formulation is not conservative (this is also the case for the 1.5-fluid formulation). The non conservative terms are present in the energy equations. They are related to the energy fluxes due to the particle emission in the beam. Recall that we consider an ion emission but the results are identical in the case of an electron emission. Thus, the model can not be used for non continuous solutions. But, in our plasma expansion test case the densities are smooth in the plasma bubble.

Like in the isentropic case, this formulation is conditionally hyperbolic. The hyperbolic zone is characterized by

$$\gamma_e p_e + \gamma_i p_i \geq \frac{\varepsilon j^2}{(1+\varepsilon)\, n}. \tag{3.41}$$

In this region, there are four eigenvalues u_e, $u_i = u_e + j/n$ and $u_\pm = u_p \pm c$. The velocity u_p is the averaged velocity in the plasma given by $u_p = (\varepsilon\, u_e + u_i)/(1+\varepsilon)$ and c is the sound speed in the plasma taking into account the pressure terms due to the ion emission in the beam

$$c = \left(\frac{1}{(1+\varepsilon) n} \left(\gamma_e p_e + \gamma_i p_i - \frac{\varepsilon j^2}{(1+\varepsilon) n} \right) \right)^{1/2}.$$

The plasma is now characterized by the presence of electrons. Then, the bubble moves with the electron velocity. Since, some ions are emitted from the interface towards the cathode, the current at the plasma-beam interface, $j = n_i\, u_i - n_e\, u_e$, is positive. And, the eigenvalues u_i and u_+ are both larger than the interface velocity u_e. Furthermore, we show that if $\gamma_e p_e + \gamma_i p_i \in [\varepsilon j^2/((1+\varepsilon) n), j^2/n]$ we have $u_- \geq u_e$. In this case, the interface is supersonic and no boundary condition is necessary for the quasi-neutral model at the plasma-beam interface. But, if $\gamma_e p_e + \gamma_i p_i > j^2/n$,

we have $u_- < u_e$ and one boundary condition have to be imposed. This boundary condition will be precised with the connexion to the beam model.

To describe the beam, we proceed like in the isentropic case. In this region there are only ions. And, we consider the one-fluid Euler-Poisson model constituted of the ion equations of (3.36)-(3.40) with $n_e = 0$ in the Poisson equation. We rescale the ion velocity, and we pass to the limit $\lambda \to 0$. We obtain the Child-Langmuir model with an energy equation. In one space dimension, this model has an analytical solution. The resolution of the energy equation shows that the ion pressure law is isentropic in the beam region, $p_i(n) = C_i\, n^{\gamma_i}$. The constant C_i will be determined with the connection to the plasma model, we have $C_i = p_i(X(t),t)/n_i^{\gamma_i}(X(t),t)$. We obtain the same problem as in the isentropic case and the solution is given by Proposition 3.1 in the one-dimensional case.

The connection of the models is done introducing a transmission problem. It is obtained from the Euler-Poisson model (3.36)-(3.40), zooming on the plasma-beam interface in the normal direction. The limit $\lambda \to 0$ gives the connection problem. It can be expressed in terms of the variable normal to the interface. And, the multi-dimensional case consists of one-dimensional problems in the normal direction on each point of the plasma-beam interface. Consequently, we only describe the one-dimensional analysis. The resulting transmission problem differs from the one studied in the isentropic case, in the presence of energy equations. These equations show that the pressure laws are isentropic in the boundary layer near the interface. Then, the transmission problem is formally equivalent to the isentropic transmission problem. We denote by j, n_-, u_{e-}, p_{i-}, p_{e-} the solution of the quasi-neutral model at $x = X(t)$ for $t > 0$ and by j_i and C_i the current and the pressure constant in the beam at $X(t)$. Using the analysis described in [**A1**], we have the following connection relations:

$$dX/dt = u_e(X(t),t), \qquad j(t) = j_i(t), \qquad C_i = \frac{p_{i-}}{n_-^{\gamma_i}}, \qquad \frac{j^2}{n_-} \geq \gamma_e p_{e-} + \gamma_i p_{i-}.$$

The last relation is the Bohm sheath criterion which imposes that the plasma must be supersonic at the plasma-beam interface. I recall that we use this criterion to determine a boundary condition when the interface leaves the supersonic regime. In this case, we impose $j(t)^2/n(X(t),t) = \gamma_e\, p_e(X(t),t) + \gamma_i\, p_i(X(t),t)$.

The transmission problem does not give the current (like in the isentropic case). We assume a maximal current regime for the Child-Langmuir model corresponding to a vanishing electric field at the interface.

We present numerical results in one dimension. The space discretization is uniform (Δx =constant) except in the neighborhood of the interface where the mesh matches the interface position. In one space dimension the Child-Langmuir model has an analytical solution and the current is known in all the domain. The non conservative 1-fluid formulation of the quasi-neutral model is discretized with an upwind scheme splitting the Jacobian matrix in its positive and negative parts. We solve an exact fluid-vacuum Riemann problem at the interface for the quasi-neutral model. This gives an accurate approximation of the plasma-beam interface position. The analysis of this Riemann problem is not classical since there are additional pressure terms due to the ion emission in the beam. the reader can refer to [**A5**] for the details.

We perform two test cases, one for the ion beam and one for the electron beam. Here, I only show the results for the first test case. The values of the rescaled parameters are given by $\varepsilon = 2.7 \times 10^{-4}$ and $\lambda = 4.2 \times 10^{-4}$. The mesh used for the two-fluid Euler-Poisson model has 7000 cells while the one used for the quasi-neutral model has only 2000 cells. It is important to note that it is not possible to use a coarser mesh for the two-fluid model because numerical instabilities occur at the plasma-beam interface. Furthermore, the computational time for the asymptotic model is 70 seconds while the one of the Euler-Poisson model is more than 12 hours. Therefore, there is a very important time saving using the asymptotic model.

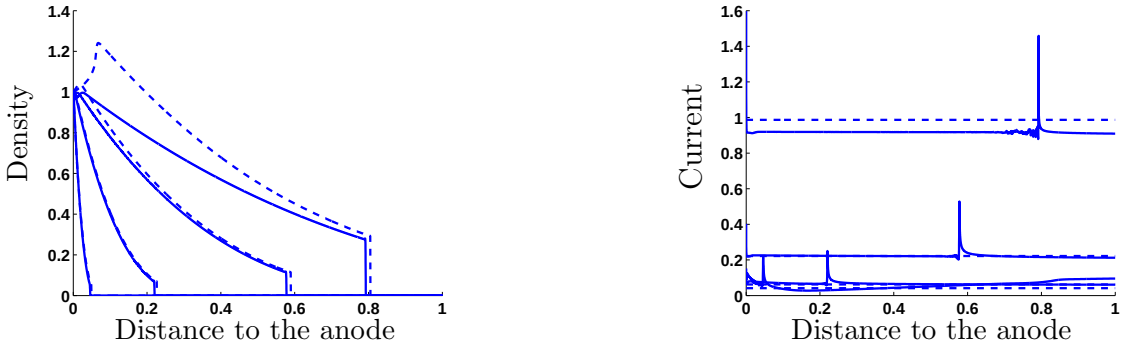

Figure 3.6: The results are given at the rescaled times 0.01, 0.05, 0.15 and 0.3. On the left-hand side: quasi-neutral density in the plasma region given by the Euler-Poisson model (solid line) and the quasi-neutral model (dotted line). On the right-hand side: current in the domain given by Euler-Poisson model (solid line) and the Child-Langmuir model (dotted line).

Figure 3.6 gives on the left-hand side the plasma density and on the right-hand side the current. The results are given by the two-fluid Euler-Poisson model and the asymptotic model. We note a very good agreement of the curves at the beginning of the plasma expansion, but a discrepancy between the results at the end of the simulation. This discrepancy manifests itself on the plasma-beam interface position, computed by the quasi-neutral model, a little bit ahead of the one of the Euler-Poisson model and on the particle density being too large around the anode for the quasi-neutral model. These problems certainly result from the presence of a boundary layer at the injection point. They were already observed in the isentropic case but it seems that they are magnified when the energy conservation laws are considered. The study of this boundary layer is detailed in the following chapter.

In the second test case, the results have overall an identical behavior compared to the results of the previous test case. But, the comparison of the results stops earlier in the expansion process. This is due to the fact that we can not give results at larger times for the asymptotic model. Just after the rescaled time $t = 0.6$, the hyperbolicity of the quasi-neutral model is lost and the simulation of the asymptotic model stops. In the case of an electron beam, the hyperbolicity region of the quasi-neutral model and the Bohm sheath criterion impose the following condition $\gamma_e p_e + \gamma_i p_i \in [\varepsilon j^2/((1+\varepsilon)\, n), \varepsilon j^2/n]$. The smallness of ε produces a very small range between the critical

values $\varepsilon j^2/((1+\varepsilon)\,n)$ and $\varepsilon j^2/n$. This yields an unstable numerical resolution of this problem and explains why, contrary to the previous test case, we quickly lose the hyperbolicity of the quasi-neutral model. In the previous section, it has been showed that this breakdown of the model can be attributed to a physical two-stream instability. This instability occurs when the plasma current reaches large values as the interface moves closer to the anode. In this case, non quasi-neutral modes are excited and the quasi-neutral model fails to describe them. For these particular situations, the problem can be cured by using the Euler-Poisson model which describes both quasi-neutral and non quasi-neutral modes but it is necessary to discretize it with an asymptotic preserving scheme in the quasi-neutral limit. Such a scheme has been developed in the isentropic case, see Chapter 4. Investigation of this scheme for the full Euler case is in progress.

3.6 Towards a two dimensional modeling

In this section, I present the results published in [**A6**]. They deals with the two dimensional extension of the quasi-neutral model with a zero current.

In two dimensions, the interface is no more a point but a curve. This leads to new difficulties in the modeling as well as in the numerical scheme. Here, we want to focus our attention on the difficulties related to the numerical simulation of the plasma-beam interface and not on the modeling intensively studied in the previous sections. The zero current model presented in section 3.3 gives a less accurate approximation of the two-fluid Euler-Poisson model compared to the quasi-neutral with a non vanishing current. But, it is simpler to discretize, essentially because it does not need to compute the current in the plasma. For this reason, we choose to extend this model.

Then, the asymptotic model is constituted of the isentropic Euler equations in the plasma bubble. They give the quasi-neutral density n and the total momentum $(m_i+m_e)u$, where m_i and m_e are the ion and electron masses. To describe the beam, we use a simplified Child-Langmuir model. It is based on the one dimensional Child-Langmuir solution and consists in assuming that any electron emitted in the beam satisfies a one dimensional Child-Langmuir law along its trajectory. We approximate these trajectories by arcs of circle. These models are connected at the plasma-beam interface by pressure forces modeling the reaction of the beam onto the plasma when electrons are emitted. Furthermore, the dynamics of the interface is given by the ion velocity u.

Then, we focus our attention on the numerical method to follow the interface. We assimilate this problem to an interface problem between two fluids: the plasma and the vacuum of plasma. We use a V.O.F. method (Volume Of Fluid). This is an Eulerian method, i.e. the mesh is given at the beginning and kept during all the simulation. The principle of the V.O.F. methods is the following, see [27], [55]. We follow the interface through the volume fraction of fluid present in each cell of the mesh. At each time step and in each cell, the unknowns are the volume fraction of plasma in the cell and the fluid quantities (here the density and the velocity) averaged on the cell.

Furthermore, we use a splitting method in the x and y directions where x is the abscissa and y is the ordinate. Thus, at each time step, the considered V.O.F. method consists in two steps alternately applied in the directions x and y. The first step is the transport of the averaged quantities using a Lagrangian scheme, i.e. following the characteristic curves of the considered system. Then, during the second step, we project the transported quantities on the Eulerian grid and we update the volume fraction on each cells. But, in mixed cells, i.e. those containing both plasma and vacuum, for this update, we have to determine the plasma flowing from a cell into its neighbors. For this, we use the S.L.I.C. algorithm (for Simple Line Interface Calculation, [35]) which defines transfer priorities for plasma between the cells.

In our problem, the major difficulty relies in taking account the reaction-pressure term at a discrete level. This is done by splitting the interface pressure force in the directions x and y. Then, we have to reconstruct the unit normal to the interface in each concerned cells. For this, we use Youngs' method, [56] which directly gives an oblique representation of the interface.

We present the results for two test cases. The first test case consists in a two dimensional fluid compression. The fluid is initially located in a ball and a uniform pressure applied on its boundary compresses it on the radius center. Since we know an analytic solution, it is given in [4] and **[A6]**, we can study the accuracy of our discretization and the treatment of the pressure terms at the interface. Figure 3.7 shows, on its left-hand side, the relative error in L^2 norm, on the density between the exact solution and the approximate solution given by the V.O.F. scheme. The numerical solution converges towards the exact solution when the mesh is refined. Figure 3.7 shows, on middle, the relative error between the exact and approximate

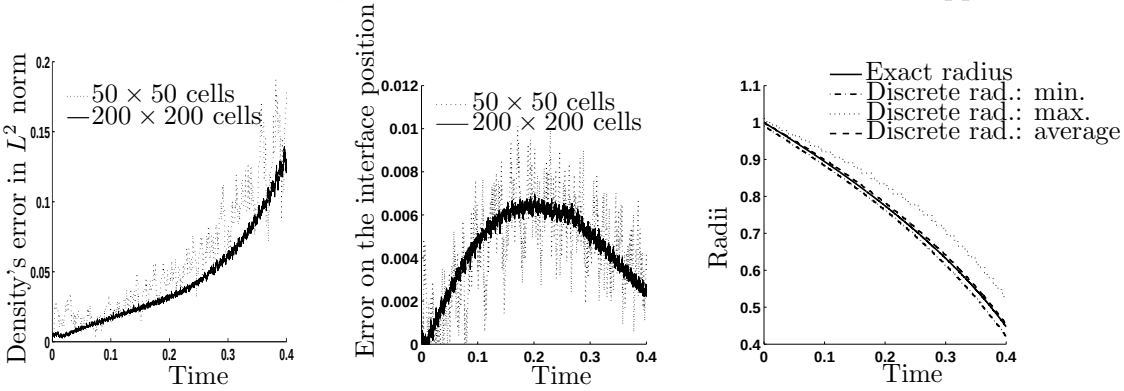

Figure 3.7: On the left-hand side and on the middle: relative errors in L^2 norm on the fluid density (left) and in absolute value on the fluid-vacuum interface position (middle) as functions of time for different meshes: in solid line for $\Delta x = \Delta y = 2/200$ and in dotted line for $\Delta x = \Delta y = 2/50$. On the right-hand side: exact and approximate radii of the fluid bubble as a function of time for $\Delta x = \Delta y = 2/100$. The approximate values are the minimum (dashed-dotted line), the maximum (dotted line) and the averaged radius (dashed line).

radii of the plasma bubble and on the right, a comparison between the exact radius and different values of the approximate radius: the minimum, the maximum and

the averaged value. We can see that even if the error between the exact radius and the averaged value is decreasing, the approximation of the radius is less and less accurate since the variance increases. But, even with a rough mesh (50×50 cells) the error on the interface position is of order 1.% and so it is very small. This is an important property for our problem. Indeed, we recall that getting precisely the interface position is a key point in the high current diodes problem because it governs the value of the current in the electron beam.

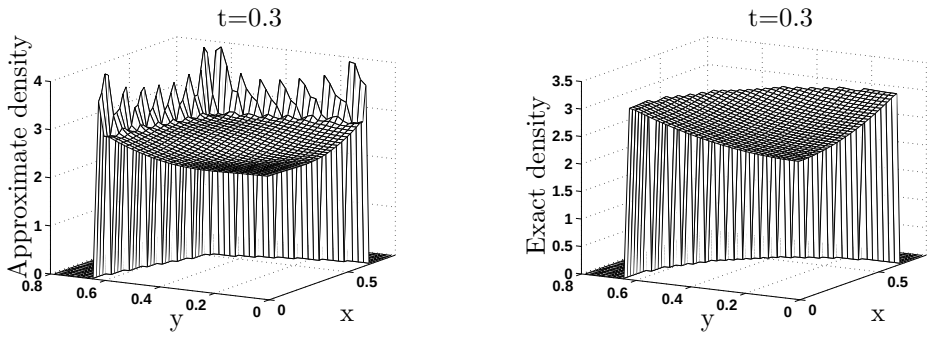

Figure 3.8: On the left-hand side: approximate density given by the V.O.F. scheme at time $t = 0.3$ for $\Delta x = \Delta y = 2/100$. On the right-hand side: exact density given by the analytical solution and projected on the mesh at time $t = 0.3$.

Figure 3.8 shows on the left-hand side, the approximate density and on the right-hand side the exact density at time $t = 0.3$. The final compression time is 0.5. Then, more than the half of the simulation is done. We can see that the error is large on the boundary cells but small on interior cells. This error increases with time but does not introduce instabilities since in the interior cells the error is small during all the simulation. Figure 3.9 presents the fluid bubble for different times on the top given by the approximate solution with the space steps $\Delta x = \Delta y = 2/50$, in the middle given by the approximate solution with the space steps $\Delta x = \Delta y = 2/200$ and on the bottom given by the exact solution projected on an intermediate mesh with steps $\Delta x = \Delta y = 2/100$. We can see that the approximate bubble becomes a square while the exact bubble remains circular. This is due to the splitting of the Euler system and to the S.L.I.C. algorithm used in the projection step. Indeed the transport in the directions x and y are uncoupled and this privileges the Cartesian deformations. Furthermore the S.L.I.C. algorithm gives a square reconstruction of the interface and increases this phenomena. Figure 3.9 shows that the convergence towards a circular bubble is very slow since multiplying the number of cells by 4×4, the difference between the results is not significant. This point will have to be improved in future work. This can be done discretizing directly the Euler system and using Youngs' method (see [56]) instead of the S.L.I.C algorithm in the projection step. This error on the location of boundary cells explains the error encountered on the density for boundary cells, see Figure 3.8 . It is important to note that in spite of the bad approximation of the density and velocity for boundary cells, we have a very good prediction of the mean interface position (see Figure 3.7 middle and right).

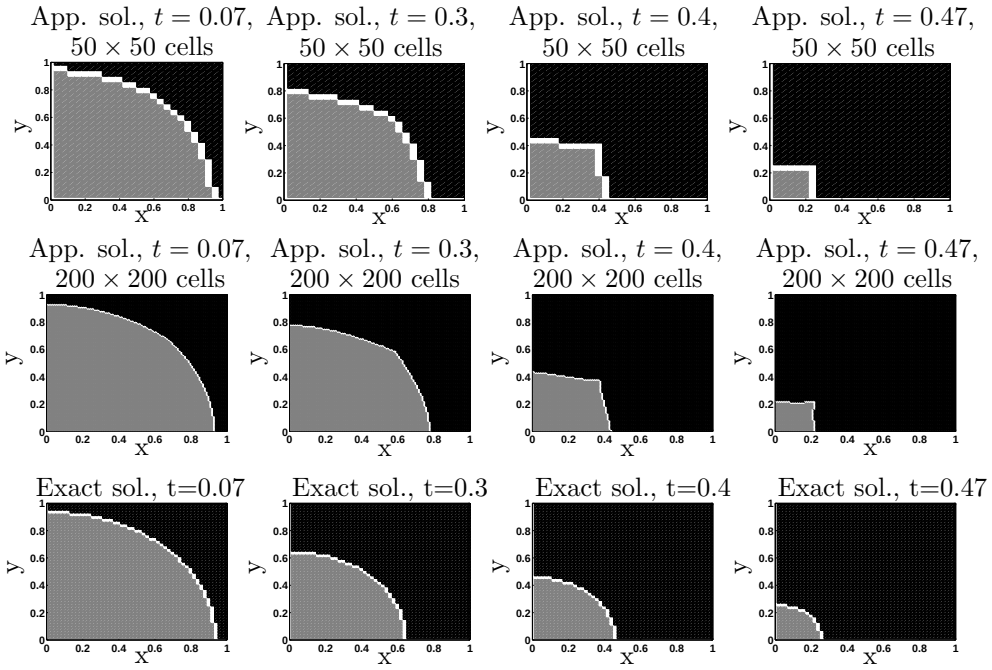

Figure 3.9: Fluid bubble for different times $t = 0.07$, $t = 0.3$, $t = 0.4$ and $t = 0.47$. We can see the different type of cells: in gray, the full cells, in white, the mixed cells and in black, the empty cells. Top and middle, the results are computed with the V.O.F. scheme with $\Delta x = \Delta y = 2/50$ (top) and $\Delta x = \Delta y = 2/200$ (middle). Bottom: the results are given by the exact solution projected on an intermediate mesh with $\Delta x = \Delta y = 2/100$.

Furthermore, we stress that Figure 3.9 proves that we have the right behavior of the bubble and the **right compression time** since at exactly $t = 0.5$ the numerical bubble has disappeared completely from the domain as does the exact bubble.

The second test case models the expansion of a plasma bubble between two electrodes. It is related to high current diodes. The domain is assumed to be a square and the plane electrodes are located at $x = 0$ and $x = 1$. The plasma is injected from a part of the cathode at $x = 0$. The domain is discretized with a uniform square mesh constituted of 100×100 cells. Figure 3.10 shows the density in the plasma region at the rescaled times $t = 0.20$ and $t = 0.40$. The plasma bubble expands between the cathode and the anode. It is slowed down by the reaction pressure force which expresses the reaction of the plasma to the emission of electrons in the beam. We can observe that due to this reaction-pressure force, the plasma region stays connected during the simulation, there is no instability at the interface. Furthermore, the front of the plasma is very stiff near the interface, and we see again the non physical peak of density before the interface as seen in the one dimensional case. We recall that this peak is due to the model itself since the reaction pressure force is concentrated at the interface instead of being applied in all the plasma. This point can be improved using the quasi-neutral model with a non vanishing current.

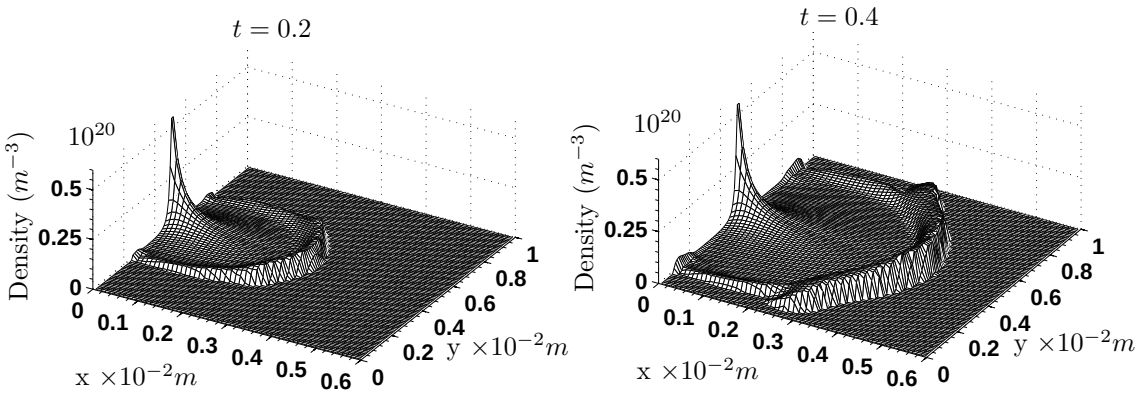

Figure 3.10: Plasma density at the rescaled times $t = 0.2$ and $t = 0.4$. The solution is calculated with the V.O.F. scheme on a uniform squared mesh containing 100×100 cells.

3.7 Conclusions and future prospects

In this chapter, I have presented the mathematical and numerical modeling of the expansion of a plasma bubble between two electrodes. This model has been studied to determine its validity domain and its possible extensions in multi-dimensional cases. Several future prospects are possible.

First, the complexity of methods used for the numerical simulations of moving interfaces in two or three dimensions as well as the necessity to relax the quasi-neutral model in a neighborhood of the interface, have convinced us to use a different method. We began to use fictitious mixture techniques (see as instance [6] or [42]). Theses techniques consist in establishing a global mixture model from the original two models each of them being valid in different zones. It is based on a smooth characteristic function α such that $\alpha = 1$ in a region and $\alpha = 0$ in the other one. Then, the interface is enlarged and corresponds to values of α in $]0, 1[$. In our case, the first region is the plasma bubble and the second region is the beam. Thus, we can split the solution of the Euler-Poisson model in a plasma component and a beam component. The quasi-neutral limit can be taken on the plasma component giving the mixture model. This method, which consists in passing to the limit in only a part of the domain, has been applied in [16] for kinetic-fluid coupling. The main difficulty is in the reconstruction of the solution in the mixture zone, i.e. the region where $\alpha \in]0, 1[$. However, let us emphasize that the asymptotic preserving scheme in the quasi-neutral limit for the Euler-Poisson system, described in the following chapter, performs the same work at a discrete level.

An other future prospect deals with the boundary conditions at the injection point. Indeed, in numerical simulations, we have observed that the boundary conditions of the two-fluid Euler-Poisson model are not well-adapted to the quasi-neutral regime. They generate a boundary layer in the asymptotic model at the injection point. This boundary layer is more penalizing when the full Euler system is considered. This

boundary layer problem is studied in the following chapter in one dimension of space. This analysis allows to determine boundary conditions well-adapted to the quasi-neutral regime. It would be interesting to use these boundary conditions for the asymptotic model presented here and extend them in multi-dimensions.

Chapter 4

An asymptotic preserving scheme and a boundary layer problem

4.1 Introduction

In this chapter, I detail the results published in [**N5**], [**A4**], [**A7**] and [**A8**]. They have been done in collaboration with Pierre Crispel, Pierre Degond, Jian-Guo Liu and Dominique Savelief. They deal with the establishment of an asymptotically consistent and stable scheme in the quasi-neutral limit for a plasma fluid model.

For the sake of simplicity, we assume that the plasma consists of electrons and one ion species but the methodology can be extended to models containing more than two species. The model consists of the isentropic Euler equations for each species coupled with the Poisson equation

The schemes, classically used to discretize this system are subject to severe numerical constraints. They are related to two physical parameters well known in plasma physics (see [7, 28]): the Debye length and the plasma period. Although these parameters have been already presented in the previous chapter, I recall their definition. The Debye length, denoted by λ_D and the plasma period, denoted by τ_p are given by

$$\lambda_D = \left(\frac{\epsilon_0 \, k_B \, T_0}{e^2 \, n_0} \right)^{1/2} \qquad \text{and} \qquad \tau_p = \left(\frac{\epsilon_0 \, m_e}{n_0 \, e^2} \right)^{1/2}, \tag{4.1}$$

where ϵ_0 is the vacuum permittivity, k_B is the Boltzmann constant, T_0 and n_0 are the characteristic temperature and density of the plasma, $e > 0$ is the elementary charge and m_e is the electron mass. The Debye length measures the scale at which electric interactions occur in the plasma. Indeed, these interactions are such that a particular charge in the plasma is screened by the other charges beyond the distance λ_D. The second parameter is a time scale. It is related to the electric unbalances in the plasma. The electric interactions between the particles imply local charge unbalances, at the scale of the Debye length. The electric forces tend to restore the particles towards their equilibrium position. The particles oscillate around this position. The electrons being smaller than ions, their oscillation period is smaller than ions' and so this period plays a more important role in plasmas. Then, this is the electron plasma period that we call plasma period.

In [23], S. Fabre shows that the classical explicit discretizations of the linearized Euler-Poisson system must resolve the scale of the plasma period. Hence, the time

step must be smaller than the plasma period otherwise a numerical instability is generated. The satisfaction of this constraint requires huge computational resources in the quasi-neutral regions where the plasma period is small. This makes the use of classical explicit methods almost impracticable for realistic applications.

They are two possible ways to overcome this limitation. The first way consists in using a quasi-neutral model in the region where the Debye length is small. This approach is particularly well adapted to problems such that all the domain is quasi-neutral. But, when there are both quasi-neutral and non quasi-neutral regions in the domain it is necessary to use a different model for the non quasi-neutral region. Then, we have to determine the interface position and reconnect the models. This method has been detailed in the previous chapter and we have seen the difficulties related to this approach.

The second way consists in finding a discretization of the Euler-Poisson system which preserves the quasi-neutral asymptotic and which does not need to resolve the small scale of the plasma period. Such a scheme has been developed in [**A4**], we call it AP scheme, for "Asymptotic Preserving". This result is presented in section 4.2.

The stability analysis of this scheme for the Euler-Poisson system linearized around a constant solution is done in [**A7**] and described in section 4.3. This analysis confirms the asymptotic stability of the AP scheme.

In [**A4**], two test cases in one dimension are presented. The first test case is a periodic perturbation of a constant quasi-neutral solution. The second test case is the expansion of a quasi-neutral plasma bubble between two electrodes presented in details in the previous chapter. The simulations are performed using the modified Lax-Friedrichs solver. This solver is well known to be very diffusive but also to be very robust. So it was well adapted to the validation step. The extension of the AP scheme to more general Roe type solvers gives identical results in the first test case. Let us note that in this test case the boundary conditions for the fluid quantities are periodic. But, in the second test case, the AP scheme as well as the classical scheme develop numerical instabilities when the space step is larger than the Debye length for general solvers. This constraint is as penalizing as the one related to the plasma period. Indeed, in quasi-neutral regions, the Debye length is very small. In section 4.4, which presents the results submitted for publication in [**A8**], I numerically show that these instabilities are related to the presence of a boundary layer at the injection point. The study of this boundary layer allows to determine boundary conditions well-adapted to the quasi-neutral regime. Then, I present numerical results which show that these boundary conditions stabilize the classical and AP schemes without resolving the Debye length.

4.2 An asymptotic consistent and stable scheme in the quasi-neutral limit for the Euler-Poisson system

In this section, I present the results published in [**N5**] and [**A4**].

4.2.1 The Euler-Poisson model and its quasi-neutral limit

We consider a plasma constituted of one ion species and of electrons. We use a fluid model, and the particles are described by their density, $n_{i,e}(x,t)$ and their momentum, $q_{e,i}(x,t)$ where $x \in \mathbb{R}^d$, $d = 1$, 2 or 3, is the space variable and $t > 0$ is the time. We consider the scaled variables, the rescaling step is detailed in **[A4]** and in the previous chapter. The rescaled Euler-Poisson model is given by

$$\partial_t n_i + \nabla.q_i = 0, \qquad \partial_t n_e + \nabla.q_e = 0, \tag{4.2}$$

$$\partial_t q_i + \nabla f_i = -n_i \nabla\phi, \qquad \partial_t q_e + \nabla f_e = n_e \nabla\phi/\varepsilon, \tag{4.3}$$

$$-\lambda^2 \Delta\phi = n_i - n_e, \tag{4.4}$$

where f_i and f_e are the rescaled momentum fluxes defined by $f_i = q_i \otimes q_i/n_i + p_i(n_i)\,\mathrm{Id}$ and $f_e = q_e \otimes q_e/n_e + \frac{1}{\varepsilon} p_e(n_e)\,\mathrm{Id}$, where $p_{e,i}(n) = C_{i,e}\, n^{\gamma_{i,e}}$, $C_{i,e} > 0$, $\gamma_{i,e} > 1$ are the pressure laws.

The parameters ε and λ are respectively the mass ratio $\varepsilon = m_e/m_i$ and the rescaled Debye length $\lambda = \lambda_D/L$ where λ_D is the Debye length given by (4.1) and L is the macroscopic length scale.

The mathematical theory of the Euler-Poisson system is studied in [11] and [39] in the isothermal case and in [32] in the isentropic case. In the previous chapter, we studied the formal quasi-neutral limit, $\lambda \to 0$, of this system considering plasmas carrying a non zero current. The rigorous quasi-neutral limit for simplified cases are studied in [10], [38], [54] and [48]. All these articles consider a vanishing current in the plasma. I briefly recall the results for the two-fluid Euler-Poisson model with a non vanishing current.

The formal limit $\lambda \to 0$ in the two-fluid Euler-Poisson system consists in replacing the Poisson equation (4.4), by the quasi-neutrality constraint $n_i = n_e$. The Poisson equation is lost, while the electrostatic potential becomes the Lagrange multiplier of this constraint. An elliptic equation can be determined for the potential. We subtract the mass equations (4.2), and using the quasi-neutrality constraint, we obtain the divergence-free constraint for the scaled electric current $j = n_i u_i - n_e u_e$. Then, we take the divergence of the difference of the momentum equations (4.3). And finally, we use the divergence-free constraint for the current, we obtain:

$$-\nabla \cdot \left(\left(n_i + \frac{n_e}{\varepsilon} \right) \nabla\phi \right) = \nabla^2 : (f_i - f_e)\,, \tag{4.5}$$

where the symbols ∇^2 and : respectively denote the tensor of second order derivatives and the contracted product of two tensors.

Then, the quasi-neutral model is formally equivalent to the system of equations (4.2), (4.3) and (4.5). It is important to note that one of the numerical singularities of the problem comes from the fact that the Poisson equation degenerates into and algebraic equation. And, we must transform the system to obtain an equation for the electric potential. Thus to build an asymptotically consistent scheme, we must capture the quasi-neutral limit without transformations. This is one of the key points of the AP scheme presented here. For this, we reformulate the Poisson equation using the same transformations as those used to obtain (4.5). We go back to the

Euler-Poisson system, and we take the divergence of the difference of the momentum equations (4.3), to obtain

$$\nabla \cdot \partial_t j + \nabla^2 : (f_i - f_e) = -\nabla \cdot \left(\left(n_i + \frac{n_e}{\varepsilon} \right) \nabla \phi \right) . \tag{4.6}$$

In order to eliminate the current in this equation, we subtract the time derivative of the difference of the mass equations (4.2). Then, we use the Poisson equation (4.4) to express the total charge $n_i - n_e$, as a function of the potential. We obtain the reformulated Poisson equation

$$\varepsilon \lambda^2 \, \partial_{tt}^2 (-\Delta \phi) - \nabla \cdot ((\varepsilon n_i + n_e) \, \nabla \phi) = \varepsilon \, \nabla^2 : (f_i - f_e) \, . \tag{4.7}$$

First, note that this equation is formally equivalent to the Poisson equation if the fluid quantities satisfy the Euler equations and if the Poisson equation and its time derivative are satisfied initially. The second important remark is that this formulation explicitly raises the time singularity of the problem: the oscillations related to the plasma period. Indeed, in rescaled variables, the plasma period is given by $\tau = \sqrt{\varepsilon} \, \lambda$, where $\tau_p = t_0 \, \tau$ with t_0 the macroscopic time scale and τ_p the plasma period. Finally, let us remark that this limit is dispersive. Indeed, considering (4.7) as an equation on the total charge $\rho = -\Delta \phi$ and linearizing this equation around a constant solution of the problem, we obtain a Klein-Gordon equation on the total charge ρ. Then, we prove that in the limit $\lambda \to 0$, there are solutions with order 1 magnitude which oscillate with a period of order $\tau = \sqrt{\varepsilon} \, \lambda$. This point is developed in section 4.3.

4.2.2 The classical and AP schemes for the Euler-Poisson model

We only investigate semi-discretizations in time of the two-fluid Euler-Poisson system. Indeed, the breakdown of the standard time-stepping strategies in the quasi-neutral regime is primarily a time stability problem. We refer to [**A4**] for the description of the space discretization using the modified Lax-Friedrichs solver and to [**A8**] for more general Roe type solvers.

We first recall the classical discretization of the Euler-Poisson system. We denote by Δt the time step and g^m an approximation of the function $x \mapsto g(x, t^m)$ where $t^m = m \Delta t$, $m \geq 0$. The classical discretization of the two-fluid Euler-Poisson system (3.22)-(3.24) is given by

$$\frac{n_{i,e}^{m+1} - n_{i,e}^m}{\Delta t} + \nabla \cdot q_{i,e}^m = 0 \quad , \qquad \frac{q_i^{m+1} - q_i^m}{\Delta t} + \nabla f_i^m = -n_i^{m+1} \nabla \phi^{m+1},$$

$$\frac{q_e^{m+1} - q_e^m}{\Delta t} + \nabla f_e^m = \frac{n_e^{m+1}}{\varepsilon} \nabla \phi^{m+1}, \qquad -\lambda^2 \Delta \phi^{m+1} = n_i^{m+1} - n_e^{m+1}.$$

The fluxes are explicitly discretized while the electric force terms are implicit. In [23], it is shown, on the linearized Euler-Poisson system, that if these force terms are explicitly discretized, the scheme is unconditionally unstable. Furthermore, as in the

continuous case, we can determine the associated discretization of the reformulated Poisson equation (4.6). It is given by

$$-\varepsilon\lambda^2\,\frac{(\Delta\phi^{m+1}-2\Delta\phi^{m}+\Delta\phi^{m-1})}{\Delta t^2}-\nabla\cdot((\varepsilon\, n_i^m+n_e^m)\nabla\phi^m)=\varepsilon\nabla^2:(f_i^{m-1}-f_e^{m-1})\,.$$

This discretization is explicit. But, the reformulated Poisson equation (4.6) is an harmonic oscillator equation on the total charge $n_i - n_e = -\Delta\phi$. And, it is well known that an explicit discretization of this equation is conditionally stable. In [23], it is proved for the linearized Euler-Poisson system, that this scheme is stable if and only if it resolves the plasma period. Then, we have to impose

$$\Delta t \leq \tau,$$

where τ is the rescaled plasma period i.e. the ratio between the plasma period τ_p, given by (4.1), and the macroscopic time scale. Finally, let us remark that the cost of the classical scheme is given by the cost of the resolution of the elliptic equation. Indeed, the resolution is uncoupled, the mass conservation equations allow the update of the densities. Then, using the discrete Poisson equation we determine the potential and we finish with the explicit resolution of the momentum equations.

Now, we describe the new approach of the AP scheme. This scheme consists in an implicit treatment of the mass fluxes, an explicit treatment of the momentum fluxes and a semi-implicit treatment of the electric force terms (explicit for the densities and implicit for the potential). We get

$$\frac{n_i^{m+1}-n_i^m}{\Delta t}+\nabla\cdot q_i^{m+1}=0,\qquad \frac{n_e^{m+1}-n_e^m}{\Delta t}+\nabla\cdot q_e^{m+1}=0, \tag{4.8}$$

$$\frac{q_i^{m+1}-q_i^m}{\Delta t}+\nabla f_i^m=-n_i^m\,\nabla\phi^{m+1},\qquad \frac{q_e^{m+1}-q_e^m}{\Delta t}+\nabla f_e^m=\frac{n_e^m}{\varepsilon}\,\nabla\phi^{m+1}, \tag{4.9}$$

$$-\lambda^2\Delta\phi^{m+1}=n_i^{m+1}-n_e^{m+1}. \tag{4.10}$$

Now, the associated discretization of the reformulated Poisson equation (4.6), is given by

$$-\varepsilon\lambda^2\,\frac{(\Delta\phi^{m+1}-2\Delta\phi^{m}+\Delta\phi^{m-1})}{\Delta t^2}-\nabla\cdot\big((\varepsilon\, n_i^m+n_e^m)\nabla\phi^{m+1}\big)=\varepsilon\nabla^2:(f_i^{m}-f_e^{m})\,. \tag{4.11}$$

We can see that now the discretization is implicit. Furthermore, using this equation, we obtain an uncoupled formulation of the AP scheme which has the same cost as the classical scheme. Indeed, using (4.11) we update the potential. The cost is given by the cost of the elliptic operator as in the classical scheme. Then, we calculate the momenta using (4.9). And, we finish with the update of the densities with (4.8). Thus, the cost is the same as the classical scheme.

4.2.3 Numerical results

I present numerical results for two test cases in one dimension of space and a two dimensional test case.

The first test case consists in a periodic perturbation of a constant quasi-neutral solution with a non vanishing current. The constant solution is given by $(n_i^0 = n_e^0 = 1, q_i^0 = 0, q_e^0 = 1, E^0 = 0)$ where $E = -\partial_x \phi$ is the electric field.

We consider the following initial perturbation

$$n_i(x,0) = n_e(x,0) = 1, \qquad q_i(x,0) = \delta \cos 2\pi x, \qquad q_e(x,0) = 1 + \delta \cos 2\pi x.$$

where $\delta = 10^{-2}$ is the magnitude of the perturbation. This test case has been studied in [**N4**] and [**A2**] where the analytical solutions of the linearized two-fluid Euler-Poisson system are given. For small perturbations, these solutions are believed to be close to the solution of the non linear system. Then, we compare the approximate solutions given by the classical and AP schemes to the analytical solution. For this test case, we use the modified Lax-Friedrichs solver.

We select parameters issued from plasma arc physics (see (see [9], [5]) such that $C_i = C_e = 1$, $\gamma_i = \gamma_e = 5/3$, $\varepsilon = 10^{-4}$, $\lambda = 10^{-4}$ which give a rescaled plasma period given by $\tau = 10^{-6}$.

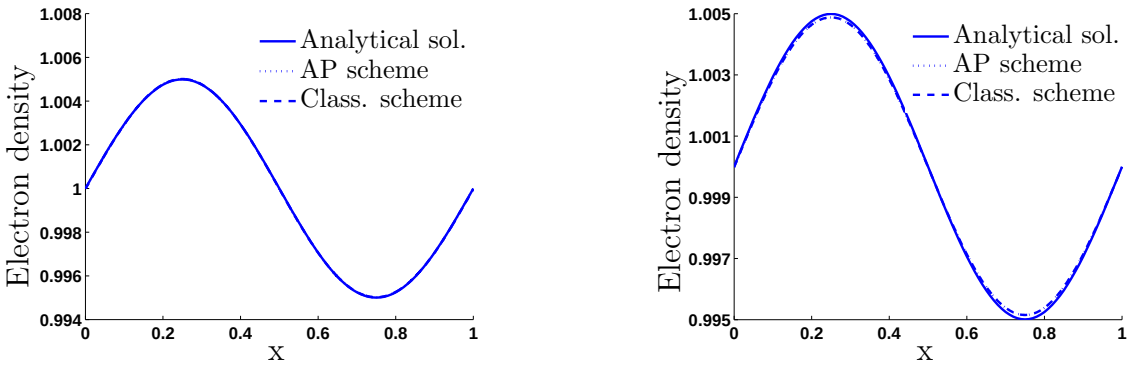

Figure 4.1: Electron density at the rescaled time $t = 0.1$ for the periodic perturbation test case. The classical scheme (dashed line) and the AP scheme (dotted line) are compared to the analytical solution (solid line). On the left-hand side the plasma period and the Debye length are resolved: $\Delta t < \tau$ and $\Delta x = \lambda$ and all curves are identical. On the right-hand side the plasma period is resolved but the Debye length is not: $\Delta t < \tau$ and $\Delta x = 10^{-2} > \lambda$. The curves given by the classical and AP schemes are identical.

Figure 4.1 shows the electron density at the rescaled time $t = 0.1$. The classical and AP schemes are compared to the exact solution of the linearized system. On the left-hand side, the time and space discretizations respectively resolve the Debye length and the plasma period. We can see that all curves are identical, both schemes are stable. The curves for the other quantities (given in [**A4**]) show the same behavior. On the right-hand side, the plasma period is still resolved but the Debye length is not. Both schemes are still stable. The results are more diffusive but we have divided the number of cells by one hundred. The results on the ion density and velocity, and on the potential have the same behavior. But, on the electron velocity curve there is a difference with the analytical solution essentially in the computation of the

phase. In [**A4**], we numerically show that this difference can be imputed to the bad consistency of the scheme for the electron velocity equation due to the mass ratio stiffness as $\varepsilon = 10^{-4} \ll 1$. We are in a low Mach number regime well known to generate numerical problems.

Figure 4.2 shows the electron density at the rescaled time $t = 0.1$ in the non resolved case in space and time. On the left-hand side, the curve given by the classical scheme shows that it is unstable when the discretization does not resolve the Debye length and the plasma period. While, on the right-hand side the AP scheme is still stable even if the discretization does not resolve the Debye length and the plasma period.

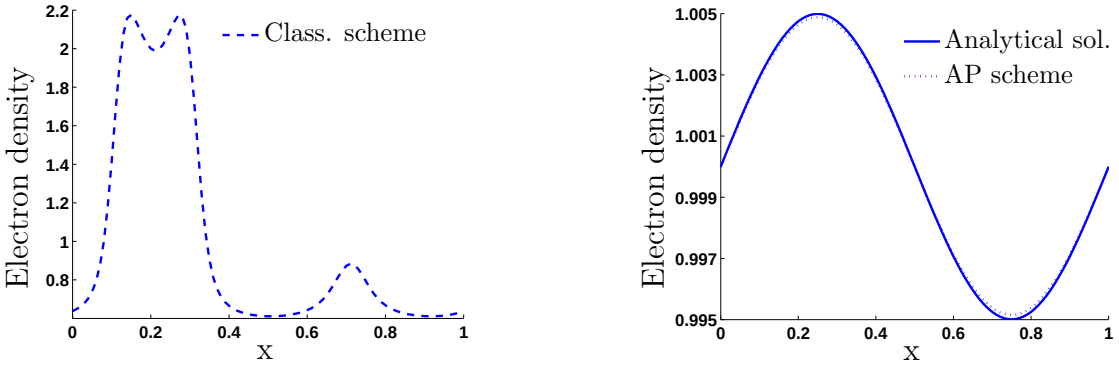

Figure 4.2: Electron density at the rescaled time $t = 0.1$ for the periodic perturbation test case. The classical scheme (dashed line on the left-hand side) and the AP scheme (dotted line on the right-hand side) are compared to the analytical solution of the linearized system (solid line on the right-hand side). The plasma period and the Debye length are not resolved: $\Delta t > \tau$ and $\Delta x = 10^{-2} > \lambda$.

The second test case is the expansion of a quasi-neutral plasma between two electrodes. This test case is detailed in the previous chapter. I recall that we inject at $x = 0$, the cathode, a quasi-neutral plasma in the domain initially supposed devoid of plasma. Here, we choose $n_i(x = 0) = n_e(x = 0) = 1$ and $q_i(x = 0) = q_e(x = 0) = 1$. The anode is located at $x = 1$ and the rescaled difference of potential is given by 100. The parameters are the same as previously $C_i = C_e = 1$, $\gamma_i = \gamma_e = 5/3$, $\varepsilon = 10^{-4}$ and $\lambda = 10^{-4}$. I recall that they yield a rescaled plasma period $\tau = 10^{-6}$.

The results presented here are not in [**A4**], indeed in [**A4**] we use the modified Lax-Friedrichs solver but here the space discretization uses the degree 0 polynomial solver. It is a Roe type solver proposed in [17]. This solver has several advantages. First it is very robust for this test case. We will see in section 4.4, that it gives a stable resolution of the boundary layer problem. Furthermore, it is less diffusive than the modified Lax-Friedrichs solver. Figure 4.3 shows on the left-hand side the electron density and the right-hand side the electric potential. I present results for the classical and AP scheme in the resolved case (solid line and cross markers) i.e. when the space and time space are respectively lower than the Debye length and the plasma period. These curves are identical for the density and for the potential. Finally, the

curves in dashed and dotted lines show the same schemes when the space and time discretizations do not resolve the Debye length and the plasma period. These curves clearly show the instability of the classical scheme whereas the AP scheme remains stable.

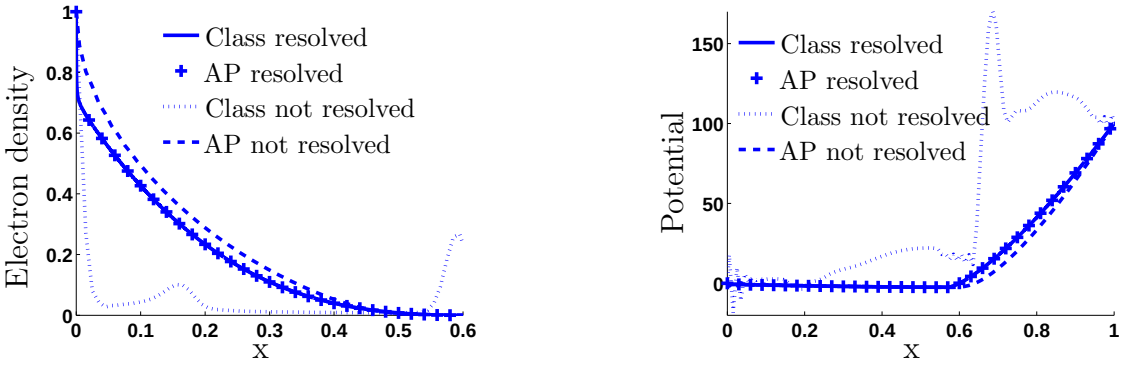

Figure 4.3: Electron density (left-hand side) and electric potential (right-hand side) at the rescaled time $t = 0.06$ for the plasma expansion test case. The results are given in the resolved case in time and space ($\Delta t < \tau$ and $\Delta x = \lambda$) for the classical scheme (solid line) and the AP scheme (crosses) and in the non resolved case in time and space ($\Delta t > \tau$ and $\Delta x = 10^{-1} > \lambda$) for the classical scheme (dotted line) and the AP schema (dashed line).

Finally, the last test case deals with the expansion of a plasma bubble between two electrodes in two dimensions. The electrodes are plane and located at $x = 0$ and $x = 1$. The plasma is injected from a part of the cathode $x = 0$ with a Gaussian profile in the ordinate direction y. The values of the parameters are the same as the previous test case, $C_i = C_e = 1$, $\gamma_i = \gamma_e = 5/3$, $\varepsilon = 10^{-4}$ and $\lambda = 10^{-4}$ which give a rescaled plasma period $\tau = 10^{-6}$. The mesh is squared with 100×100 cells. The results presented on Figure 4.4 are obtained with the AP scheme using the degree 0 polynomial solver. They confirm the stability of the AP scheme in the non resolved case.

The numerical results show the good asymptotic behavior of the AP scheme. In the following section, we prove the asymptotic stability of the AP scheme for a one-fluid Euler-Poisson system linearized around a constant solution.

4.3 Numerical analysis of the asymptotic preserving scheme in the quasi-neutral regime

In this section, I present the results submitted for publication in [**A7**]. In this article, we prove the asymptotic stability in the quasi-neutral limit of the AP scheme presented in the previous section (or in [**A4**]). In [**A7**] the Debye length is denoted by ε but to be consistent with the notations used here, I will continue to denote it by λ.

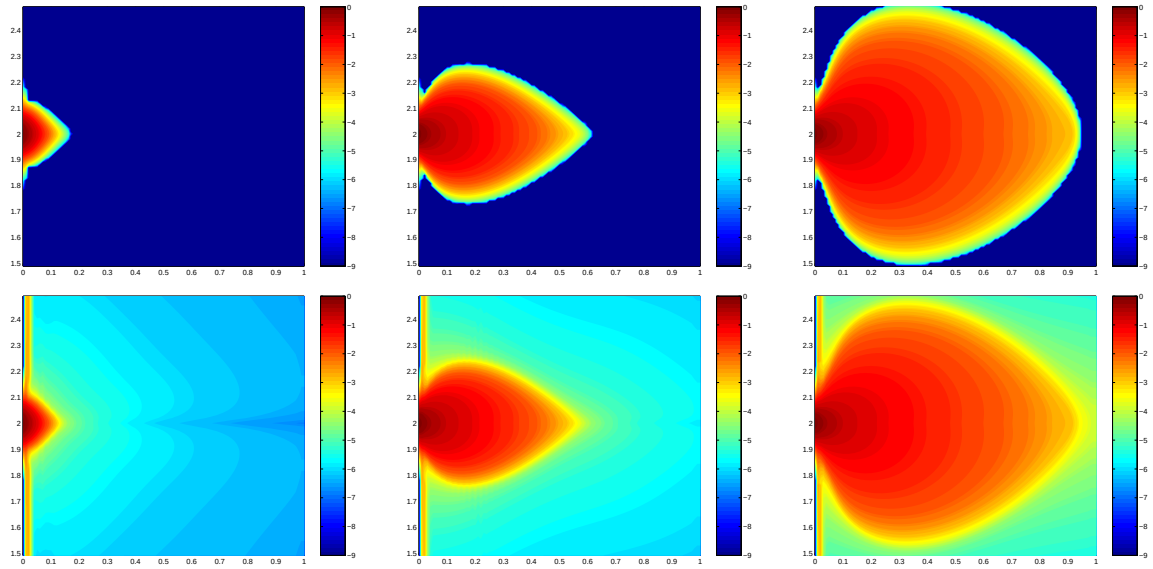

Figure 4.4: Ion density (on the top) and electron density (on the bottom) in logarithm scale, at the rescaled times $t = 0.01$ (left), $t = 0.1$ (middle) and $t = 0.2$ (right) for the two-dimensional plasma expansion test case. The results are obtained with the AP scheme in the non resolved case in time and space.

4.3.1 Linearization and discretization of the one-fluid Euler-Poisson model

Here, we consider a simplified model. It consists to assume static ions and to look at the electron dynamics. Here, we consider electrons with scaled charge equal to -1 and the right-hand side of the Poisson equation involves a uniform ion background density equal to 1 in the scaled variables. The one dimensional model in rescaled variables is given by

$$\partial_t n + \partial_x q = 0\,, \qquad \partial_t q + \partial_x \left(\frac{q^2}{n} + p(n) \right) = n \partial_x \phi\,, \tag{4.12}$$

$$\lambda^2 \partial_{xx}^2 \phi = n - 1\,. \tag{4.13}$$

where $x \in \mathbb{R}$ is the space variable, $t > 0$ is the time, $n = n(x,t)$ and $q = q(x,t)$ are respectively the electron density and momentum, $p(n) = C\, n^\gamma$, $C > 0$ and $\gamma > 1$, is the pressure and $\phi = \phi(x,t)$ is the potential.

The parameter λ is the scaled Debye length, i.e. the ratio between the Debye length λ_D, given by (4.1), and the macroscopic length scale.

The quasi-neutral limit of this system yields the incompressible Euler equations. Indeed, letting λ formally tend to 0 in (4.12)-(4.13), we obtain (4.12) and the quasi-neutrality constraint $n = 1$. This can be equivalently rewritten

$$n = 1, \qquad \partial_x q = 0\,, \qquad \partial_t q + \partial_x q^2 - \partial_x \phi = 0\,.$$

Thus, by switching ϕ into $-\pi$, we recognize the incompressible Euler equations and ϕ is the Lagrange multiplier of the constraint $\partial_x q = 0$.

In the stability analysis studied in the following sections, we work with the Euler-Poisson system linearized around a constant solution. This constant solution is given by $n = 1$, $q = q_0$, $E = (-\partial_x \phi) = 0$. The constant q_0 is a real number, at the beginning of the analysis it will be considered equal to 0, which corresponds to a quasi-neutral limit with a vanishing current in the plasma. In a second step, q_0 will be considered not zero. We will see that a non vanishing current in the plasma yield different conclusions in the stability analysis of the scheme. The Euler-Poisson system linearized around the constant state $(1, q_0, 0)$ is given by

$$\partial_t n + \partial_x q = 0\,, \qquad \partial_t q + 2\,q_0\,\partial_x q + (c_s^2 - q_0^2)\,\partial_x n = \partial_x \phi\,, \qquad \lambda^2 \partial_{xx}^2 \phi = n. \quad (4.14)$$

The sound speed c_s is equal to 1 since $c_s = \sqrt{p'(1)/1}$, but to highlight how our conclusions may depend on its value, the notation c_s is kept.

First, let us remark that u and ϕ can be eliminated. When $|q_0| < |c_s|$, the resulting equation is a Klein-Gordon equation with a mass equal to $1/\lambda^2$. It is given by

$$\partial_{tt}^2 n + 2q_0 \partial_{tx}^2 n - (c_s^2 - q_0^2)\partial_{xx}^2 n + \frac{1}{\lambda^2} n = 0\,. \quad (4.15)$$

Multiplying this equation by $\partial_t n$ and assuming periodic boundary conditions, we obtain an energy estimate:

$$\partial_t \int_a^b \left((\partial_t n)^2 + (c_s^2 - q_0^2)(\partial_x n)^2 + \frac{1}{\lambda^2} n^2 \right) dx = 0\,.$$

This energy estimate shows that when $\lambda \to 0$, more and more energy is stored in the last term which can be interpreted as a potential.

Furthermore, we find again the dispersive nature of the quasi-neutral limit already mentioned in the previous section. Indeed, taking the Fourier transform in space of equation (4.15) and denoting by $\hat{n}(\xi, t)$ the Fourier transform of n, we get

$$\partial_{tt}^2 \hat{n} + 2\,i\,q_0 \xi\,\partial_t \hat{n} + \left(c_s^2 - q_0^2 + \frac{1}{\lambda^2} \right) \hat{n} = 0.$$

The solutions of this equation are of the form

$$\hat{n}(\xi, t) = A(\xi)\,\exp(i\,\theta^\lambda(\xi)\,t) + B(\xi)\,\exp(-i\,\theta^\lambda(\xi)\,t),$$

where A and B only depend on the initial condition, but not on λ. The oscillation frequency is defined by

$$\theta^\lambda(\xi) = -2\,q_0 \xi + \left(c_s^2\,\xi^2 + \frac{1}{\lambda^2} \right)^{1/2}.$$

The magnitude of the solutions are of order 1 and they oscillate at the frequency $\theta^\lambda(\xi) = \mathcal{O}(1/\lambda)$ where λ is, in this case, the plasma period since the electron mass equals 1 in the rescaled variables.

To study the stability of the classical and asymptotic preserving discretizations presented in the previous section, we use the Fourier analysis. The considered Fourier transform only acts on the space variable of systems discretized in time. This analysis is a model for the analysis of a fully discrete scheme (in space and time) using a centered space differencing. Then, to study the stability of an upwind space discretization we add diffusion terms. We introduce the following linearized viscous Euler-Poisson system

$$\partial_t n+\partial_x q = \beta\partial^2_{xx} n, \quad \partial_t q+2q_0\partial_x q+(c_s^2-q_0^2)\partial_x n = \beta\partial^2_{xx} q+\partial_x\phi, \quad \lambda^2\partial^2_{xx}\phi = n, \tag{4.16}$$

where $\beta > 0$.

To be convinced by these remarks, let us look at the simplest transport equation, i.e.

$$\partial_t u + c\,\partial_x u = 0, \tag{4.17}$$

where $c > 0$ as instance. The centered and upwind discretizations of this equation are given by

$$\frac{u_j^{m+1}-u_j^m}{\Delta t} + c\,\frac{u_{j+1}^m-u_{j-1}^m}{2\,\Delta x} = 0, \qquad \frac{u_j^{m+1}-u_j^m}{\Delta t} + c\,\frac{u_j^m-u_{j-1}^m}{\Delta x} = 0.$$

But, the upwind scheme can be rewritten

$$\frac{u_j^{m+1}-u_j^m}{\Delta t} + c\,\frac{u_{j+1}^m-u_{j-1}^m}{2\,\Delta x} - \frac{c\,\Delta x}{2}\,\frac{u_{j+1}^m-2\,u_j^m+u_{j-1}^m}{\Delta x^2} = 0,$$

which is a centered discretization of the equation

$$\partial_t u + c\,\partial_x u - \frac{c\,\Delta x}{2}\,\partial^2_{xx} u = 0. \tag{4.18}$$

It is well known that the centered scheme is unconditionally unstable whereas the upwind scheme is stable under the C.F.L. condition (Courant-Friedrichs-Levy) given by $\Delta t \leq \Delta x/c$. Let us find again these results with the Fourier analysis in space of equations (4.17) and (4.18) discretized in time. We obtain

$$\begin{aligned} \hat{u}^{m+1} &= \hat{u}^m\,(1-c\,\Delta t\,i\,\xi), \\ &= \hat{u}^0\,(1-c\,\Delta t\,i\,\xi)^m, \end{aligned} \qquad \begin{aligned} \hat{u}^{m+1} &= \hat{u}^m\left(1-c\,\Delta t\,i\,\xi-\frac{c\,\Delta x}{2}\,\Delta t\,\xi^2\right), \\ &= \hat{u}^0\left(1-c\,\Delta t\,i\,\xi-\frac{c\,\Delta x}{2}\,\Delta t\,\xi^2\right)^m. \end{aligned}$$

Then, we have

$$|1-c\,\Delta t\,i\,\xi|^2 = 1+c^2\,\Delta t^2\xi^2 > 1,$$

and we find again the unconditional instability of the centered scheme. On the other hand,

$$\begin{aligned} \left|1-c\,\Delta t\,i\,\xi-\frac{c\,\Delta x}{2}\,\Delta t\,\xi^2\right|^2 &= \left(1-\frac{c\,\Delta x}{2}\,\Delta t\,\xi^2\right)^2 + c^2\,\Delta t^2\xi^2, \\ &= 1-c\,\Delta x\,\Delta t\,\xi^2 + c^2\,\Delta t^2\,\xi^2\left(\frac{\Delta x^2}{4}\,\xi^2+1\right). \end{aligned}$$

We obtain the sufficient stability condition

$$\Delta t \leq \frac{\Delta x}{c\left(\dfrac{\Delta x^2}{4}\,\xi^2 + 1\right)}.$$

Choosing $\xi = \mathcal{O}(1/\Delta x)$ which mimics the fact that a fully discrete scheme can not resolve large wave-numbers, we find a C.F.L. condition of same order as expected. Finally, let us note that in the linear case, the upwind scheme and the modified Lax-Friedrichs scheme, used in **[A4]**, are identical.

4.3.2 Stability of the linearized model

We begin with the presentation of the classical and asymptotic preserving schemes of the linearized Euler-Poisson system (4.16). Both discretizations use an implicit treatment of the electric source terms. They differ from the explicit or implicit treatment of the flux in the mass conservation law. The classical scheme consists in discretizing this term explicitly while the AP scheme discretizes it implicitly. In the following we call the classical scheme, EI scheme and the AP scheme II scheme in relation with the Explicit or Implicit mass flux term and with the Implicit treatment of the electric force term. We denote by Δt the time step and by g^m an approximation of $x \mapsto g(x, t^m)$ where $t^m = m\,\Delta t$ for $m \geq 0$. The EI scheme (classical) is given by

$$\frac{n^{m+1} - n^m}{\Delta t} + \partial_x q^m = \beta \partial^2_{xx} n^m, \qquad \lambda^2 \partial^2_{xx} \phi^{m+1} = n^{m+1}, \tag{4.19}$$

$$\frac{q^{m+1} - q^m}{\Delta t} + 2\,q_0\,\partial_x q^m + (c_s^2 - q_0^2)\,\partial_x n^m = \beta \partial^2_{xx} q^m + \partial_x \phi^{m+1}. \tag{4.20}$$

The II scheme (AP) is given by

$$\frac{n^{m+1} - n^m}{\Delta t} + \partial_x q^{m+1} = \beta \partial^2_{xx} n^m, \qquad \lambda^2 \partial^2_{xx} \phi^{m+1} = n^{m+1}, \tag{4.21}$$

$$\frac{q^{m+1} - q^m}{\Delta t} + 2\,q_0\,\partial_x q^m + (c_s^2 - q_0^2)\,\partial_x n^m = \beta \partial^2_{xx} q^m + \partial_x \phi^{m+1}. \tag{4.22}$$

Furthermore, we introduce the following IE discretization, in order to verify if the implicit treatment of the electric force term is necessary for the AP scheme as it is for the classical scheme. It is given by

$$\frac{n^{m+1} - n^m}{\Delta t} + \partial_x q^{m+1} = \beta \partial^2_{xx} n^m, \qquad \lambda^2 \partial^2_{xx} \phi^{m+1} = n^{m+1}, \tag{4.23}$$

$$\frac{q^{m+1} - q^m}{\Delta t} + 2\,q_0\,\partial_x q^m + (c_s^2 - q_0^2)\,\partial_x n^m = \beta \partial^2_{xx} q^m + \partial_x \phi^{m}. \tag{4.24}$$

In [23], S. Fabre studies the stability of the full discretization of the linearized Euler-Poisson system (4.14) with $q_0 = 0$. This discretization consists in the classical Euler

scheme in time and the upwind scheme in space. Here, this corresponds to the EI scheme (classical) given by (4.19)-(4.20) with $q_0 = 0$ and $\beta \neq 0$. In [**A7**], we prove the following results.

Lemma 4.1 *We consider the linearized viscous Euler-Poisson system (4.16) with $q_0 = 0$. Then*

1. *If $\beta = 0$, the discretization II (AP) given by (4.21)-(4.22) is stable under the condition*
$$\Delta t \leq \delta_{ii}^{\star} = 2\left(\frac{\Delta x}{\pi c_s}\right)^2 \left(\frac{1}{\lambda^2} + \left(\frac{\pi c_s}{\Delta x}\right)^2\right)^{1/2}.$$
The discretization IE given by (4.23)-(4.24) is stable under the condition
$$\Delta t \leq \delta_{ie}^{*} = \frac{2}{\left(\frac{1}{\lambda^2} + \left(\frac{\pi c_s}{\Delta x}\right)^2\right)^{1/2}}.$$

2. *If $\beta \neq 0$, the discretization II (AP) given by (4.21)-(4.22) is stable under the condition*
$$\Delta t \leq \delta_{ii}^{v} = \frac{2\,\beta}{c_s^2} \min\left(\frac{1}{C^{\star 2}}, \sqrt{1 + C^{\star}} - 1\right), \tag{4.25}$$
where $C^{\star} = \beta\,\pi/(c_s\,\Delta x)$.
The discretization EI (classical) given by (4.19)-(4.20) is stable under the condition
$$\Delta t \leq \min(\delta_{ei}^{v}, \delta^{\star}) = \min\left(\frac{2\beta}{c_s^2}\frac{1}{1 + C^{*2}}, \frac{2}{\sqrt{1 + C^{*2}}}\lambda\right),$$
for all $\lambda \in [0, \frac{\beta}{c_s^2\sqrt{1+C^{*2}}}]$ and if $2\lambda < \Delta t \leq \delta^{\star}$, the scheme is unstable.

Point *1.* of this lemma clearly shows the asymptotic stability of the II scheme (AP) in the quasi-neutral limit. Indeed, $\delta_{ii}^{\star} \to +\infty$ when $\lambda \to 0$. The IE scheme is subject to a severe constraint in quasi-neutral zones since $\delta_{ie}^{*} \to 0$ when $\lambda \to 0$. Then, the implicit treatment of the electric force term is necessary to obtain the asymptotic stability. Finally, let us note that when $1/\lambda$ is small, i.e. in non quasi-neutral zones, we find again the classical C.F.L. condition i.e. Δt of order $\Delta x/c_s$.

Point *2.* confirms the asymptotic stability of the AP scheme. Indeed, δ_{ii}^{v} does not depend on λ, furthermore the stability condition is a C.F.L. condition, which only depends on the purely hydrodynamic part of the scheme. Indeed, I recall that for the upwind scheme, the viscosity term β is given by $c_s\,\Delta x/2$. Thus, $C^{\star}$ does not depend on Δx and condition (4.25) is equivalent to $\Delta t \leq C\,\Delta x/c_s$. Finally, the last result shows that the stability domain of the EI scheme (classical) is an interval of size exactly $\mathcal{O}(\lambda)$. We find again the result already established by S. Fabre.

In the case of a non vanishing current, we prove the following result.

Lemma 4.2 *We consider the linearized viscous Euler-Poisson system (4.16) with $q_0 \neq 0$. Then*

1. *If $\beta = 0$, for all constant $0 < K < 1$, there exists $\Delta t^\star > 0$ such that the discretization II (AP) given by (4.21)-(4.22) is stable under the conditions*

$$\Delta t \leq \Delta t^\star \qquad \text{and} \qquad \lambda < K\Delta t,$$

where $\delta^\star \to 0$ when $K \to 1$.

2. *If $\beta \neq 0$ is such that there exists $B > B^\star$, where $B^\star$ does not depend on q_0 and c_s, such that $\beta = B\,\Delta t$ then there exists $\Delta t^\star$ non depending on q_0 and c_s such that the discretization II (AP) given by (4.21)-(4.22) is stable for all $\lambda > 0$, under the condition*

$$\Delta t \leq \Delta t^\star.$$

Point *1.* gives a stability property but for λ sufficiently small. Thus, the **centered** AP scheme is unstable in the non quasi-neutral regime. But, point *2.* shows that the AP scheme is uniformly stable for all values of λ. The diffusion constant is taken proportional to δ, whereas classically it is taken proportional to Δx. The result would also remain true in this case but this choice simplifies the, already quite technical, proof. Also, the result in itself is interesting as it shows that the AP scheme is stable even with a vanishingly small diffusion term proportional to δ.

4.4 A boundary layer problem related to the quasi-neutrality

In this section, I present the results submitted for publication in [**A8**]. They deal with the study of a boundary layer in the test case of the plasma expansion between two electrodes presented in section 4.2.

4.4.1 The two-fluid Euler-Poisson model

We consider the rescaled two-fluid Euler-Poisson model, that I recall here precising the boundary conditions. We denote by $n_i(x,t)$ and $n_e(x,t)$ the ion and electron densities, by $q_i(x,t)$ and $q_e(x,t)$ their momentum and by $\phi(x,t)$ the electric potential, where $x \in \mathbb{R}$ is the space variable and $t > 0$ is the time. These quantities satisfy the following system

$$\partial_t n_i^\lambda + \partial_x q_i^\lambda = 0, \qquad \partial_t q_i^\lambda + \partial_x f_i(n_i^\lambda, q_i^\lambda) = -n_i^\lambda\,\partial_x \phi^\lambda, \tag{4.26}$$

$$\partial_t n_e^\lambda + \partial_x q_e^\lambda = 0, \qquad \varepsilon\,\partial_t q_e^\lambda + \varepsilon\,\partial_x f_e(n_e^\lambda, q_e^\lambda) = n_e^\lambda\,\partial_x \phi^\lambda, \tag{4.27}$$

$$-\lambda^2\,\partial_{xx}^2 \phi^\lambda = n_i^\lambda - n_e^\lambda, \tag{4.28}$$

for $x \in]0,1[$ and $t > 0$, and where the momentum fluxes are given by $f_i(n,q) = q^2/n + p_i(n)$ and $f_e(n,q) = q^2/n + p_e(n)/\varepsilon$. The isentropic pressure laws are defined by $p_{i,e}(n) = C_{i,e} n^{\gamma_{i,e}}$, with $C_{i,e} > 0$ and $\gamma_{i,e} > 1$.

Remind that the rescaled parameters ε and λ are respectively the ratio between electron and ion masses $\varepsilon = m_e/m_i$ and the rescaled Debye length $\lambda = \lambda_D/L$ where

λ_D is the Debye length, given by (4.1) and L is the macroscopic length scale. These parameters give the rescaled plasma period $\tau = \sqrt{\varepsilon}\,\lambda$.

The domain is initially devoid of plasma and the hyperbolic systems are assumed supersonic at the point $x = 1$. Thus, we need no boundary condition at $x = 1$ for the fluid quantities. The cathode and the anode are respectively located at $x = 0$ and $x = 1$ and a quasi-neutral plasma is present outside the domain for $x < 0$. Then, we set

$$\phi^\lambda(0,t) = 0, \qquad \phi^\lambda(1,t) = \phi_A(t) > 0, \tag{4.29}$$

$$(n_i^\lambda, q_i^\lambda)(0,t) = (n_{i0}^\lambda, q_{i0}^\lambda)(t), \qquad (n_e^\lambda, q_e^\lambda)(0,t) = (n_{e0}^\lambda, q_{e0}^\lambda)(t), \tag{4.30}$$

for all $t > 0$ and where $(n_{i0}^\lambda, q_{i0}^\lambda)$ and $(n_{e0}^\lambda, q_{e0}^\lambda)$ are the respective solutions at the point $x = 0$ of the following Riemann problems

$$\begin{cases} \partial_t n_i + \partial_x q_i = 0, \\ \partial_t q_i + \partial_x f_i(n_i, q_i) = 0, \\ \begin{pmatrix} n_i \\ q_i \end{pmatrix}(x,0) = \begin{cases} \begin{pmatrix} n_0 \\ q_0 \end{pmatrix}(t), & x < 0, \\ \begin{pmatrix} n_i^\lambda \\ q_i^\lambda \end{pmatrix}(0^+,t), & x > 0, \end{cases} \end{cases} \quad \begin{cases} \partial_t n_e + \partial_x q_e = 0, \\ \partial_t q_e + \partial_x f_e(n_e, q_e) = 0, \\ \begin{pmatrix} n_e \\ q_e \end{pmatrix}(x,0) = \begin{cases} \begin{pmatrix} n_0 \\ q_0 \end{pmatrix}(t), & x < 0, \\ \begin{pmatrix} n_e^\lambda \\ q_e^\lambda \end{pmatrix}(0^+,t), & x > 0, \end{cases} \end{cases} \tag{4.31}$$

where $(n_{i,e}^\lambda, q_{i,e}^\lambda)(0^+,t) = \lim_{x\to 0^+}(n_{i,e}^\lambda, q_{i,e}^\lambda)(x,t)$ and where (n_0, q_0) is the state outside the domain, it is assumed subsonic, i.e. such that $q_0/n_0 + \sqrt{p_i'(n_0)} > 0$, $q_0/n_0 + \sqrt{p_e'(n_0)/\varepsilon} > 0$, $q_0/n_0 - \sqrt{p_i'(n_0)} < 0$ and $q_0/n_0 - \sqrt{p_e'(n_0)/\varepsilon} < 0$.

4.4.2 Numerical problems related to the boundary layer

In [**A4**], summarized in section 4.2, two test cases in one dimension of space are considered. The first test case is a periodic perturbation of a uniform stationary plasma with a non vanishing current. For this test case, the boundary conditions on the fluid quantities are periodic and not given by (4.30). Then, we compare the classical and asymptotic preserving (AP) discretizations. Numerically, we observe that the AP scheme remains stable for time steps greater than plasma period while the classical scheme develops instabilities. In these simulations, we use the modified Lax-Friedrichs solver (see [22]). This solver is well known to be very diffusive but is also very robust. So, it is well adapted to the validation step of the AP scheme. Now, we have extended these results to more general Roe type solvers like the degree 0 or 2 polynomial solvers (see [17]), HLLE, HLLC and to the order 2 Lax-Wendroff solver (see [51]). We obtain the same results. The second test case used in [**A4**], is the expansion of a quasi-neutral plasma between two electrodes. This test case is particularly well adapted to the asymptotic preserving scheme, since a transition between a quasi-neutral region (the plasma) to a non quasi-neutral one (the beam) occurs. As in the previous test case, the numerical simulations presented in [**A4**], are performed using the modified Lax-Friedrichs solver. They show that the asymptotic preserving scheme remains stable while the classical scheme is unstable when the

time steps are greater than the electron plasma period. Here, we present the results obtained with more general order 1 solvers: the degree 0 and 2 polynomial solvers.

The parameters are issued from plasma arc physics (see [9]). We set $\gamma_i = \gamma_e = 5/3$, $C_i = C_e = 1$, $\varepsilon = 10^{-4}$, $\lambda = 10^{-4}$, $\phi_A = 100$. Furthermore, the quasi-neutral plasma present outside the domain is chosen such that $(n_0, q_0) = (1, 1)$. The results are given on Figures 4.5 and on the left-hand side of Figure 4.6.

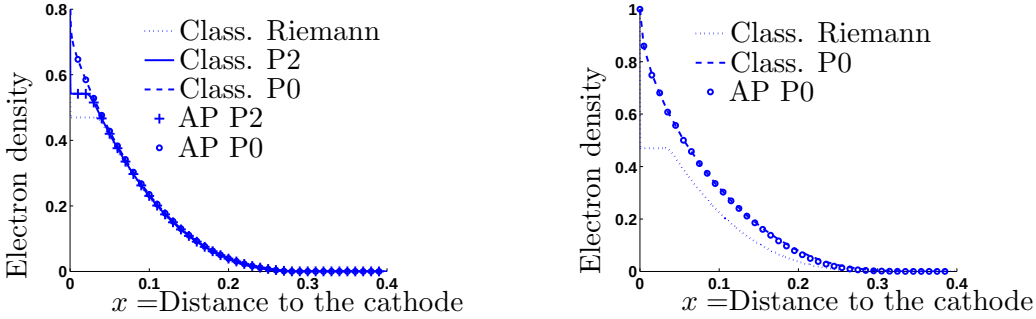

Figure 4.5: Electron density as a function of x, at the rescaled time $t = 0.05$. The results are obtained with the classical scheme and the Riemann solver (dotted line, left and right) in the resolved case: $\Delta x = 10^{-4} = \lambda$ and $\Delta t \leq \tau = 10^{-6}$, with the degree 0 polynomial solver for the classical scheme (dashed line) in the resolved case on the left-hand side and partially resolved on the right-hand side: $\Delta x = 10^{-2} > \lambda$ and $\Delta t \leq \tau$, with the degree 0 polynomial solver for the AP scheme (circle markers) in the resolved case on the left-hand side and in the non resolved case on the right-hand side: $\Delta x = 10^{-2} > \lambda$ and $\Delta t > \tau$. Finally for the degree 2 polynomial solver with the classical scheme (solid line on the left-hand side) and the AP scheme (cross markers on the left-hand side) in the resolved case.

The reference solution is the one given by classical scheme with the exact Riemann solver in the resolved case, i.e. when the space step Δx and the time step Δt satisfy $\Delta x \leq \lambda$ and $\Delta t \leq \tau$. We compare this reference solution to the classical and AP schemes with degree 0 and 2 polynomial solvers. Note that the degree 0 polynomial solver has diagonal numerical viscosity matrices which is also the case for the modified Lax-Friedrichs solver used in [**A4**]. On the contrary, the degree 2 polynomial solver has non diagonal numerical viscosity matrices like the general Roe type solvers HLLE, HLLC,$\cdots$.

The left-hand side of Figure 4.5 shows the results in the resolved case for all discretizations. We can see that the classical and AP schemes give the same curves for a given solver. Furthermore, the different solvers give the same results in the core of the plasma but not in a neighborhood of $x = 0$. These differences show the presence of a boundary layer which is not identically resolved by all solvers. The right-hand side of Figure 4.5 on the left-hand side of Figure 4.6 show the same results when the Debye length is not resolved, i.e. when $\Delta x = 10^{-2} > \lambda = 10^{-4}$. The classical scheme resolves the plasma period ($\Delta t \leq \tau$) and the AP scheme does not ($\Delta t > \tau$). We compare these results to the reference curve (classical scheme, Riemann solver,

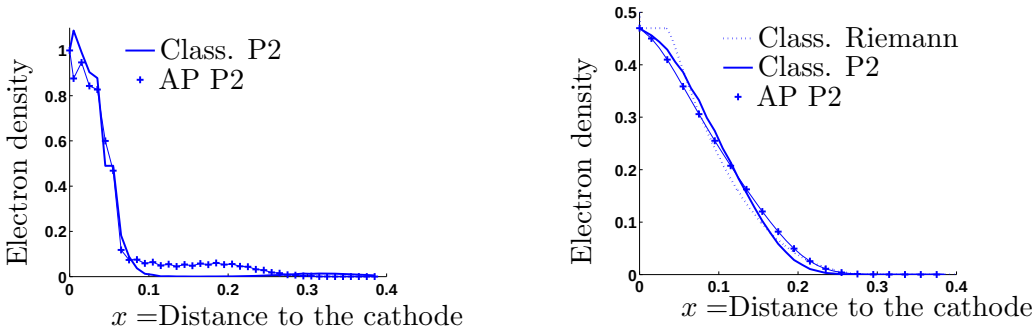

Figure 4.6: Electron density as a function of x, at the rescaled time $t = 0.05$. The results are computed with the classical scheme (solid line) and the AP scheme (cross marker) and with the degree 2 polynomial solver in the non resolved case $\Delta x = 10^{-2} > \lambda = 10^{-4}$. The classical scheme resolves the plasma period: $\Delta t \leq \tau$ and the AP scheme does not: $\Delta t > \tau$. On the left-hand side the boundary conditions are given by (4.30). On the right-hand side, we use the values given at the end of the boundary layer by the reference curve, i.e. the curve obtained with the classical scheme, the Riemann solver and the boundary conditions (4.30) in the resolved case. This curve is plotted on the right-hand side in dotted line.

resolved case in space and time). It clearly shows that the degree 0 polynomial solver ($P0$) is stable while the degree 2 polynomial solver ($P2$) is unstable. This instability is due to the boundary layer, which is not properly resolved. Indeed, when we choose for boundary conditions the values given by the reference curve at the end of the boundary layer, the $P2$ solver gives stable results for both schemes (classical and AP) as we can see on the right-hand side of Figure 4.6.

4.4.3 Solution of the boundary layer problem

To determine boundary conditions well adapted for the quasi-neutral regime, we introduce a boundary layer problem. It is obtained by writing the following asymptotic expansion

$$(n_{i,e}^{\lambda}, q_{i,e}^{\lambda}, \phi^{\lambda})(x,t) = (\bar{n}_{i,e}, \bar{q}_{i,e}, \bar{\phi})(x,t) + (\tilde{n}_{i,e}, \tilde{q}_{i,e}, \phi)(x/\lambda, t) + \lambda\,(\hat{n}_{i,e}^{\lambda}, \hat{q}_{i,e}^{\lambda}, \hat{\phi})(x,t),$$

where $\lim_{\lambda\to 0} \lambda\,(\hat{n}_{i,e}^{\lambda}, \hat{q}_{i,e}^{\lambda}, \hat{\phi}^{\lambda}) = (0,0,0)$ and $(\bar{n}_{i,e}, \bar{q}_{i,e}, \bar{\phi})$ is solution of the quasi-neutral system obtained by letting λ tend to 0 in system (4.26)-(4.28).

Inserting this expansion in the two-fluid Euler-Poisson system, we get the following result.

Lemma 4.3 (Formal) *The boundary layer* $(\tilde{n}_{i,e}, \tilde{q}_{i,e}, \phi)$ *is solution of system*

$$n_{i,e}(y,t) = \tilde{n}_{i,e}(y,t) + \bar{n}_{i,e}(0,t), \qquad q_{i,e}(y,t) = \tilde{q}_{i,e}(y,t) + \bar{q}_{i,e}(0,t), \tag{4.32}$$

$$\partial_y q_i = 0, \qquad \partial_y(q_i^2/n_i + p_i(n_i)) = -n_i\,\partial_y\phi, \tag{4.33}$$

$$\partial_y q_e = 0, \qquad \partial_y(\varepsilon\, q_e^2/n_e + p_e(n_e)) = n_e\,\partial_y\phi, \tag{4.34}$$

$$-\partial^2_{yy}\phi = n_i - n_e, \tag{4.35}$$

for all $y > 0$ *and all* $t > 0$. *The boundary conditions are given by*

$$\phi(0,t) = -\bar{\phi}_0, \qquad \phi(+\infty,t) = 0, \tag{4.36}$$

$$(n_i, q_i)(0,t) = (n_{i0}, q_{i0})(t), \qquad (n_i(+\infty), q_i(+\infty)) = (\bar{n}_0, \bar{q}_{i0}), \tag{4.37}$$

$$(n_e, q_e)(0,t) = (n_{e0}, q_{e0})(t), \qquad (n_e(+\infty), q_e(+\infty)) = (\bar{n}_0, \bar{q}_{e0}), \tag{4.38}$$

with $(\bar{\phi}_0, \bar{n}_0, \bar{q}_{i0}, \bar{q}_{e0}) = (\bar{\phi}, \bar{n}, \bar{q}_i, \bar{q}_e)|_{(0,t)}$ *and where* (n_{i0}, q_{i0}) *and* (n_{e0}, q_{e0}) *are the respective solutions at the point* $x = 0$ *of the following Riemann problems*

$$\begin{cases} \partial_t n_i + \partial_x q_i = 0, \\ \partial_t q_i + \partial_x((q_i)^2/n_i + p_i(n_i)) = 0, \\ \begin{pmatrix} n_i \\ q_i \end{pmatrix}(x,0) = \begin{cases} \begin{pmatrix} n_0 \\ q_0 \end{pmatrix}, & \text{if } x < 0, \\ \begin{pmatrix} n_i^+ \\ q_i^+ \end{pmatrix}, & \text{if } x > 0, \end{cases} \end{cases} \quad \begin{cases} \partial_t n_e + \partial_x q_e = 0, \\ \varepsilon\partial_t q_e + \partial_x(\varepsilon\,(q_e)^2/n_e + p_e(n_e)) = 0, \\ \begin{pmatrix} n_e \\ q_e \end{pmatrix}(x,0) = \begin{cases} \begin{pmatrix} n_0 \\ q_0 \end{pmatrix}, & \text{if } x < 0, \\ \begin{pmatrix} n_e^+ \\ q_e^+ \end{pmatrix}, & \text{if } x > 0, \end{cases} \end{cases} \tag{4.39}$$

where $(n_{i,e}^+, q_{i,e}^+) = \lim_{y\to 0}(n_{i,e}(y,t), q_{i,e}(y,t))$ *for all* $t > 0$.

The aim of this section is to find $\bar{n}_0$, $\bar{q}_{i0}$, $\bar{q}_{e0}$ and $\bar{\phi}_0$, such that the boundary layer problem has a solution. It is important to note that the boundary conditions (4.39) are implicitly determined by the boundary layer since $(n_{i,e}^+, q_{i,e}^+)$ are given by the solution of the boundary layer problem. This makes the problem strongly non linear.

To resolve this problem, we introduce the ion and electron total enthalpies of the systems. They are given as functions of the density since in the boundary layer the momenta are constant.

$$k_i(n) = \frac{(\bar{q}_{i0})^2}{2\,n^2} + \frac{C_i\,\gamma_i}{\gamma_i - 1} n^{\gamma_i - 1}, \quad k_e(n) = \frac{\varepsilon(\bar{q}_{e0})^2}{2\,n^2} + \frac{C_e\,\gamma_e}{\gamma_e - 1} n^{\gamma_e - 1}. \tag{4.40}$$

These functions k_i and k_e are non monotonous. They are decreasing respectively on $(0, n_{iS})$ and $(0, n_{eS})$, and increasing respectively on $(n_{iS}, +\infty)$ and $(n_{eS}, +\infty)$, where n_{iS} and n_{eS} are the ion and electron sonic points defined by

$$n_{iS} = \left(\frac{(\bar{q}_{i0})^2}{C_i\,\gamma_i}\right)^{1/(\gamma_i+1)}, \quad n_{eS} = \left(\frac{\varepsilon(\bar{q}_{e0})^2}{C_e\,\gamma_e}\right)^{1/(\gamma_e+1)}. \tag{4.41}$$

Let us remark that a state $(n, \bar{q}_{i0})$ is supersonic if $n < n_{iS}$ and subsonic if $n > n_{iS}$, which explains the name sonic point for n_{iS}. The same results hold for electrons. We

assume $n_{iS} > n_{eS}$. This is the case if ε is small, if $\bar{q}_{i0}$ and $\bar{q}_{e0}$ are of same order and if C_e, C_i, γ_i and γ_e are order 1 parameters.

In a same way, we define the total enthalpy of the plasma by $k(n) = k_i(n) + k_e(n)$ for all $n > 0$. This function has the same behavior as k_i and k_e, we denote by n_S the plasma sonic point. The assumption $n_{iS} > n_{eS}$ implies $n_{iS} > n_S > n_{eS}$.

We prove the following result considering all the possible cases in the resolution of the Riemann problems (4.39).

Theorem 4.1 *We consider the boundary layer problem (4.32)-(4.39), where (n_0, q_0) is a subsonic state for ions and electrons. Furthermore, we assume $q_{i0}, q_{e0} > 0$ (i.e. the plasma incomes the domain). Then*

1. *If $\bar{n}_0 > n_{iS} > n_{eS}$ we have*

   1.1. *If (n_{i0}, q_{i0}) is given by $n_{i0} = n_{ic} \leq n_0$, with n_{ic} defined by*

$$n_{lc} = \left(\left(\frac{q_0}{n_0} + \frac{2\sqrt{k_l\,\gamma_l}}{\gamma_l - 1}\, n_0^{(\gamma_l - 1)/2} \right) \left(\frac{1}{\sqrt{k_l\,\gamma_l} + \frac{2\sqrt{k_l\,\gamma_l}}{\gamma_l - 1}} \right) \right)^{2/(\gamma_l - 1)}, \quad (4.42)$$

   for $l = i$ or e and with $k_i = C_i$ and $k_e = C_e/\varepsilon$, furthermore if $q_{i0} = \sqrt{C_i\,\gamma_i}\, n_{i0}^{(\gamma_i+1)/2}$ and if (n_{e0}, q_{e0}) satisfies

$$n_0 \geq n_{e0} > n_{ec}, \quad q_{e0} = n_{e0} \left(\frac{q_0}{n_0} + \frac{2\sqrt{\gamma_e\, C_e/\varepsilon}}{\gamma_e - 1} \left(n_0^{\frac{\gamma_e - 1}{2}} - n_{e0}^{\frac{\gamma_e - 1}{2}} \right) \right), \quad (4.43)$$

   or if (n_{e0}, q_{e0}) satisfies

$$n_{e0} > n_0, \quad q_{e0} = n_{e0} \left(\frac{q_0}{n_0} - (n_{e0} - n_0) \sqrt{\frac{p_e(n_{e0}) - p_e(n_0)}{\varepsilon\,(n_{e0} - n_0)\, n_{e0}\, n_0}} \right), \quad (4.44)$$

   problem (4.32)-(4.39) has a solution. Then three cases are possible.

   - *The solution exists if n_{i0} and n_{e0} satisfy*

$$k_i(n_{i0}) + k_e(n_{e0}) \geq k_i(n_S) + k_e(n_S), \quad (4.45)$$

   where n_S is the plasma sonic point. This solution is continuous with increasing potential ϕ and electron density n_e and a decreasing ion density n_i. It satisfies

$$\bar{\phi}_0 = k_i(n_{i0}) - k_i(\bar{n}_0), \quad \bar{q}_{i0} = q_{i0}, \quad \bar{q}_{e0} = q_{e0}, \quad (4.46)$$

$$k_i(n_{i0}) + k_e(n_{e0}) = k_i(\bar{n}_0) + k_e(\bar{n}_0). \quad (4.47)$$

   - *The solution exists if n_{i0} and n_{e0} satisfy (4.45). It is continuous with decreasing potential, ϕ, and electron density, n_e, and an increasing ion density, n_i. Furthermore, it satisfies (4.46), (4.47).*

• *The solution is unsmooth with a jump of n_i from a left state $n_i^{\star,-}$ to a right state $n_i^{\star,+}$. The ion density, n_i, is non monotonous, the potential, ϕ, and the electron density, n_e, are decreasing. This solution exists if the following condition is satisfied*

$$k_e(n_{e0}) > k_e(n_S) + k_i(n_S) - k_i(n_i^{\star,+}) + k_i(n_i^{\star,-}) - k_i(n_{iS}), \tag{4.48}$$

1.2. If (n_{i0}, q_{i0}) satisfies

$$n_0 \geq n_{i0} > n_{ic}, \quad q_{i0} = n_{i0}\left(\frac{q_0}{n_0} + \frac{2\sqrt{C_i\,\gamma_i}}{\gamma_i - 1}\left(n_0^{(\gamma_i-1)/2} - n_{i0}^{(\gamma_i-1)/2}\right)\right),$$

or if (n_{i0}, q_{i0}) satisfies

$$n_{i0} > n_0, \quad q_{i0} = n_{i0}\left(\frac{q_0}{n_0} - (n_{i0} - n_0)\sqrt{\frac{p_i(n_{i0}) - p_i(n_0)}{(n_{i0} - n_0)\,n_{i0}\,n_0}}\right).$$

1.2.1. If (n_{e0}, q_{e0}) is given by $n_{e0} = n_{ec} \leq n_0$, with n_{ec} defined by (4.42), and $q_{e0} = \sqrt{\gamma_e\,C_e/\varepsilon}\,n_{e0}^{(\gamma_e+1)/2}$, problem (4.32)-(4.39) has a solution. Two cases are possible.

• *The solution exists if n_{i0} and n_{e0} satisfy (4.45). It is continuous with increasing potential, ϕ, and electron density, n_e, and a decreasing ion density, n_i. It satisfies (4.46), (4.47).*

• *The solution is unsmooth with a jump of n_e from a left state $n_e^{\star,1,-}$ to a right state $n_e^{\star,1,+}$. The electron density, n_e, is non monotonous and the potential, ϕ, and the ion density, n_i, are respectively increasing and decreasing. This solution exists if*

$$k_i(n_{i0}) > k_i(n_S) + k_e(n_S) - k_e(n_e^{\star,1,+}) + k_e(n_e^{\star,1,-}) - k_e(n_{eS}).$$

1.2.2. If (n_{e0}, q_{e0}) satisfies (4.43) or (4.44), problem (4.32)-(4.39) has a solution. Two cases are possible.

• *The solution exists if $n_{e0} \leq \bar{n}_0$ and if n_{i0} and n_{e0} satisfy (4.45). It is continuous with increasing potential, ϕ, and electron density, n_e, and a decreasing ion density, n_i. It satisfies (4.46), (4.47).*

• *The solution is unsmooth with a jump of n_i from a left state $n_i^{\star,-}$ to a right state $n_i^{\star,+}$. The ion density, n_i, is non monotonous, the potential, ϕ, and the electron density, n_e, are decreasing. This solution exists if (4.48) is satisfied.*

2. If $n_{iS} > n_S > \bar{n}_0 > n_{eS}$, if (n_{i0}, q_{i0}) is given by $n_{i0} = n_{ic} \leq n_0$ and $q_{i0} = \sqrt{C_i\,\gamma_i}\,n_{i0}^{(\gamma_i+1)/2}$, and if (n_{e0}, q_{e0}) satisfies (4.43) or (4.44) then, the boundary layer problem (4.32)-(4.39) has a solution. This solution exists if (4.45) is satisfied. It is continuous, with decreasing potential, ϕ, and ion and electron densities, n_i and n_e. Furthermore, it satisfies (4.46), (4.47).

4.4.4 Numerical results using the boundary conditions well-adapted to the quasi-neutrality

We use the resolution of the boundary layer problem to determine boundary conditions well-adapted to the quasi-neutral regime. Let us note that Theorem 4.1 shows that several boundary conditions (depending on the information contained in the domain) give a solution of the boundary layer problem. We must select the right one. For this, we use the numerical results performed in the resolved case. We look for a solution of the boundary layer problem giving decreasing electron and ion densities. But, only one solution corresponds to this condition, the one of point *2.* in Theorem 4.1. For this solution, the ion state at $x = 0$ in the boundary layer problem, denoted by (n_{i0}, q_{i0}), is fully determined by the information coming from the left-hand side, i.e. outside the domain. This is not the case for the electron state. But, this is not surprising. Indeed, ε being small, the state at the end of the boundary layer is subsonic for electrons (one positive eigenvalue and one negative eigenvalue). Thus, it can not be fully determined by the information coming from outside the domain. To determine the boundary conditions, we must use the information coming from the right-hand side, i.e. from the core of the plasma.

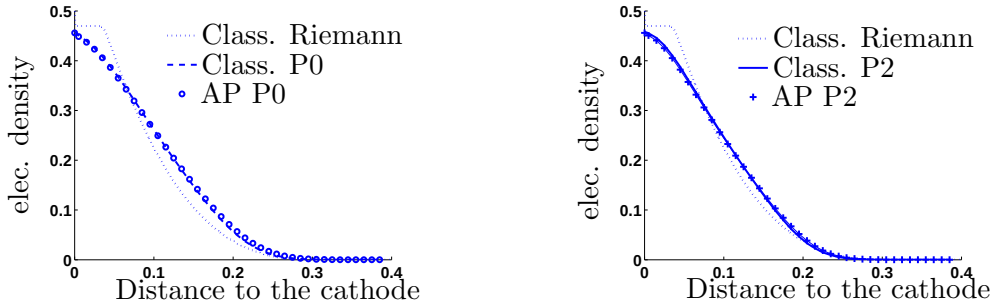

Figure 4.7: Electron density as a function of x at the rescaled time $t = 0.05$ in the non resolved in space case: $\Delta x = 10^{-2} > \lambda = 10^{-4}$. The classical scheme resolves the plasma period: $\Delta t \leq \tau$, and the AP scheme does not: $\Delta t > \tau$. We use the solvers $P0$ and $P2$ with the boundary conditions well-adapted to the quasi-neutral regime and given by $n_e = n_i = \bar{n}_0$, $q_e = \bar{q}_{e0}$, $q_i = \bar{q}_{i0}$ and $\phi = \bar{\phi}_0$. The curves are compared to the reference curve obtained with the classical scheme, the Riemann solver and the non well-adapted boundary conditions: $n_e = n_i = n_0$, $q_e = q_i = q_0$ and $\phi = 0$, in the resolved case $\Delta x = \lambda$ and $\Delta t \leq \tau$.

However, neglecting ε, we can determine the quasi-neutral density $\bar{n}_0$, the ion momentum $\bar{q}_{i0}$ and the potential $\bar{\phi}_0$, at the end of the boundary layer. For this, we use (4.46), (4.47) and we remark that the limit of the total electron enthalpy k_e when $\varepsilon \to 0$ is the enthalpy $h_e(n) = C_e\, \gamma_e/(\gamma_e - 1)\, n^{\gamma_e - 1}$ which does not depend on $\bar{q}_{e0}$. For the electron momentum, we set $\bar{q}_{e0} = \lim_{x \to 0} \bar{q}_e(x, t)$ where $\bar{q}_e$ is the quasi-neutral solution, since in the boundary layer q_e is constant.

We use these boundary conditions to perform numerical simulations of the test case previously presented. The results are given on Figure 4.7.

We use the same reference curve as previously, i.e. the one given by the classical scheme, the Riemann solver in the resolved case ($\Delta x = \lambda$ and $\Delta t \leq \tau$) and the non well-adapted boundary conditions. We compare this reference curve to the classical and AP schemes with the $P0$ and $P2$ solvers in the non resolved space case, ($\Delta x = 10^{-2} > \lambda = 10^{-4}$) and using the well-adapted boundary conditions. The classical scheme resolves the plasma period, $\Delta t \leq \tau$, and the AP scheme does not, $\Delta t > \tau$. We can see that all schemes give results similar to the reference curve. Only the plateau at the end of the boundary layer is not well described. But we stress that the $P2$ solver is now stable, I recall it was not with the non well-adapted boundary conditions. These boundary conditions allow to use general Roe type solvers without resolving the Debye length.

4.5 Conclusions and future prospects

In this chapter, I have presented an asymptotic preserving scheme in the quasi-neutral limit for the two-fluid Euler-Poisson system. Numerical simulations and a stability analysis have proven the good behavior of the scheme compared to the classical scheme. This new scheme drastically reduces the cost of the numerical simulations. Furthermore, the analysis of a boundary layer problem at the injection point, allows to determine boundary conditions well-adapted to the quasi-neutral regime. Thus, extension of the AP scheme to general Roe type solvers is possible without resolving the Debye length.

Many future prospects can be considered at the end of this work. First, prospects dealing with the AP scheme for the Euler-Poisson system. On coarse meshes the scheme is still stable but is less accurate. Using higher order solvers is necessary to increase the accuracy. For this, we can use discontinuous Galerkin methods, that I have started to do in collaboration with Pierre Degond and Shi Wang Shu.

We can study extensions to other systems. The study of the system with the full Euler equations is quite straightforward. A work is in progress on this subject including the study of the boundary layer problem. Furthermore, I work on the extension of the AP scheme for the Euler-Maxwell system in collaboration with Pierre Degond, Fabrice Deluzet and Dominique Savelief.

In collaboration with Annalisa Ambroso, Pierre Degond, Fabrice Deluzet, Nadia Lemarchant, Pascal Omnès and Jacques Segré, I work on a scheme preserving the low Mach number limit for the Euler system.

Finally, the boundary layer problem still keeps its secrets. First, the approximation ε small could be certainly eliminated by exactly resolving, at least numerically, the boundary layer problem. It could help us to reproduce the plateau at the end of the boundary layer. Furthermore, I would like understand the miracle of the solvers with diagonal numerical viscosity matrices (modified Lax-Friedrichs and degree 0 polynomial solvers) which are stable even when the mesh does not resolve the boundary layer.

Chapter 5

Kinetic models for the transport of particles

In this chapter, we are interested in kinetic models describing the transport of particles. These results are published in [**N1**], [**A3**], [**CR1**] and [**CR3**]. They have been realized in collaboration with Pierre Degond, Komla Domelevo, Céline Parzani and Rachid Talaalout.

The first section deals with the transport of charged or non charged particles, confined close to a surface by an external potential.

In the second section, we study a simplified diphasic model for the modeling of the transport of droplets in a gas.

5.1 Particles trapped in a surface potential

In this section, we describe the results published in [**CR1**], [**CR3**] and those published in [**A3**].

5.1.1 Introduction

We are interested in the modeling of particles submitted to an external potential in a half space. The applied potential confines the particles close to the surface of the half space. We start from the Vlasov equation describing the transport of the particles. It is classical in mathematical modeling, to derive an asymptotic model containing a smaller number of variables than the kinetic description. This is possible when the physical context allows for it. As instance, when the particles are subject to a large number of collisions. The resulting model depends of the nature of the considered collisions. In the problem studied here, the particles being confined close to the surface, they frequently collide with the surface. This allows us to derive different model according to the considered collisions.

This work is related to a physical application proposed by Jean-Pierre Catani and Denis Payan from CNES. The problem deals with electric arc phenomena on satellite solar panels already described in section 3.2. I briefly recall the physical context. The satellite solar panels are constituted of strings of photo-voltaic cells. When the delivered tension exceeds the threshold value of fifty volts, some electric

arc phenomena occur yielding sometimes the short-circuit of all the concerned string. The scenario, proposed by physicists, is split into three steps, see [5], [8] and [9]. First, a primary discharge ignites and creates a high density plasma. This plasma expends between two cells. When the plasma has filled the gap between the cells, an electric arc may establish. Here, we want to model the primary discharge.

Following [8], we assume that the primary discharge is due to a differential charging of the dielectric surface and of the conducting media (semiconductor or metallic inter-connectors). Indeed the plasma environment of the satellite contributes to positively charge the dielectric surface compared to the conductor with potential difference ranging up to 1000 volts. This large electric field triggers an enhanced field electron emission at the triple point. This local increase of the electric field has two origins: the contact between metallic parts, dielectric and vacuum and the presence of micro-dielectric impurities at the triple point. Due to the electric field parallel to the dielectric boundary, the emitted electrons reach the top of the cell. On their way, they are attracted by the positive potential of the surface and collide with it. These collisions generate secondary electrons from the dielectric surface as well as desorbed neutral particles. Furthermore, during their way to the top of the dielectric, the electrons collide with the neutral particles and create some ions. Due to the increase of the electron density by secondary emission, an avalanche breakdown occurs and generates a high density plasma.

I begin with the brief description of the results published in **[CR1]**, **[CR3]**. This preliminary work clarifies what are the dominant physical mechanisms in the plasma formation for the physical application previously described.

In section 5.1.3, I present the results published in **[A3]**. In this work, we consider a more general situation than the previous one. We consider particles trapped along a surface by a confining potential. From a kinetic description, we derive a two dimensional model along the surface. This analysis is rigorous in the case of non charged particles and formal when the coupling with the Poisson equation is considered.

5.1.2 Energy-transport asymptotic model

In **[CR1]**, **[CR3]**, we want to establish a model to describe of the high density plasma along the solar cell surface. We suppose that the collisions between the electrons and the surface are diffusive. We denote by $x = (\underline{x}, z) \in \mathbb{R}^2 \times \mathbb{R}^-$ the space variable split into the parallel components $\underline{x}$ and the transverse component z. We assume that the applied potential is given by $\phi(\underline{x}, z) = \phi_0(\underline{x}) + \psi(z)$ with $\psi(z) = -E_T\, z$ where $E_T > 0$ is given. The potential ψ is called the confining potential. In [13], P. Degond, considering the same problem, derives a diffusion model (called SHE model for Spherical Harmonic Expansion, see [53]) from a kinetic model. This model consists in a diffusion equation on the particle distribution function F. This distribution is an averaged value in the transverse direction (z) and in the velocity for a given energy (ε). Then, here we assume that the particles are in a local equilibrium and their distribution $F(\underline{x}, \varepsilon, t)$ is a Maxwellian function

$$F(\underline{x}, \varepsilon, t) = \exp\left(\frac{\mu(\underline{x}, t) - \varepsilon}{T_e(\underline{x}, t)}\right),$$

where $\mu \in \mathbb{R}$ and $T_e > 0$ are the chemical potential and the temperature of the electrons. Integrating the SHE model by respect to the energy, we obtain an energy-transport model on the surface particle density (n_e) and on the energy (W_e):

$$\partial_t n_e + \nabla_{\underline{x}} \cdot J_n = Q_n,$$
$$\partial_t W_e + \nabla_{\underline{x}} \cdot J_w - J_n \cdot \nabla_{\underline{x}} \phi_0 = Q_w.$$

These quantities are connected to the chemical potential and the temperature by the relations $n_e = (2\,\pi\,e/m_e)^{3/2}\,T_e^{5/2}/E_T\,\exp(\mu/T_e)$ and $W_e = 5\,n_e\,T_e/2$, where $e > 0$ is the elementary charge and m_e is the electron mass. Furthermore, the particle and energy currents are given by

$$J_n = -D_{11}\,(\nabla_{\underline{x}}(\mu/T_e) - \nabla_{\underline{x}}\phi_0/T_e) - D_{12}\,\nabla_{\underline{x}}(-1/T_e),$$
$$J_w = -D_{21}\,(\nabla_{\underline{x}}(\mu/T_e) - \nabla_{\underline{x}}\phi_0/T_e) - D_{22}\,\nabla_{\underline{x}}(-1/T_e),$$

where $D_{i,j}$ are the coefficients of the diffusion matrix D given as a function of n_e, T_e and E_T, see [**CR1**].

This model is enriched with physics through source terms Q_n and Q_w. They model the inelastic collisions with the surface (i.e. those non conserving the energy) like the neutral desorption, the secondary electron emission or the electron attachment on the surface. When an electron collides with the surface, if it has enough energy, it extracts a neutral molecule or electrons. In the last case, the surface is positively charged allowing the capture of electrons with low energy.

To update the potential, we resolve a two dimensional Poisson equation

$$-\Delta_{\underline{x}}\phi_0 = \frac{e}{d}\left(\frac{n_s}{\epsilon_d} - \frac{n_e}{\epsilon_0}\right),$$

where d is an approximation of the electron cloud width in the transverse direction, ϵ_d and ϵ_0 are the dielectric (constituting the surface) and the vacuum permittivities. Finally, n_s is the density of the positive charges resulting from the secondary electron emission process. We will see in the following section that this two dimensional Poisson equation is not valid. Indeed, the formal derivation of the two dimensional model shows that a three dimensional Poisson equation must be considered with a density concentrated (with a Dirac function) on the surface. But at this stage, this result was not known.

The initial and boundary conditions are such that the domain is devoid of particles at the beginning of the process and electrons are emitted from the bottom of the cell with an enhanced field electron emission (like for the high current diodes with a micro spike lattice described in section 3.2 of Chapter 3).

We performed numerical simulations in one space dimension. Figure 5.1 shows the electron density and the density of neutral molecules desorbed by electron impact. We clearly see the expected avalanche phenomenon which creates a high density plasma. Let us note that the plasma creation is more important at the top of the cell where the electrons have gained sufficiently energy to extract neutral molecules or electrons from the surface.

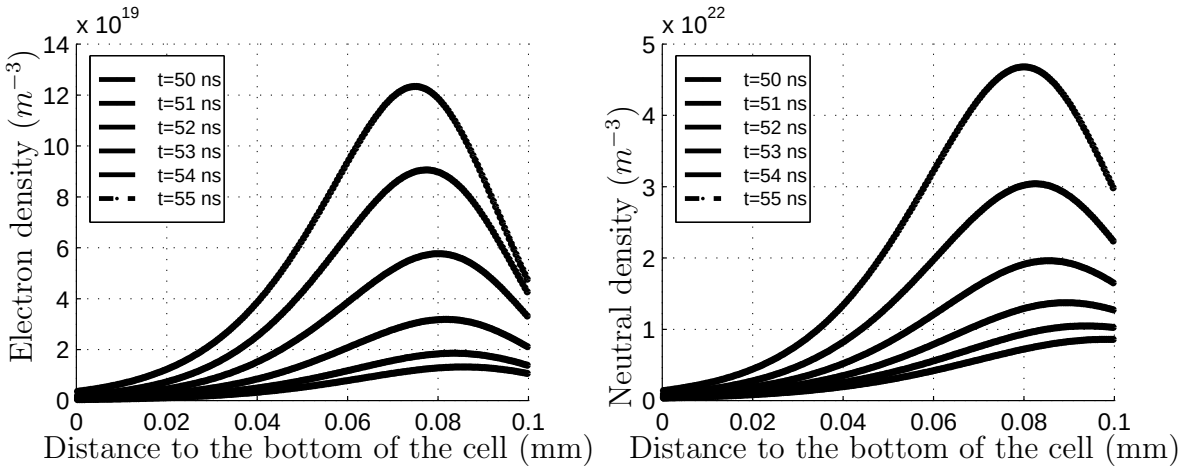

Figure 5.1: On the left-hand side: volume electron density along the surface of the cell at different times. It is obtained from the surfacic density n_e given by the energy transport model, divided by the approximate width d of the electron cloud. On the right-hand side: neutral density desorbed from the surface by electron impact.

5.1.3 Derivation of a Boltzmann model for particles trapped in a surface potential

In [**A3**], we are interested in the modeling of particles confined close to a surface by an external potential. We consider the domain $\Omega = \mathbb{R}^2 \times (-\infty, 0)$ and we assume a wall present on the boundary of Ω: $\partial\Omega = \mathbb{R}^2 \times \{0\}$. We denote by $x = (\underline{x}, z) \in \mathbb{R}^2 \times \mathbb{R}^-$, $v = (\underline{v}, v_z) \in \mathbb{R}^2 \times \mathbb{R}$ the space and velocity vectors. Due to their geometric relation with the surface, $\underline{x}$ and $\underline{v}$ are called the parallel space and velocity vectors. Similarly, z and v_z are called the transverse components.

Let f be the particle distribution function. It satisfies the Vlasov equation

$$\partial_t f + v \cdot \nabla_x f + \frac{E}{m} \cdot \nabla_v f = 0, \tag{5.1}$$

for all $(x, v, t) \in \Omega \times \mathbb{R}^3 \times \mathbb{R}^+$, where m is the particle mass and E is the resultant force applied on the particles. Here we assume that it derives from a potential.

Two cases are considered for E. First, the case of non charged particles with $E = -\nabla_x \phi$ and ϕ is a given potential. Finally, the case of charged particles and $E = -q\nabla_x(\phi + \phi_s)$ where q is the particle charge, ϕ is the applied external potential and so it is given. And, ϕ_s is the self-consistent potential given by the resolution of the Poisson equation

$$-\epsilon_0 \Delta_x \phi_s = q \int_{\mathbb{R}^3} f(v)\, dv, \tag{5.2}$$

for $(x, t) \in \Omega \times \mathbb{R}^+$ and where ϵ_0 is the vacuum permittivity.

To derive an asymptotic model, first we rescale the problem. I consider the case of charged particles but the other case can be easily deduced. The aim of this work is to derive an asymptotic model in situations such that the external potential confines the particles close to the surface $\partial\Omega$. We denote by $L_\parallel$ and $L_\perp$ the characteristic lengths

respectively in the parallel and transverse directions. We suppose that $\alpha = L_\perp/L_\parallel$ is a small (dimensionless) parameter. We denote by ϕ_c (chosen such that $\mathrm{sign}(\phi_c) = \mathrm{sign}(q)$), $v_c = \sqrt{q\,\phi_c/m}$, and f_c the characteristic scale of the potential, velocity and distribution function. Then, we introduce the following change of variables $\underline{x} = L_\parallel\,\hat{\underline{x}}$, $z = L_\perp \hat{z} = \alpha\, L_\parallel\,\hat{z}$, $v = v_c\,\hat{v}$ and $t = L_\parallel/v_c\,\hat{t}$. In space, it amounts to zoom on the transverse direction. We assume that there exists $\hat{\phi}$, independent of α and such that $\phi(x,t) = \phi_c\,\hat{\phi}(\hat{x},\hat{t})$, for all $(x,t) \in \Omega \times \mathbb{R}^+$. Furthermore, we define f^α and ϕ_s^α by

$$\begin{aligned} f(x,v,t) &= f_c\, f^\alpha(\hat{x},\hat{v},\hat{t}) \quad \text{for } (x,v,t) \in \Omega \times \mathbb{R}^3 \times \mathbb{R}^+, \\ \phi_s(x,t) &= \phi_c\,\phi_s^\alpha(\hat{\underline{x}},\alpha\hat{z},\hat{t}) \quad \text{for } (x,t) \in \Omega \times \mathbb{R}^+. \end{aligned}$$

It is important to note that we do not localize the self-consistent potential in the transverse variable. This is due to the fact that the Laplacian operator is non local. Indeed, it is well known that a local variation of the density close to the surface modifies the self-consistent potential in all the domain.

This rescaling leads to introduce a dimensionless parameter defined by $(f_c\,v_c) \times (q\,L_\parallel^2/\epsilon_0\,\phi_c)$. We choose it equal to $1/\alpha$. This hypothesis corresponds to the assumption that the number of particles is large since they are confined close to the surface. Indeed, we have $f_c\,v_c = (\epsilon_0\,\phi_c/q\,L_\parallel^2)/\alpha$.

Inserting this change of variables in (5.1), (5.2), we obtain for all $(\underline{x},z)\times(\underline{v},v_z)\times t \in \Omega \times \mathbb{R}^3 \times \mathbb{R}^+$:

$$\begin{aligned} \partial_t f^\alpha(z) + \underline{v}\cdot\nabla_{\underline{x}} f^\alpha(z) - \Big(\nabla_{\underline{x}}\phi(z) + \nabla_{\underline{x}}\phi_s^\alpha(\alpha\,z)\Big)\cdot\nabla_{\underline{v}} f^\alpha(z) \qquad (5.3)\\ -\partial_z\phi_s^\alpha(\alpha\,z)\,\partial_{v_z} f^\alpha(z) + \frac{1}{\alpha}\Big(v_z\,\partial_z f^\alpha(z) - \partial_z\psi(z)\,\partial_{v_z} f^\alpha(z)\Big) = 0, \\ -\Delta_{\underline{x}}\phi_s^\alpha(\underline{x},\alpha\,z,t) - \partial_{zz}^2\phi_s^\alpha(\underline{x},\alpha\,z,t) = \frac{1}{\alpha}\int_{\mathbb{R}^3} f^\alpha(\underline{x},z,v,t)\,dv, \qquad (5.4) \end{aligned}$$

where ψ is the transverse component of the external potential defined by

$$\psi(\underline{x},z,t) = \phi(\underline{x},z,t) - \phi_0(\underline{x},t) \quad \text{and} \quad \phi_0(\underline{x},t) = \phi(\underline{x},0,t). \qquad (5.5)$$

In the case of non charged particles, the rescaled Vlasov equation is given, in $\Omega \times \mathbb{R}^3 \times \mathbb{R}^+$, by

$$\partial_t f^\alpha + \underline{v}\cdot\nabla_{\underline{x}} f^\alpha - \nabla_{\underline{x}}(\phi_0+\psi)\cdot\nabla_{\underline{v}} f^\alpha + \frac{1}{\alpha}\Big(v_z\,\partial_z f^\alpha - \partial_z\psi\,\partial_{v_z} f^\alpha\Big) = 0. \qquad (5.6)$$

We add to these equations an initial condition $f^\alpha(t=0) = f_0$, and boundary conditions. For this, we introduce the outgoing and incoming traces of f on the surface $\partial\Omega$. They are respectively denoted by $\gamma^-(f)(\underline{x},(\underline{v},v_z),t)$ for all $v_z < 0$ and by $\gamma^+(f)(\underline{x},(\underline{v},v_z),t)$ for all $v_z > 0$. Then, we consider the boundary condition given by

$$\gamma^-(f^\alpha)(v_z) = \beta\,\mathcal{S}\gamma^+(f^\alpha)(v_z) + (1-\beta)\,\mathcal{K}\gamma^+(f^\alpha)(v_z) \quad \text{for all } v_z < 0, \qquad (5.7)$$

where $\mathcal{S}$ is the specular reflection operator and $\mathcal{K}$ is a general collision operator on $\partial\Omega$. Furthermore, β is the probability for an incoming particle on the surface $\partial\Omega$ to

be specularly re-emitted. This parameter will be chosen equal to 1 or $1-\alpha$ which corresponds to a case such that only specular collisions are considered or such that the specular collisions is the dominant collision process on the surface. These operators are given by

$$\mathcal{S}\gamma^+(f)(v_z) = \gamma^+(f)(-v_z), \quad \text{and} \quad \mathcal{K}\gamma^+(f)(v_z) = \int_{\{v'=(\underline{v}',v'_z)\in\mathbb{R}^2\times\mathbb{R}^+\}} K(v',v)\,\gamma^+(f)(v'_z)\,v'_z\,dv',$$

where $K(v',v)\,|v_z|\,dv$ is the number of re-emitted particles in $[v, v+dv]$ for an incoming particle on the surface $\partial\Omega$, with a velocity given by v'.

In the case of charged particles, we assume the following boundary conditions for the Poisson equation

$$\partial_z\phi_s^\alpha(z=0) = 0 \text{ on } \partial\Omega\times\mathbb{R}^+, \qquad \lim_{|x|\to+\infty}\phi_s^\alpha(x,\cdot) = 0 \text{ in } \mathbb{R}^+. \tag{5.8}$$

In [**A3**], we consider the case of an attractive potential for the particles. Then, we assume

Assumption 5.1 *For all $(\underline{x},t)\in\mathbb{R}^2\times\mathbb{R}^+$, the function $z\in\mathbb{R}^-\mapsto\psi(\underline{x},z,t)\in\mathbb{R}$ is decreasing, continuous and satisfies $\lim_{z\to-\infty}\psi(\underline{x},z,t)=+\infty$.*

We prove the following result.

Theorem 5.1 *Let $\alpha>0$, $f_0\in L^\infty(\Omega\times\mathbb{R}^3)$ with a compact support in $\bar\Omega\times\mathbb{R}^3$ and $\phi\in C^2(\bar\Omega)$. We assume $\beta=0$ and we denote by ϕ_0 and ψ the parallel and transverse components of ϕ defined by (5.5). We suppose that ψ satisfies Assumption 5.1. Let f^α be the weak solution to (5.6) and (5.7). Then, there exists $f\in L^\infty(\Omega\times\mathbb{R}^3\times[0,T])$ for all $T>0$ such that*

$$\lim_{\alpha\to0} f^\alpha = f \quad \text{ in } L^\infty(\Omega\times\mathbb{R}^3\times[0,T]) \text{ for the weak-}\star \text{ topology.}$$

Furthermore, there exists $F\in L^\infty(\mathbb{R}^2\times\mathbb{R}^2\times\mathbb{R}^+\times[0,T])$ for all $T>0$ such that

$$f(\underline{x},z,\underline{v},v_z,t) = F(\underline{x},\underline{v},\varepsilon_z,t),$$

for almost all $(\underline{x},z,\underline{v},v_z,t)\in\mathbb{R}^2\times\mathbb{R}^-\times\mathbb{R}^3\times\mathbb{R}^+$, where $\varepsilon_z = |v_z|^2/2+\psi(\underline{x},z,t)$. The function F satisfies

$$\begin{aligned}\Big[\partial_t + \underline{v}\cdot\nabla_{\underline{x}} - \Big(\nabla_{\underline{x}}\phi_0 + \langle\nabla_{\underline{x}}\psi\rangle\Big)\cdot\nabla_{\underline{v}}\Big](N_z\,F)& \\ +\partial_{\varepsilon_z}\Big[\Big(\langle\partial_t\psi\rangle + \underline{v}\cdot\langle\nabla_{\underline{x}}\psi\rangle\Big)(N_z\,F)\Big] = 0,&\end{aligned} \tag{5.9}$$

in $\mathcal{D}'(\mathbb{R}^2\times\mathbb{R}^2\times(0,+\infty)\times(0,+\infty))$, where for all function g from $\mathbb{R}^-$ into $\mathbb{R}^n$ ($n\geq1$), $\langle g\rangle$ is the mean value of g in the transverse direction and is given by

$$\langle g\rangle = \frac{2}{N_z(\underline{x},\varepsilon_z,t)}\int_{\mathcal{Z}(\underline{x},\varepsilon_z,t)}^0 \frac{g(z)}{v_z(\underline{x},z,\varepsilon_z,t)}\,dz,$$

where $v_z(\underline{x}, z, \varepsilon_z, t) = \sqrt{2(\varepsilon_z - \psi(\underline{x}, z, t))}$, *and* $\varepsilon_z \mapsto \mathcal{Z}(\underline{x}, \varepsilon_z, t)$ *is the inverse function of the one to one function* $z \mapsto \psi(\underline{x}, z, t)$ *from* $\mathbb{R}^-$ *into* $\mathbb{R}^+$. *The density of state,* N_z, *is given by*

$$N_z(\underline{x}, \varepsilon_z, t) = 2 \int_{\mathcal{Z}(\underline{x}, \varepsilon_z, t)}^{0} \frac{1}{v_z(\underline{x}, z, \varepsilon_z, t)}\, dz.$$

Several remarks will clarify the asymptotic model.

First, let us note that $\varepsilon_z(v_z, z) = |v_z|^2/2 + \psi(z)$ is the total energy in the transverse direction. When a particle leaves the surface with a given total transverse energy, it gains potential energy and thus loses a part of its kinetic energy. Its velocity vanishes when all the kinetic energy is transformed into potential energy. Then, it can only go back to the surface. We mathematically find again this result. Indeed, for a given positive energy and a given initial transverse velocity, we have $\varepsilon_z = \psi(z) + |v_z|^2/2 \geq 0$ and $0 \leq \psi(z) = \varepsilon_z - |v_z|^2/2 \leq \varepsilon_z$. But, ψ is a decreasing function, its inverse is also decreasing and $0 \geq z \geq \mathcal{Z}(\varepsilon_z)$.

The asymptotic model for F is obtained by integrating the limit equation in the transverse direction and by taking the averaged value in the transverse velocities for a given transverse energy. This formally means that we multiply the limit equation on f by $\delta(\varepsilon_z(z, v_z) - \bar{\varepsilon}_z)$ where $\bar{\varepsilon}_z$ is a fixed energy and we integrate by respect to z and v_z. The previous remark clarifies why the resulting quantities are finite even if we integrate for $z \in]-\infty, 0]$.

A simple calculus shows that $N_z(\underline{x}, \varepsilon_0, t) = \int_{\mathbb{R}\times\mathbb{R}^-} \delta(\varepsilon_z - \varepsilon_0)\, dz\, dv_z$. Thus, N_z is the bouncing time between two successive collisions of a given particle with the surface. Furthermore, $N_z(\underline{x}, \varepsilon_z, t)\, F(\underline{x}, \underline{v}, \varepsilon_z, t)\, d\underline{x}\, d\underline{v}\, d\varepsilon_z$ is the number of particles with a parallel position in $[\underline{x}, \underline{x}+d\underline{x}]$, a parallel velocity in $[\underline{v}, \underline{v}+d\underline{v}]$, a total transverse energy in $[\varepsilon_z, \varepsilon_z + d\varepsilon_z]$ and a transverse position in $[\mathcal{Z}(\underline{x}, \varepsilon_z, t), 0]$.

In the case of the coupling with the Poisson equation (5.4), we prove the following result.

Theorem 5.2 (Formal) *Let* $\alpha > 0$, f_0 *and* ϕ *be given, we suppose* $\beta = 1-\alpha$ *and that* ϕ_0 *and* ψ, *the parallel and transverse components of the external potential* ϕ, *defined by (5.5), satisfy assumption (5.1). Let* f^α, ϕ_s^α *be a solution of (5.3), (5.4), (5.7). then, the formal limit* $\alpha \to 0$ *gives* $f^\alpha \to f$ *and* $\phi_s^\alpha \to \phi_s$ *with*

$$f(x, v, t) = F(\underline{x}, \underline{v}, \varepsilon_z, t),$$

where $\varepsilon_z = |v_z|^2/2 + \psi(\underline{x}, z, t)$ *and where* F *satisfies,*

$$\partial_t(N_z F) + \underline{v} \cdot \nabla_{\underline{x}}(N_z F) - \Big(\nabla_{\underline{x}} \tilde{\phi}_s + \nabla_{\underline{x}} \phi_0 + < \nabla_{\underline{x}} \psi > \Big) \cdot \nabla_{\underline{v}}(N_z F) \qquad (5.10)$$
$$\partial_{\varepsilon_z}\Big(\Big(< \partial_t \psi > + \underline{v} \cdot < \nabla_{\underline{x}} \psi > \Big)\, N_z\, F\Big) = \mathcal{K}(F) - F,$$

The quantities N_z *and* $\langle\cdot\rangle$ *are defined in Theorem 5.1. The function* $\tilde{\phi}_s$ *is the trace on the surface* $\partial\Omega$, *of the self-consistent potential* ϕ_s. *We have* $\tilde{\phi}_s = \phi_s(z = 0)$ *with*

ϕ_s given by

$$\begin{cases} -\Delta_{\underline{x},z}\phi_s = 0, \ \textit{in} \quad \mathbb{R}^2 \times (-\infty, 0), \\ \lim\limits_{|(\underline{x},z)|\to+\infty} \phi_s(\underline{x}, z, t) = 0, \\ \partial_z\phi_s(z=0) = \rho = \displaystyle\int_{\mathbb{R}^2\times\mathbb{R}^+} N_z\, F\, d\varepsilon_z\, d\underline{v}, \quad \textit{on} \quad \mathbb{R}^2. \end{cases} \tag{5.11}$$

finally, the operator $\mathcal{K}$ is a collision operator modeling the non specular collisions on the surface. It is given as a function of K in [**A3**].

First, let us remark that the non specular part of the collisions is modeled in the source term like a volume collision operator. Furthermore, the limit Poisson equation is an equation on the entire half space with a density concentrated on the surface. In [**A3**], we prove that the solution is the restriction to the half space $\Omega = \mathbb{R}^2 \times \mathbb{R}^-$ of the solution to the Poisson equation on all the space $\mathbb{R}^3$ with a density, on the right-hand side term, concentrated on $z = 0$ given by $\rho(\underline{x}, t)\,\delta(z)$. We find again the non locality of the electric forces. Finally, a similar result have been rigorously established in [3] in the quantum case and on the entire space.

In [**A3**], we use this model to perform numerical simulations of the primary discharge presented in the introduction.

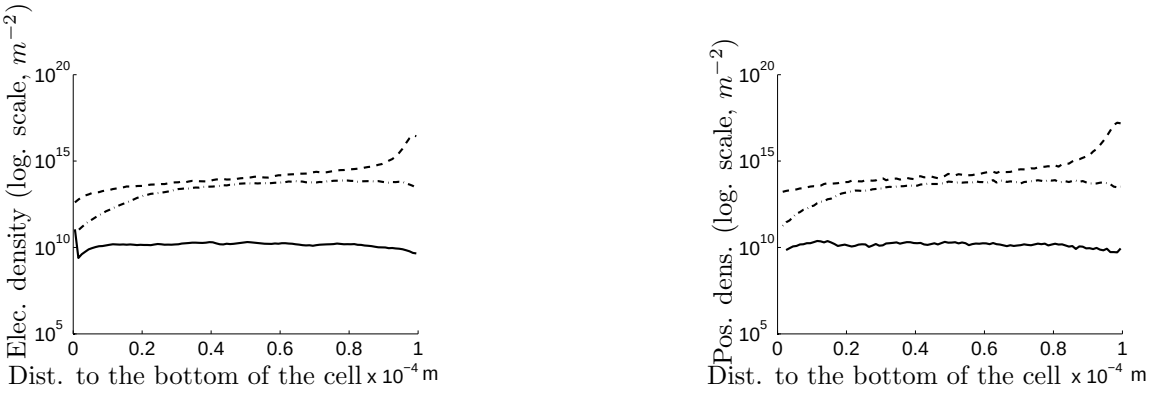

Figure 5.2: Surfacic electron density (left) and surfacic positive charges (right) in logarithm scale at times $t = 5 \times 10^{-11}$s (solid line), $t = 15 \times 10^{-11}$s (dashed-dotted line) and $t = 20 \times 10^{-11}$s (dotted line).

We simplify the model assuming a one dimensional process and assuming that the external transverse potential only depends on the transverse space variable z. These simplifications give a model for which the transverse energy ε_z is only a parameter of the transport equation (5.10). Like in section 5.1.2, we take into account the electron secondary emission and the enhanced field electron emission in the collision term and in the boundary conditions. We discretize system (5.10), (5.11) with a P.I.C. method (Particles in Cells, see [12], [15], [34]) based on a particular discretization of the Boltzmann equation and on a Fourier approximation of the Poisson equation. The electron secondary emission yields the creation of a large number of numerical

particles. We use a collapsing process to reduce this number and avoid numerical problems. On Figure 5.2, we see on the left-hand side the electron density and on the right-hand side the positive charges on the solar cell surface resulting of the electron secondary emission process. These curves show the expected avalanche phenomenon with the creation of an electron cloud more and more dense. The simultaneous increase of the positive charges on the surface shows that these electrons come from the electron secondary emission and not from the injection. This confirms the dominant role of this process.

5.2 Transport of droplets in a gas

I finish this chapter with the description of a work which is different from the other results. It has been done in collaboration with Komla Domelevo when I arrived in Toulouse. This work is published in [**N1**].

We are interested in a simplified model for a droplet flow in a gas. The gas is described by its constant density, normalized to 1 and its velocity u satisfying the viscous Burgers equation. The unknown for the droplets is a distribution function solution of a Fokker-Planck equation. These equations are coupled through force terms modeling the Stokes drag in turbulent gas flow. The model is given by

$$(\mathcal{P}^{\varepsilon,\eta}) \quad \begin{cases} \partial_t u^{\varepsilon,\eta} + u^{\varepsilon,\eta}\partial_x u^{\varepsilon,\eta} - \varepsilon\partial^2_{xx} u^{\varepsilon,\eta} = \displaystyle\int_{v\in\mathbb{R}} f^{\varepsilon,\eta}(v - u^{\varepsilon,\eta})dv, \\ \partial_t f^{\varepsilon,\eta} + v\partial_x f^{\varepsilon,\eta} + \partial_v(f^{\varepsilon,\eta}(u^{\varepsilon,\eta} - v)) - \eta\partial^2_{vv} f^{\varepsilon,\eta} = 0, \end{cases}$$

where $\varepsilon \geq 0$ and $\eta \geq 0$ are given. We have studied the different limit and problems summarized in the following figure:

$$\begin{array}{ccc} (\mathcal{P}^{\varepsilon,\eta}) & \xrightarrow{\quad\varepsilon\to 0\quad} & (\mathcal{P}^{0,\eta}) \\ \Big\downarrow{\scriptstyle \eta\to 0} & & \Big\downarrow{\scriptstyle \eta\to 0} \\ (\mathcal{P}^{\varepsilon,0}) & \xrightarrow{\quad\varepsilon\to 0\quad} & (\mathcal{P}^{0,0}) \end{array}$$

We recall the following result proven in [20]

Theorem 5.3 (Case $\varepsilon > 0$, $\eta = 0$)) *Let $T > 0$, we consider u_0 in $L^\infty(\mathbb{R}_x)$ and f_0 in $\mathcal{M}_0(\mathbb{R}_x \times \mathbb{R}_v)$ a bounded measure with a compact support.*

For all $\varepsilon > 0$, problem $(\mathcal{P}^{\varepsilon,0})$ has a unique weak entropy solution $(u^{\varepsilon,0}, f^{\varepsilon,0})$ in $\mathcal{C}([0,T]; L^\infty(\mathbb{R}_x)) \cap L^1([0,T]; W^{1,\infty}(\mathbb{R}_x)) \times \mathcal{C}([0,T]; \mathcal{M}_0(\mathbb{R}_x \times \mathbb{R}_v))$.

We establish the following results

Theorem 5.4 (Case $\varepsilon > 0$, $\eta > 0$)) *Let $T > 0$, we consider u_0 in $L^\infty(\mathbb{R}_x)$ and f_0 in $\mathcal{M}_0(\mathbb{R}_x \times \mathbb{R}_v)$ a bounded measure with a compact support.*

For all $\varepsilon > 0$ and all $\eta > 0$, problem $(\mathcal{P}^{\varepsilon,\eta})$ has a unique weak solution $(u^{\varepsilon,\eta}, f^{\varepsilon,\eta})$ in $\mathcal{C}([0,T]; L^\infty(\mathbb{R}_x)) \cap L^1([0,T]; W^{1,\infty}(\mathbb{R}_x)) \times \mathcal{C}([0,T]; \mathcal{M}(\mathbb{R}_x \times \mathbb{R}_v))$.

Theorem 5.5 (Case $\varepsilon = 0$, $\eta > 0$) *Let $T > 0$, we consider u_0 in $L^\infty(\mathbb{R}_x)$ and f_0 in $L^1_0(\mathbb{R}_x \times \mathbb{R}_v) \cap L^\infty_0(\mathbb{R}_x \times \mathbb{R}_v)$ with a compact support.*

Then, for all $\eta > 0$, problem $(\mathcal{P}^{0,\eta})$ has a unique weak entropy solution $(u^{0,\eta}, f^{0,\eta})$ in $\mathcal{C}([0,T]; L^\infty(\mathbb{R}_x)) \cap L^1([0,T]; W^{1,\infty}(\mathbb{R}_x)) \times \mathcal{C}([0,T]; L^1(\mathbb{R}_x \times \mathbb{R}_v) \cap L^\infty(\mathbb{R}_x \times \mathbb{R}_v))$.

Finally, we look at the existence of solutions for problem $(\mathcal{P}^{0,0})$. In this case, we only consider cases for which f_0 is in $L^1_0(\mathbb{R}_x \times \mathbb{R}_v) \cap L^\infty_0(\mathbb{R}_x \times \mathbb{R}_v)$ with a compact support.

Theorem 5.6 (Existence for $(\mathcal{P}^{0,0})$) *Let $(\varepsilon, \eta) > (0,0)$, we consider u_0 in $L^\infty(\mathbb{R}_x)$ and f_0 in $L^1_0(\mathbb{R}_x \times \mathbb{R}_v) \cap L^\infty_0(\mathbb{R}_x \times \mathbb{R}_v)$ with a compact support. We denote by $(u,f)^{\varepsilon,\eta}$, the solution of problem $(\mathcal{P}^{\varepsilon,\eta})$. Then, $(u,f)^{\varepsilon,\eta}$ weakly tends towards $(\tilde{u}, \tilde{f})$, up to a subsequence, in $\mathcal{C}([0,T]; L^1_{loc}(\mathbb{R}_x) \cap L^\infty(\mathbb{R}_x)) \times L^\infty([0,T]; L^1(\mathbb{R}_x \times \mathbb{R}_v) \cap L^\infty(\mathbb{R}_x \times \mathbb{R}_v))$, and $(\tilde{u}, \tilde{f})$ is a weak solution of $(\mathcal{P}^{0,0})$.*

5.3 Conclusions and future prospects

In this chapter, I have presented the mathematical and numerical modeling of the transport of particles confined close to a surface by an external potential. Furthermore, a Boltzmann model has been rigorously derived in the case of non charged particles and formally in the case of charged particles. A future prospect regarding this work is the rigorous derivation of the model in the non linear case, i.e. the case of the coupling with the Poisson equation. Furthermore, it would be interesting to perform more realistic simulations of the primary discharge. In particular, we could take into account the transverse energy in the model.

In the last section, I have presented results dealing with the transport of droplets in a gas. This last part has been done when I arrived in Toulouse. I did not pursue this work, thus I do not have future prospect regarding this work. However, the uniqueness of the non viscous limit system is an interesting problem, but the hyperbolic system property of the problem is a well known difficult study.

Bibliography

[1] R. Abgrall, R. Saurel, Discrete equations for physical and numerical compressible multiphase mixtures, J. Comput. Phys. **186** (2003) no. 2, 361–396.

[2] N. Ben Abdallah, S. Mas-Gallic, P.A. Raviart, Analysis and asymptotics of a one-dimensional ion extraction model, Asymptotic analysis **10** (1995) 1–28.

[3] N. Ben Abdallah, F. Mehats, O. Pinaud, *Adiabatic approximation of the Shrödinger-Poisson system with a partial confinement*, SIAM J. Math. Anal., 36 (2005), pp. 986–1013.

[4] S. Bouquet, Une solution analytique décrivant la compression d'un milieu soumis à une pression extérieure uniforme, CEA, private communication.

[5] J.P. Catani, D. Payan, Electrostatic behaviour of materials in a charging space environment, Proceedings of the 9th International Symposium on Materials in a Space Environment, 16-20 June 2003, Noordwijk, The Netherlands (ESA Publications Division 2003), p. 3.

[6] G. Chanteperdrix, P. Villedieu, J.P. Vila, *Un modèle bifluide compressible pour la simulation numérique d'écoulements diphasiques à phases séparées*, Rapport interne, ONERA (CT), mars **2002**.

[7] F.F. Chen, Introduction to plasma physics (Plenum, New-York, 1974).

[8] M. Cho, Arcing on High Voltage Solar Arrays in Low Earth Orbit: Theory and Computer Particle Simulation, Phd thesis, Massachusetts Institute of Technology, 1992.

[9] M. Cho, D.E. Hastings, Dielectric charging process and arcing rates of high voltage solar arrays, J. Spacecraft and Rockets **28** (1990) 698–706.

[10] S. Cordier and E. Grenier, Quasineutral limit of Euler-Poisson system arising from plasma physics, Comm. Partial Differential Equations **25** (2000) 1099–1113.

[11] S. Cordier, Y.J. Peng, Système Euler-Poisson non linéaire. Existence globale de solutions faibles entropiques, RAIRO Modél. Math. Anal. Numér. **32** (1998) no. 1, 1–23.

[12] G.H. Cottet, P.A. Raviart, Particle methods for the one-dimensional Vlasov-Poisson equation, Siam J. Numer. Anal. **21** (1984) no. 1, 52–76.

[13] P. Degond, Transport of trapped particles in a surface potential, Nonlinear partial differential equations and their applications. Collège de France Seminar, Vol. XIV (Paris, 1997/1998), 273–296, Stud. Math. Appl., **31** (2002), North-Holland, Amsterdam.

[14] P. Degond, The Child-Langmuir Law in the Kinetic Theory of Charged-Particles. Part 1, Electron Flows in vacuum, Advances in Kinetic Theory (B. Perthame, ed), World Scientific, Singapore (1994) 3–44.

[15] P. Degond, F. Guyot-Delaurens, Particle simulations of the semiconductor Boltzmann equation for one-dimensional inhomogeneous structures, J. Comput. Phys., **90** (1990) no. 1, 65–97.

[16] P. Degond, S. Jin, L. Mieussens, A smooth transition model between kinetic and hydrodynamic equations, J. Comput. Phys. **209** (2005) no. 2, 665–694.

[17] P. Degond, P.F. Peyrard, G. Russo and Ph. Villedieu, Polynomial upwind schemes for hyperbolic systems, C. R. Acad. Sci. Paris, Ser. I, **328** (1999) 479-483.

[18] P. Degond, P.A. Raviart, An Asymptotic Analysis of the One-Dimensional Vlasov-Poisson System : the Child-Langmuir Law, Asymptotic Analysis **4** (1991) 187–214.

[19] P. Degond, P.A. Raviart, On a penalization of the Child-Langmuir emission condition for the one-dimensional Vlasov-Poisson equation, Asymptotic Analysis **6** (1992) 1–27.

[20] K. Domelevo, Long time behaviour for a kinetic modelling of two-phase flows with thin polydisperse sprays, Rapport Interne n^{o}99-21., Laboratory MIP, University Paul Sabatier, Toulouse, FRANCE, (1999).

[21] R. Eymard, T. Gallouët, R. Herbin, Existence and uniqueness of the entropy solution to a nonlinear hyperbolic equation, Chinese Annals of Mathematics, Series B, **16** (1995) no. 1, 1–14.

[22] R. Eymard, T. Gallouët and R. Herbin, Finite Volume methods, in: P.G. Ciarlet, J.L. Lions (Eds), Handbook of Numerical Analysis, vol. VII, (North-Holland, 2000), p. 713.

[23] Sylvie Fabre, Stability analysis of the Euler-Poisson equations, J. Comp. Phys. **101** (1992) no. 2, 445–451.

[24] R.N. Franklin, J.R. Ockendon, Asymptotic matching of plasma and sheath in an active low pressure discharge, Journal of plasma physics **4** (1970) 3521–3528.

[25] S.Y. Ha, M. Slemrod, Global existence of plasma ion sheaths and their dynamics, Comm. Math. Phys. **238** (2003) no. 1-2, 149–186.

[26] R. Herbin, An error estimate for a finite volume scheme for a diffusion convection problem on a triangular mesh, Numerical Methods in Partial Differential Equations **11** (1995) no. 2, 165–173.

[27] C.W. Hirt, J.L. Cook, T.D. Butler, A Lagrangian method for calculating the dynamics of an incompressible fluid with free surface, J. Comput. Phys. **5** (1970) 103–124.

[28] N.A. Krall, A.W. Trivelpiece, Principles of plasma physics (San Francisco Press, 1986).

[29] Ya.E. Krasik, A. Dunaevsky, A. Krokhmal, J. Felsteiner, Emission properties of different cathodes at $E \leq 10^5\, V/cm$, Journal of Applied Physics, **89** (2001) no. 4, 2379–2399.

[30] S.N. Kruskov, First order quasilinear equations with several space variables, Math. USSR. Sb. **10** (1970) 217–243.

[31] I. Langmuir, K.T. Compton, Electrical discharges in gases, part II, fundamental phenomena in electrical discharges, Rev. Modern Phys. **3** (1931) 191–257.

[32] P. Marcati, R. Natalini, Weak solutions to a hydrodynamic model for semiconductors: the Cauchy problem, Proc. Roy. Soc. Edinburgh Sect. A **125** (1995) no. 1, 115–131.

[33] G.A. Mesyats, Explosive electron emission, URO-Press, Ekaterinburg, 1998.

[34] R.L. Morse, Multidimensional Plasma Simulation by the Particle-in-Cell Method, Methods Comput. Phys. **9** (1970) 213–239.

[35] W.F. Noh, P. Woodward, SLIC Simple Line Interface Calculation, proceedings of the fifth international conference on Numerical Methods in Fluid Dynamics, Lecture Notes in Physics, Springer, **59** (1976) 330–340.

[36] S.E. Parker, R.J. Procassini, C.K. Birdsall, A suitable boundary condition for bounded plasma simulation without sheath resolution, J. Comput. Phys. **104** (1993) 41–49.

[37] D. Payan, A model of inverted voltage gradient discharge inducing a secondary arc between cells on a solar array, CNES, European Round Table on modelling of S/C-plasma Interactions, 24-25 February 2000, ESA-ESTEC.

[38] Y.J. Peng and Y.G. Wang, Boundary layers and quasi-neutral limit in steady state Euler-Poisson equations for potential flows, Nonlinearity **3** (2004) no. 17, 835–849.

[39] F. Poupaud, M. Rascle, J. P. Vila, Global solutions to the isothermal Euler-Poisson system with arbitrary large data, J. Diff. Equ. **123** (1995) 93–121.

[40] K.U. Riemann, The Bohm criterion and sheath formation, J. Phys. D: Appl. Phys. **24** (1991) 493–518.

[41] K.U. Riemann, Th. Daube, Analytical model of the relaxation of a collisionless ion matrix sheath, J. Appl. Phys. **86** (1999) 1201–1207.

[42] R. Saurel, R. Abgrall, A simple method for compressible multifluid flows, SIAM J. Sci. Comput. **21** (1999) no. 3, 1115–1145.

[43] R. Saurel, R. Abgrall, A multiphase Godunov method for compressible multifluid and multiphase flows, J. Comput. Phys. **150** (1999) no. 2, 425–467.

[44] D. Shiffer, M. Ruebush, D. Zagar, M. LaCour, M. Sena, K. Golby, M. Haworth, R. Umstattd, Cathode and anode plasma in short-pulse explosive field emission cathodes, Journal of Applied Physics **91** (2002) no. 9, 5599–5603.

[45] K.M. Shyue, A fluid-mixture type algorithm for compressible multicomponent flow with van der Waals equation of state, J. Comput. Phys. **156** (1999) no. 1, 43–88.

[46] M. Slemrod, Shadowing and the plasma-sheath transition layer, J. Nonlinear Sci. **11** (2001) 193–209.

[47] M. Slemrod, The radio frequency driven plasma sheath: asymptotics and analysis, SIAM J. Applied Mathematics **63** (2003) no. 5, 1737–1763.

[48] M. Slemrod, N. Sternberg, Quasi-neutral limit for Euler-Poisson system, J. Nonlinear Sci. **11** (2001) 193–209.

[49] N. Sternberg, V.A. Godyak, Solving the mathematical model of the electrode sheath in symmetrically driven rf discharges, J. Comput. Phys. **111** (1994) 347–353.

[50] H. Sze, J. Benford, W. Woo, B. Harteneck, Dynamics of a virtual cathode oscillator driven by a pinched diode, Phys. Fluids **29** (1986) 3873-3880.

[51] E.F. Toro, Riemann Solvers and Numerical Methods for Fluid Dynamics. A practical introduction. Springer-Verlag, Berlin, 1997.

[52] B. Van Leer, Towards the ultimate conservative difference scheme V: a second order sequel to Godunov's method, J. Comp. Phys. **32** (1979) 101–136.

[53] D. Ventura, A. Gnudi, G. Baccarani, F. Odeh, Multidimensional spherical harmonics expansion of Boltzmann equation for transport in semiconductors, Appl. Math. Letters **5** (1992) 85–90.

[54] S. Wang, Quasineutral limit of Euler-Poisson system with and without viscosity, Comm. Partial Differential Equations **29** (2004) 419–456.

[55] D.L. Youngs, Time dependent multi-material flow with large fluid distortion, Numerical Methods for Fluid Dynamics, Ed. K. W. Morton & M. J. Baines, Academic Press, London, New-York, (1982) p. 273.

[56] D.L. Youngs, An interface tracking method for a 3D Eulerian hydrodynamics code, report of Atomic Weapons Research Establishment, (1994).